UNIVERSITÄT ZU LÜBECK

From the Institute of Experimental and Clinical Pharmacology and Toxicology
of the University of Lübeck
Director: Prof. Dr. Markus Schwaninger

"Metabolic and cellular factors determining the therapeutic effects of dimethyl fumarate"

Dissertation
for Fulfillment of
Requirements
for the Doctoral Degree
of the University of Lübeck

from the Department of Natural Sciences

Submitted by

Joanna Kosińska
from Rzeszów, Podkarpacie, Poland

Lübeck 2024

First referee: Prof. Dr. Markus Schwaninger

Second referee: PD Dr. Misa Hirose

Date of oral examination: 6.06.2025

Approved for printing: 12.06.2025

Table of contents

List of figures

List of tables

Abbreviations

aCSF	Artificial cerebrospinal fluid
ADEM	Acute disseminated encephalomyelitis
ADRs	Adverse drug reactions
AE	Adverse effects
AMPK	Adenosine monophosphate-activated protein kinase
APCs	Antigen-presenting cells
AUC	Area under the curve
BAT	Brown adipose tissue
BBB	Blood-brain barrier
BSA	Bovine serum albumin
CACC	Calcium-activated chloride channels
cAMP	Cyclic adenosine monophosphate
CCH	Carbachol
CFA	Complete Freund's adjuvant
CFTR	Cystic fibrosis transmembrane conductance regulator
CIS	Clinically isolated syndrome
CNS	Central nervous system
CSF	Cerebrospinal fluid
CXCR2	CXC-chemokine receptor 2
DAPI	4′,6-diamidino-2-phenylindole
DCs	Dendritic cells
DIS	Diffuse in space
DIT	Diffuse in time

DMF	Dimethyl fumarate
DMT	Disease-modifying therapy
EnaC	Epithelial Na^+ channel
EAE	Experimental autoimmune encephalomyelitis
EBV	Epstein-Barr virus
EDSS	Expanded Disability Status Scale
EL	Erythrocytes lysis
EMA	European Medicines Agency
FAE	Fumaric acid ester
FCS	Fetal calf serum
FDA	Food and Drug Administration
FLT3-L	FMS-like tyrosine kinase ligand 3
fMLP	N-Formylmethionyl-leucyl-phenylalanine
FSK	Forskolin
GA	Glatiramer acetate
GC	Germinal center
G-CSF	Granulocyte colony-stimulating factor
GDP	Guanosine diphosphate
GM-CSF	Granulocyte macrophage-colony stimulating factor
GMPs	Granulocyte-monocyte progenitors
GSH	Glutathione
GPCRs	G protein-coupled receptors
GST-1	Glutathione S-transferase-1
GWAS	Genome-wide association study

HCAR2	Hydroxycarboxylic acid receptor 2
HFbD	High-fiber diet
HLA	Human leukocyte antigen
HO-1	Haem oxygenase-1
I'_{sc}	Short- circuit current
IBS	Inflammatory bowel disease
ICAM-1	Intracellular cell adhesion molecule-1
IFN-β	Interferon beta
IFN-γ	Interferon gamma
IL	Interleukin
JNK	c-Jun N-terminal kinase
LAD	Lauric acid diet
MAPK	Mitogen-activated protein kinase
MBP	Myelin basic protein
MHC	Major histocompatibility
miR	microRNA
MOG	Myelin oligodendrocyte protein
MMF	Monomethyl fumarate
MMP9	Matrix metalloproteinase-9
mRFP	Monomeric red fluorescent protein
MRI	Magnetic resonance imaging
MS	Multiple sclerosis
NA	Nicotinic acid
NBC	Na^+- bicarbonate cotransporter

NCD	Normal chow diet
NKCC1	Na^+ K^+ $2Cl^-$ cotransporter
NET	Neutrophil extracellular traps
NK	Natural killers
NF-κB	Nuclear factor “kappa-light-chain-enhancer” of activated B-cells
Nrf2	Nuclear factor erythroid-associated factor 2
NQO-1	NAD(P)H1 quinone dehydrogenase
OUT	Operational taxonomic un
PD	Pemphigoid disease
PGD2	Prostaglandin D2
PGE2	Prostaglandin E2
PI3	Phosphoinositide 3
PI3K	Phosphoinositide 3 kinase
PIP3	Phosphatidylinositol (3,4,5)-trisphosphate
PKC	Protein kinase C
PLC	Phospholipase C
PLP	Proteo- lipid-protein
PMA	Phorbol 12-myristate 13-acetate
PPMS	Primary progressive multiple sclerosis
PTX	Pertussis toxin
R_{te}	Transepithelial resistance
ROS	Reactive oxygen species
RRMS	Relapsing-remitting multiple sclerosis
S1P	Sphingosine 1-phosphate

SCF	Stem cell factor
SCFA	Short-chain fatty acids
SPMS	Secondary progressive multiple sclerosis
TCA	Tricarboxylic acid
Th	T helper cells
TLR-4	Toll-like receptors 4
TNF	Tumor necrosis factor
Treg	Regulatory T-cells
V_{te}	Transepithelial voltage
VCAM-1	Vascular cell adhesion molecule-1
WT	Wild-type

Abstract

Multiple sclerosis (MS) is an autoimmune disorder affecting the central nervous system, characterized by inflammation, demyelination, axonal loss, and gliosis. Dimethyl fumarate (DMF), metabolized in vivo to monomethyl fumarate (MMF), is approved for the treatment of relapsing-remitting MS. MMF acts as an agonist of the hydroxycarboxylic acid receptor 2 ($HCA_{2)}$, similar to butyrate, a short-chain fatty acid (SCFA) produced by the gut microbiome. I hypothesize that the therapeutic response to DMF is influenced by the diet. Using an experimental autoimmune encephalomyelitis (EAE) mouse model, I investigated the effects of dietary modulation on DMF efficacy by feeding mice a high-fiber diet (HFbD), lauric-acid-rich diet (LAD), or normal chow (NCD). Our results demonstrated that DMF significantly alleviated neurological deficits in HFbD-fed mice but showed no therapeutic effect in LAD-fed mice. Plasma MMF levels remained unaffected by dietary changes. HFbD-induced DMF efficacy was dependent on HCA_2, with increased HCA_2 expression observed in $Ly6C^{intermediate}$ monocytes and microglia, whereas neutrophils maintained high HCA_2 expression irrespective of diet.

Conditional knockout of HCA_2 in neutrophils (*Ly6G-Cre*; $Hca2^{Fl/Fl}$ mice) abolished DMF therapeutic effect, indicating that DMF exerts its benefits through HCA_2 activation in neutrophils. These findings suggest that high fiber diet may improve DMF response rates in MS treatment. My research aimed to investigate how HFbD modulates neutrophil sensitivity to MMF stimulation. Overall, these findings could potentially help clinical strategies to optimize DMF therapy in MS patients.

Zusammenfassung

Multiple Sklerose (MS) ist eine Autoimmunerkrankung des zentralen Nervensystems, die durch Entzündung, Demyelinisierung, axonalen Verlust und Gliose gekennzeichnet ist. Dimethylfumarat (DMF), das in vivo zu Monomethylfumarat (MMF) umgewandelt wird, ist für die Behandlung der schubförmig remittierenden MS zugelassen. MMF wirkt als Agonist des Hydroxycarbonsäure-Rezeptors 2 (HCA_2), ähnlich wie Butyrat, eine kurzkettige Fettsäure, die vom Darmmikrobiom produziert wird. In dieser Studie wird untersucht, ob die therapeutische Reaktion auf DMF von der endogenen Butyrat Produktion beeinflusst wird.

Zu diesem Zweck wurde ein experimentelles Autoimmun-Enzephalomyelitis (EAE)-Mausmodell verwendet und die Auswirkungen einer veränderten Ernährung auf die Wirksamkeit von DMF untersucht. Hierfür wurden die Mäuse mit einer ballaststoffreichen Diät (HFbD), einer Diät mit hohem Harnsäuregehalt (LAD) oder einer Standard Diät (NCD) gefüttert. Es konnte gezeigt werden, dass DMF die neurologischen Defizite bei Mäusen, die mit HFD gefüttert wurden, signifikant linderte, während es bei Mäusen, die mit LAD gefüttert wurden, keine therapeutische Wirkung hatte. Die Plasmaspiegel von MMF wurden durch die Ernährungsumstellung nicht verändert. Des Weiteren konnte gezeigt werden, dass die HFbD-induzierte DMF-Wirksamkeit von HCA_2 abhängig ist, bei einer erhöhten HCA_2-Expression in $Ly6C^{intermediate}$ -Monozyten und Mikroglia, im Gegensatz zu einer Ernährungsunabhängigen hohen HCA2-Expression in Neutrophilen. Die bedingte Ausschaltung von HCA_2 in Neutrophilen (*Ly6G-Cre*; $Hca2^{Fl/Fl}$ -Mäuse) hob die therapeutische Wirkung von DMF auf, was darauf hindeutet, dass DMF seine Wirkung über die Aktivierung von HCA_2 in Neutrophilen entfaltet. Diese Ergebnisse sprechen dafür, dass diätetische Maßnahmen zur Steigerung der Butyrat Produktion die Ansprechraten auf DMF bei der MS-Behandlung verbessern könnten. Ziel dieser Arbeit war es zu untersuchen, wie eine ballaststoffreiche Diät die Empfindlichkeit der Neutrophilen gegenüber der Stimulation durch MMF moduliert. Diese gewonnenen Erkenntnisse könnten zur Entwicklung klinischer Strategien zur Optimierung der DMF-Therapie bei MS-Patienten beitragen.

1. Introduction

1.1. Introduction to Multiple Sclerosis

Multiple sclerosis (MS) is one of the most common autoimmune diseases of the central nervous system (CNS), characterized by the interaction of various immunopathological and neuropathological mechanisms resulting in inflammation, demyelination, axonal loss, and gliosis (Filippi et al., 2018). Currently, 2.8 million people have been diagnosed with MS, representing 1 in 3,000 people worldwide. Over the past years the number of reported MS cases has been steadily increasing. The increasing number of MS cases can be attributed to several factors, such as better diagnosis of the disease, as well as better national and global counting methods (MSIF, 2020). MS often starts in young adults in their 20s and 30s (Huang et al., 2017). MS has been diagnosed in minors under the age of 18 years, in which the diagnosis can be difficult due to the similarity of the MS symptoms to those observed in other childhood illnesses, including acute disseminated encephalomyelitis (ADEM) (National Multiple Sclerosis Society, 2024). However, an accurate diagnosis and description of the disease course is crucial for prognosis and selection of the best available treatment (Lublin et al., 2014). MS symptoms in patients manifest differently, but the most common symptoms of the disease include fatigue, pain, bladder and bowel problems, sexual dysfunction, movement and coordination problems, vision problems, and cognitive and emotional changes (MS International Federation, 2024).To further characterize MS, four main types are distinguished: clinically isolated syndrome (**CIS**), relapsing-remitting multiple sclerosis (**RRMS**), secondary progressive multiple sclerosis (**SPMS**), and primary progressive multiple sclerosis (**PPMS**) (Ghasemi et al., 2017).

CIS refers to the first episode of neurological symptoms similar to those observed in MS due to inflammation and demyelination in the CNS, lasting at least 24 hours. However, not all patients who experienced CIS may go on to develop MS. This is dependent on multiple factors, such as sex, number of magnetic resonance imaging (MRI) lesions, the age of disease onset, as well as smoking or vitamin D deficiency. To determine the likelihood of developing MS, MRI must show brain lesions similar to those seen in patients with MS. Without these changes, the risk of developing MS is much lower. In addition,

CIS patients start a disease-modifying therapy (DMT) approved by the US Food and Drug Administration (FDA) to delay or prevent MS development (National Multiple Sclerosis Society, 2024).

The majority of patients with MS, approximately 87 %, develop the **RRMS** subtype, which describes periods of new or worsening neurological symptoms called relapses, followed by a period of partial or complete recovery (remission) (Klineova & Lublin, 2018). Further diagnosis is based on the division into active or not active, worsening or not. During the active phase, new brain lesions appear, and further progress of damage to myelin and axons carried by the activated immune cells occurs, whereas remyelination takes place during the recovery phase (Compston & Coles, 2008), (National Multiple Sclerosis Society, 2024), (Figure 1).

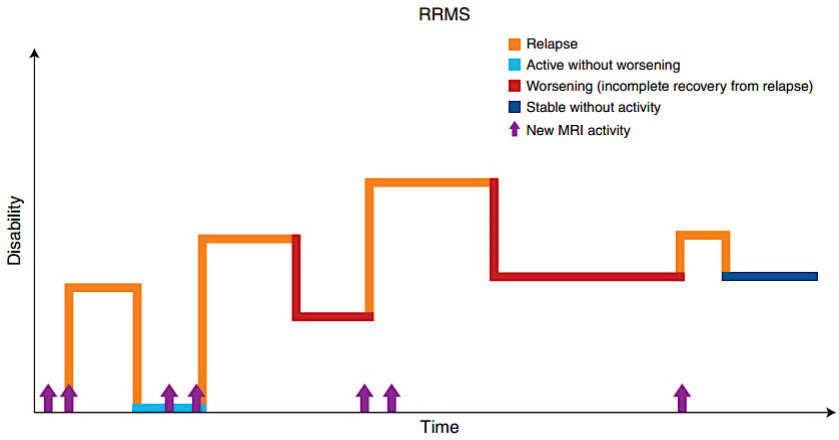

Figure 1: Representation of RRMS.

Time course and degree of disability is represented. With the onset of each relapse, new changes in MRI activity indicated by arrows can be observed. Some new symptoms may cause no worsening of the disease, while others cause an increase in disability. MS activity can also appear stable without experiencing new symptoms (Klineova & Lublin, 2018).

Patients with RRMS who experience a more rapid progression of neurological symptoms and an increase in disability go on to develop **SPMS**, which, for many patients, is a subsequent phase of the disease. Similar to RRMS, SPMS is divided into active or not active, with progression or without (National Multiple Sclerosis Society, 2024), (Figure 2).

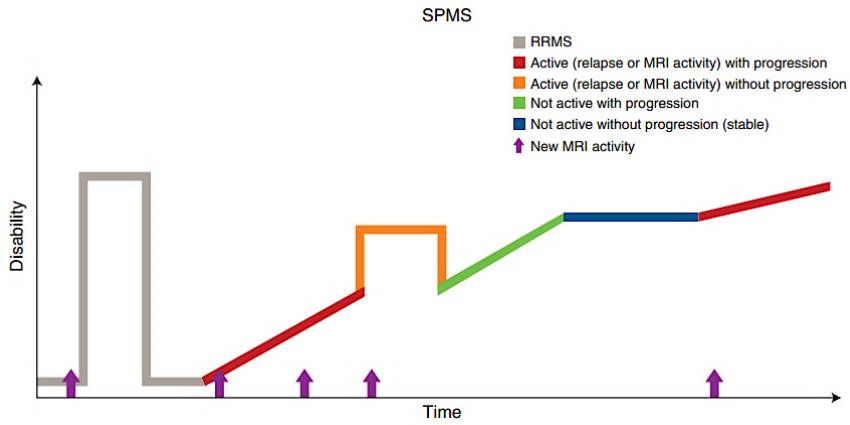

Figure 2: Representation of SPMS.

Patients with RRMS may experience a rapid increase in disability during the active phase of the disease, with or without apparent progression (occurrence of relapses or new lesions). After an active period of MS, patients enter an inactive phase, during which their disability increases or becomes stable (Klineova & Lublin, 2018).

PPMS develops in approximately 10-20 % of patients (Klineova & Lublin, 2018). As described in the other subtypes, PPMS is defined as active or not active, with or without progression (National Multiple Sclerosis Society, 2024). Patients do not experience any attacks or relapses, whereas disability accumulates, and symptoms steadily worsen, (Figure 3).

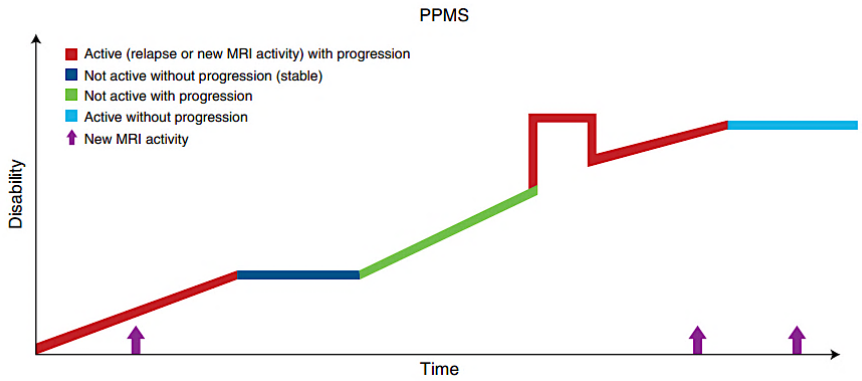

Figure 3: Representation of PPMS.

After an active period of the disease, patients may experience a stable phase with or without progression, followed shortly thereafter by a gradual worsening of symptoms (Klineova & Lublin, 2018).

1.2. Immunopathology

MS, as a multi-component disease, is characterized by a dysregulation of the immune system, including an interaction between the innate and adaptive immune systems, in which a key role has been attributed to dendritic cells (DCs) as antigen-presenting cells (APCs) (Grigoriadis & van Pesch, 2015). Activated DCs induce memory T-cell polarization by differentiating cytokines (Ifergan et al., 2008). In the presence of interleukin-12 (IL-12), naive $CD4^+$ T-cells differentiate into pro-inflammatory T helper 1 (Th1) cells that secrete interferon-γ (IFN-γ), and in the presence of IL-23, naive $CD4^+$ T-cells differentiate into Th17 cells that secrete IL-17 (Serafini et al., 2006). The presence of these pro-inflammatory factors has harmful effects on MS pathology. It contributes to the production of reactive oxygen species (ROS), leading to increased blood-brain barrier (BBB) permeability (Huppert et al., 2010). Pro-inflammatory cytokine-producing T-cells activate macrophages and microglia, producing other pro-inflammatory mediators including oxygen radicals and nitric oxide (NO), which contribute to axonal loss and demyelination (Das Sarma et al., 2009). by $CD8^+$ T lymphocytes play an essential role in the pathophysiology of MS through the production of pro-inflammatory mediators such as lymphotoxin and IL-17, which in turn lead to acute axonal damage (Bitsch et al., 2000) and neurodegeneration. Areas if neurodegeneration can be found in the white and grey matter of the brain and spinal cord, most likely located around the postcapillary venules (Dargahi et al., 2017). Helpful for the diagnosis are so-called plaques or lesions and refer to the loss of myelin sheaths and oligodendrocytes. These later, contribute to physical disability and cognitive impairment (Dendrou et al., 2015).

As previously described, lesions not only occur in the white matter but also in the gray matter, including the cortex, the basal ganglia, the brainstem, and the gray matter of the spinal cord (Lassmann, 2018). The brain is affected in several areas, such as periventricular (Figure 4), juxtacortical or cortical (Figure 5), and infratentorial (Figure 6) (Filippi et al., 2019).

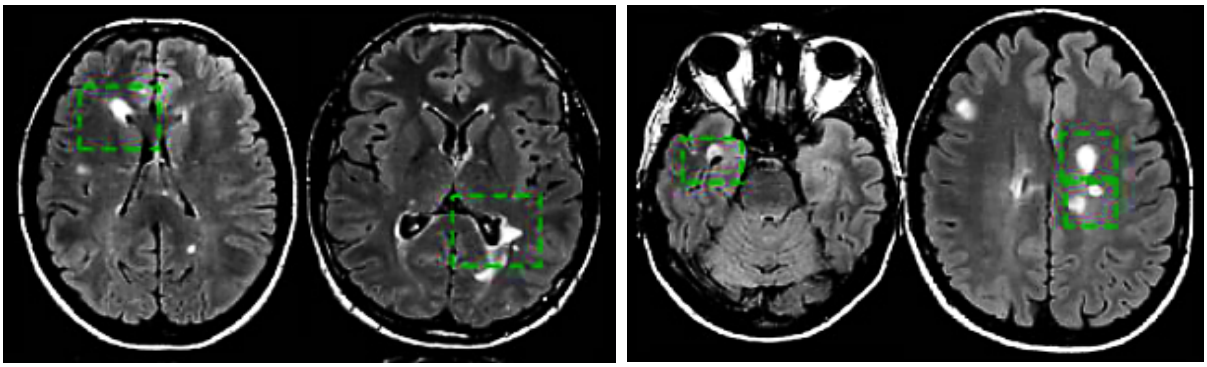

Figure 4: Characteristics of periventricular MS lesions.

Representative MRI images of periventricular MS lesion. Lesions are indicated with greens squares and are located in the vicinity of the ventricles (Filippi et al., 2019) .

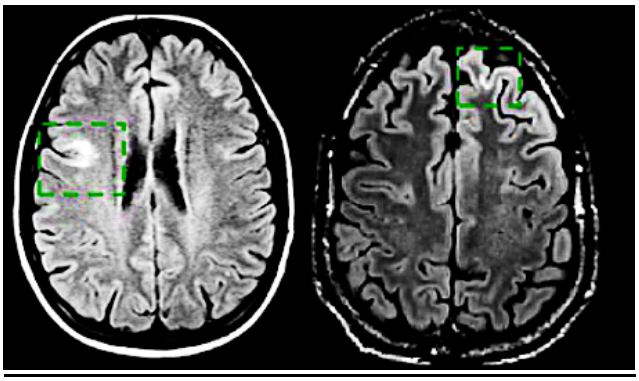

Figure 5: Characteristics of juxtacortical or cortical MS lesions.

Representative MRI images of juxtacortical or cortical MS lesion. Lesions are indicated with greens squares and are located in direct proximity to the cortex (Filippi et al., 2019).

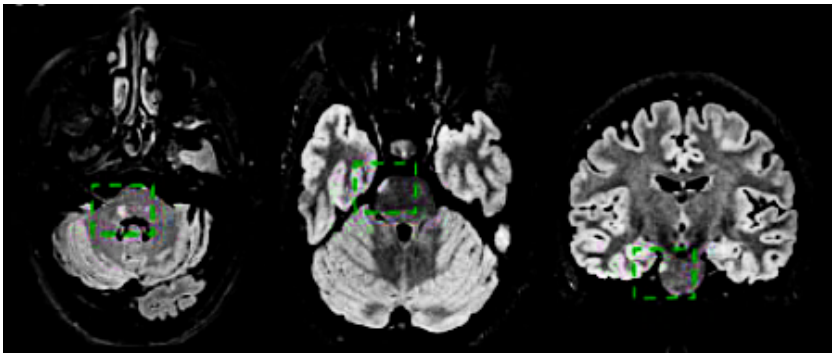

Figure 6: Characteristics infratentorial MS lesions.

Representative MRI images of infratentorial MS lesion. Lesions are indicated in the brainstem, cerebellar peduncles or cerebellum, in the vicinity of the surface (Filippi et al., 2019).

1.2.1. White matter lesions

In MS, white and gray matter damage provides a predictive marker during a single MRI scan, showing the progression and deterioration of higher functions, such as cognitive function (Lie et al., 2022).

Generally white matter lesions can be divided into active and inactive lesions as well as remyelinated shadow plaques, differing in the location and presence of infiltrating cells, the characteristics of each will be discussed further in the following paragraphs.

1.2.1.1. Active lesions

In the earliest stage of MS, active demyelinating plaques in the white matter are observed and are densely infiltrated by lymphocytes, mainly $CD8^+$ T lymphocytes, with a resident tissue memory phenotype. They play an autoinflammatory role in MS, as well as $CD20^+$ B-cells and a smaller number of infiltrating $CD4^+$ T-cells (Attfield et al., 2022). Besides lymphocytes also of activated microglia, distributed mainly at the periphery of the lesion and in the periventricular and distant white matter are found (Lassmann, 2018). However, the vast majority of infiltrating cells are activated macrophages evenly distributed throughout the lesion, that contain residual myelin. Lastly, astrocytes play an essential role in active lesions by contributing to further tissue damage through impaired redox homeostasis and increased glutamate concentrations. They also contribute to the recruitment of macrophages and lymphocytes into the parenchyma by expressing chemokines and cell adhesion molecules (Ponath et al., 2018).

1.2.1.2. Inactive lesions

Lesions progress from acute active into chronic inactive characterized by the reduction in infiltration by macrophages, microglia, and lymphocytes. Glial fibers produced by astrocytes create fibrous scar tissue filling the space between the demyelinated plaque. The consequence of axon loss and damage leads to an 80 % reduction in axon density (Popescu et al., 2013).

1.2.1.3. Remyelinated Shadow Plaques

In demyelinating plaques, so-called shadow plaques, the axons display very thin myelin sheaths and shortened interstitial distances. In these new oligodendrocytes derived from

the progenitor cell pool carry out remyelination. Completely remyelinated lesions are distinguishable areas of reduced myelin density and thin myelin thickness and represent the late remyelination phase. Plaques from older remyelination almost reach standard myelin thickness and appear difficult to distinguish from ordinary white matter (Kornek et al., 2000, Popescu et al., 2013).

1.2.2. Gray matter lesions

Over the past decade, many studies have shown that grey matter structures are involved in the process of demyelination in the early stages of MS, contributing to irreversible neuronal damage and axonal loss (Pirko et al., 2007). The process of cortical demyelination occurs in the forebrain and cerebellum, in the deep nuclei of the grey matter, and in the grey matter of the spinal cord. Compared to white matter lesions, cortical plaques differ significantly and are thought to be less inflammatory due to less infiltration of macrophages and activated microglia. They show more effective myelin repair, which occurs after demyelination. Cortical lesions are divided into four subtypes (Filippi et al., 2018):

1. Type I lesions -located at the cortico-subcortical border and affect the grey and white matter
2. Type II lesions - small perivenous intracortical lesions that do not affect white matter or the pial surface of the brain
3. Type III lesions - extend inward from the subpial layers of the cortex (subpial lesions)
4. Type IV lesions - extend through the whole width of the cortex but without passing the border between the cortex and the white matter

The most common type of cortical lesion is type 3, especially in the progressive stage of MS, located in cortical sulci or cingulate gyrus. They are often responsible for meningitis and extend from the brain surface to the deeper cortical layers (Pirko et al., 2007, Filippi et al., 2018).

Due to the diversity of the pathology, diagnosis of MS can be challenging. Thus, understanding the nature and characteristics of particular lesions could help make an

accurate and rapid diagnosis. This would be beneficial not only for a better prognosis of the disease, but also for improving therapeutic efficacy.

1.3. Etiology

Numerous factors, including genetic susceptibility in the immune system and environmental exposure such as vitamin D deficiency or smoking can trigger the development of MS. Other risk factors include previous Epstein-Barr virus (EBV) infection and sex differences with higher prevalence in female patients than male (Coyle, 2021).

1.3.1. HLA genes

A vital role in the mammalian adaptive immune system is played by the major histocompatibility (MHC) system, which in humans is known as the human leukocyte antigen (HLA) located on chromosome six and consists of three classes: HLA class I, class II and class III (Kreiter et al., 2015, Boegel et al., 2018). Within HLA class I, the three proteins HLA-A, -B, and -C are important ligands for receptors expressed by immune cells, including CD8+ T-cells, natural killers (NK) cells and DCs (Debebe et al., 2020). HLA class II includes HLA-DR, -DQ, and -D expressed exclusively on the surface of APCs (Martin et al., 2021). Class III is characterized by a high density of genes, which includes certain immune modulators, such as complement system components, e.g., C4, cytokines, such as TNF- α or regulatory genes involved in immune functions (Schott & Garcia-Blanco, 2021). Over the past decades, research has shown a strong link between HLA and MS development (Martin et al., 2021). The first genome-wide association study (GWAS) has demonstrated that the HLA DR15 haplotype is a potent risk factor for the onset of the disease. This haplotype shapes the $CD4^+$ T-cells repertoire and increases the probability of a demyelinating process (Patsopoulos et al., 2019).

1.3.2. Sex differences

In MS, women are more susceptible than men with a ratio of about 3:1. These differences may be determined by sex hormones and the effect of sex chromosomes on the immune system (Voskuhl, 2020). Compared to men, the immune response in women is more robust, and hormones such as estradiol and progesterone play an integral role. For instance, decreased hormone levels during the first day of the menstrual cycle, as well

as during menopause, contribute to increased lesion volume and worsened disease symptoms in patients with RRMS. On the other hand, females who received oral contraception showed a milder course of symptoms and improvement in MS severity (Golden & Voskuhl, 2017). Although women have a higher risk of developing RRMS, it is men who experience a worsening disability and faster progression to SPMS (Beatty & Aupperle, 2002). Various animal studies have demonstrated the neuroprotective effects of testosterone during MS by reducing the production of pro-inflammatory cytokines such as TNF-α and INFβ. And at the same time increasing regulatory interleukins such as IL-10, as well as protecting neurons from the damaging effects of oxidative stress (Collongues et al., 2018).

1.3.3. Epstein-Barr virus (EBV) infections

Patients who were previously infected with EBV have been shown to have a 2.3-fold higher risk of developing MS compared to EBV-negative patients (Ascherio, 2013). The virus affects B-cell function by reprogramming naïve B cells during the germinal center (GC) process, leading to the expansion of memory B-cells, which in turn become susceptible to autoimmunity and activation of cytotoxic T-cells (Soldan & Lieberman, 2023).

1.3.4. Environmental factors

Environmental exposure is among other risk factors for increasing the probability of developing MS. These include vitamin D deficiency, smoking, and adolescent obesity (Nourbakhsh, 2019). Insufficient levels of the vitamin D metabolite 25-OH-D, as well as any genetic abnormalities in the pathway of its metabolism, may trigger MS development (Pierrot-Deseilligny & Souberbielle, 2017). Vitamin D ability to suppress the innate and adaptive immune system contributes to the reduction of T-cell infiltration into the CNS, inhibition of monocyte proliferation into DCs, and production of pro-inflammatory cytokines. On the other hand, it leads to activation of microglia, which in turn removes myelin debris and contributes to increased production of regulatory T-cells (Treg) (Miclea et al., 2020). Furthermore, obesity has been shown to produce a higher risk for MS development. Patients suffering from obesity show higher levels of pro-inflammatory mediators produced in fat tissue, as well as an increased level of C-reactive protein, IL-

6, and leptin levels, simultaneously lowering circulating vitamin D concentration (Gianfrancesco & Barcellos, 2016). Additionally, saturated fatty acids interact with toll-like receptors 4 (TLR-4) thus activation the B-cells NF-κB pathway inducing neuroinflammation. Moreover, altered insulin sensitivity due to elevated TNF-α further contributes to the inflammation and decreased self-tolerance of immune cells (Correale & Marrodan, 2022).

1.4. Diagnostics of Multiple Sclerosis

An accurate diagnosis of MS is essential for an effective treatment. Established by Schumacher in 1965, the original criteria for the diagnosis of MS were clinical symptoms indicative of CNS demyelination. These criteria were based on two pillars: identification of the spatial and temporal spread of focal neurological deficits and elimination of critical differential diagnoses (Hartung et al., 2019). Over the decades, the diagnosis of multiple sclerosis has improved tremendously and is now based on clinical symptoms as well as MRI findings (Brownlee et al., 2017). Additionally, cerebrospinal fluid (CSF) diagnostics are essential in identifying subtype-specific biomarkers for MS and significantly improve its diagnosis (Klineova & Lublin, 2018). CSF examination provides strong evidence of MS and qualitative assessment of IgG to detect oligoclonal bands present in approximately 90 % of patients with MS (Dobson et al., 2013). These new diagnostic criteria (also referred to as the McDonald criteria) were introduced by the International Panel for the Diagnosis of Multiple Sclerosis in 2010 (Thompson et al., 2018). In 2017, the panel made specific changes to the 2010 McDonald criteria to simplify the use of MRI imaging (Hartung et al., 2019). MRI is very sensitive in detecting characteristic CNS lesions (Brownlee et al., 2017) and can substitute clinical features to meet the criteria of diffuse in space (DIS) or diffuse in time (DIT) (Wildner et al., 2020). The most common brain MRI findings are T2 lesions in four areas of the CNS: periventricular, cortical or subcortical, subthalamic, and medullary (Thompson et al., 2018). In 80-90 % of patients diagnosed with multiple sclerosis, lesions are present in the spinal cord. They are visible in the cervical, thoracic, or lumbar regions (Brownlee et al., 2017). These T2 lesions provide crucial information about the disease activity and progression (Wattjes et al., 2015).

To rule out the possibility of another disease causing the neurological symptoms, additional neurological tests are carried out. These include testing of the cranial nerve (vision, hearing, facial sensation, strength, swallowing), nerve conduction (to test sensation in the limbs), reflexes, coordination, gait, and balance (National Multiple Sclerosis Society, 2024). The results of these neurological tests are measured using a scale called the Expanded Disability Status Scale (EDSS), which assesses the progression and impact of the disease on functional systems (Srakocic, 2021). The EDSS scale ranges from 0 to 10 (Table 1), in which grades 1 to 4.5 refer to patients who can walk, while grades 5.0 to 9.5 refer to patients with impaired walking. A score of 10.0 results in patient's death (Multiple Sclerosis Trust, 2024).

Score	Description
0	Normal neurological exam, no disability in any FS
1.0	No disability, minimal signs in one FS
1.5	No disability, minimal signs in more than one FS
2.0	Minimal disability in one FS
2.5	Mild disability in one FS or minimal disability in two FS
3.0	Moderate disability in one FS, or mild disability in three or four FS. No impairment to walking
3.5	Moderate disability in one FS and more than minimal disability in several others. No impairment to walking
4.0	Significant disability but self-sufficient and up and about some 12 hours a day. Able to walk without aid or rest for 500 m
4.5	Significant disability but up and about much of the day, able to work a full day, may otherwise have some limitation of full activity or require minimal assistance. Able to walk without aid or rest for 300 m
5.0	Disability severe enough to impair full daily activities and ability to work a full day without special provisions. Able to walk without aid or rest for 200 m
5.5	Disability severe enough to preclude full daily activities. Able to walk without aid or rest for 100m
6.0	Requires a walking aid – cane, crutch, etc. – to walk about 100 m with or without resting
6.5	Requires two walking aids – pair of canes, crutches, etc. – to walk about 20 m without resting
7.0	Unable to walk beyond approximately 5 m even with aid. Essentially restricted to wheelchair, though wheels self in standard wheelchair and transfers alone. Up and about in wheelchair some 12 hours a day

7.5	Unable to take more than a few steps. Restricted to wheelchair and may need aid in transferring. Can wheel self but cannot carry on in standard wheelchair for a full day and may require a motorized wheelchair
8.0	Essentially restricted to bed or chair or pushed in wheelchair. May be out of bed itself much of the day. Retains many self-care functions. Generally, has effective use of arms
8.5	Essentially restricted to bed much of day. Has some effective use of arms retained some self-care functions
9.0	Confined to bed. Can still communicate and eat
9.5	Confined to bed and totally dependent. Unable to communicate effectively or eat/swallow
10.0	Death due to MS

Table 1: Expanded Disability Status Scale (EDSS).

MS progression is measured according to a 10-point scale that reflects the impact of MS on the functional systems such as motor function or cognitive abilities (adapted from Multiple Sclerosis Trust, 2024).

1.5. Available treatments for Multiple Sclerotic patients

Currently, the therapeutics approaches focus on reducing disease activity, delaying the onset of symptoms, and alleviating symptoms. However, to make the lives of MS patients more comfortable, disease-modifying therapies (DMTs) are used, which mechanism of action is different, as are their methods of administration. More than 25 years ago, the first drugs for RRMS were approved, including subcutaneous administration of glatiramer acetate (GA) and intramuscular interferon beta (IFN-β) (The IFNB Multiple Sclerosis Study Group, 1993, Jacobs et al., 1996). Consisting of an acetate salt and a mixture of polypeptides made up of 4 amino acids, GA induced a one-third reduction in relapse rate per year in patients suffering from MS compared to healthy controls – Additionally it decreases the diseases severity by altering the balance between pro-inflammatory and regulatory cytokines (Johnson et al., 1998). Prolonged use of GA (Copaxone) is well tolerated and maintains its clinical impact on multiple sclerosis relapse rate and disability (Johnson et al., 1995). The mechanism of action of IFNβ reduces pro-inflammatory while increasing anti-inflammatory cytokines. In addition, IFN-β inhibits T-cell proliferation and blocks inflammatory cell infiltration into the CNS (Kieseier, 2011). More than a decade later, the first humanized monoclonal antibody, Natalizumab, was approved, which acts as an inhibitor of an adhesion molecule, integrin α4β1, expressed by lymphocytes involved in transmigration across the endothelium into the CNS. Administered intravenously once every four weeks, the drug effectively reduces the number of relapses

and attenuates the progression of multiple sclerosis compared to patients receiving placebo or IFN-β (Hauser & Cree, 2020). Subsequently, oral treatment with Fingolimod was introduced. This sphingosine 1-phosphate (S1P) analog acts as an S1P antagonist, reducing the number of circulating T-cells by inhibiting their release from secondary lymphoid organs (Cohen et al., 2010). The second oral drug approved by the FDA was Teriflunomide which inhibits proliferation of autoreactive B- and T-cells (O'Connor et al., 2011). Since 2013 the FDA approved more oral drugs, such as dimethyl fumarate (DMF) (Tintore et al., 2019).

1.5.1. Dimethyl fumarate and its active metabolite monomethyl fumarate

Fumaric acid esters are a group of small molecules that exhibit immunomodulatory, anti-inflammatory, and antioxidant effects. In 1994, the first fumarate-based drug, Fumaderm, was approved as a systemic first-line therapy for Psoriasis in Germany (D.M.W., 2015). Today, DMF is not only effective in the treatment of Psoriasis but has also shown significant efficacy in the treatment of MS. Appearing under the name Tecfidera, DMF was approved by the FDA in 2013 and in 2014 by the European Medicines Agency (EMA) (Mrowietz et al., 2018). Following oral administration, exposure to the gastrointestinal mucosa leads to rapid spontaneous or esterase-mediated hydrolysis of DMF to monomethyl fumarate (MMF), the active metabolite that reaches maximum plasma concentration within 2-2.5 hours (Figure 7) (Mrowietz et al., 2018, Werdenberg et al., 2003). MMF has a short elimination half-life of approximately 1 hour, is metabolized by the tricarboxylic acid (TCA) cycle to water and carbon dioxide consequently excreted by respiration (Linker & Gold, 2013). Furthermore, DMF can form adducts with glutathione (GSH), which are then metabolized to mercapturic acid and removed from the body in the urine (Yadav et al., 2019). Due to immediate conversion to MMF, DMF is not detected in the circulation, while MMF concentrations increase significantly (Litjens et al., 2004).

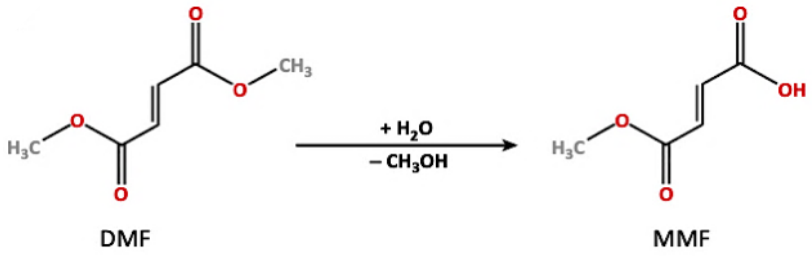

Figure 7: Metabolic conversion of DMF to MMF.

Due to high reactivity of the ester group, DMF hydrolyses into its prodrug, MMF (Mrowietz et al., 2018).

The mechanism of action of DMF and its active metabolite MMF is not yet fully understood; however, DMF has been shown to mediate neuroprotective effects through several pathways. Activation of nuclear factor erythroid-associated factor-2 (Nrf2), an important transcription factor that maintains redox homeostasis in the cell, mediates the antioxidant effect. Under the influence of MMF, the inactive form of the Nrf2 no longer binds to the Keap-1 protein in the cytoplasm, leading to the migration of Nrf2 into the nucleus, which induces the expression of antioxidant genes and detoxifying enzymes such as haem oxygenase-1 (HO-1), NAD(P)H1 quinone dehydrogenase (NQO-1) and glutathione S-transferase-1 (GST-1) (Ma, 2013). The predominant pathway involved in MMF signaling is hydroxycarboxylic acid receptor 2 (HCAR2), which has an inhibitory effect on adenylate cyclase, associated with decreased intracellular cyclic adenosine monophosphate (cAMP) and increased intracellular Ca^{2+} concentrations (Taggart et al., 2005). HCA_2 causes increased phosphorylation of mitogen-activated protein kinase (MAPK) ERK1/2, phosphoinositide 3 (PI3)/Akt kinase, and adenosine monophosphate-activated protein kinase (AMPK) α (Carretta et al., 2020). In addition, MMF inhibits nuclear factor “kappa-light-chain-enhancer” of activated B-cells (NF-κB) by reducing the production of pro-inflammatory cytokines, altering APCs function, and modulating the immune response. Furthermore, the reduced infiltration of cells in the CNS caused by DMF is driven by changes in their composition and phenotype (Yadav et al., 2019). DMF treatment reduces the number of $CD8^+$ T-cells, as well as $CD4^+$ T-cells, including pro-inflammatory Th1 and Th17 subgroups that secrete cytokines such as granulocyte macrophage-colony stimulating factor (GM-CSF), TNF, IFN-γ and Il-2, and promotes anti-inflammatory Th2 and regulatory subgroups (Smith et al., 2017). DMF significantly reduces the number of B-cells, especially $CD27^+$ memory B-cells, B-cells producing the

pro-inflammatory GM-CSF, IL-6, and TNF-α. Moreover, patients with MS show an increase in the immunomodulatory subset of NK cells ($CD56^{bright}$) and a decrease in the cytotoxic subset ($CD56^{dim}$) (Wu et al., 2017, Mehta et al., 2019). The degree of MS worsening is influenced by pro-inflammatory monocytes and monocyte-derived macrophages (M1 phenotype). During treatment with DMF, induction of anti-inflammatory M2 monocytes was observed in an Nrf2-independent manner, effectively raising their numbers with simultaneous reduction of pro-inflammatory M1 macrophages numbers. This occurs due to the activation of Nrf2 transcription factors and its target gene, *HO-1*, which promotes polarization towards the M2 type (Schulze-Topphoff et al., 2016, Han et al., 2016). DMF also reduces microRNA (miR)155 expression in monocytes responsible for the induction of TNF-α and IL-6 production and prevents infiltration of monocytes and macrophages into the CNS (Schilling et al., 2006). Neutrophils are another immune system cell affecting symptom severity and are a therapeutic target during DMF treatment. Both animal and *in vitro* studies have shown a significant inhibitory effect of DMF on neutrophils in an HCA_2-dependent manner by reducing their infiltration into the CNS (Chen et al., 2014).

1.6. The role of Hydroxycarboxylic acid receptor 2 (HCA_2)

Hydroxycarboxylic acid receptor 2 (HCA_2) belongs to the G protein-coupled receptors (GPCRs), also known as IFN-γ -regulated proteins in macrophages (PUMA-G in mice), HM74A in humans, and previously known as GPR109A (Zandi-Nejad et al., 2013). HCA_2 is expressed by a variety of cells, including white and brown adipocytes, immune cells such as monocytes, dendritic cells, macrophages, and neutrophils, but not lymphocytes (Tunaru et al., 2003). In addition, this receptor is expressed in retinal and colonic pigment epithelial cells, keratinocytes, microglia, and normal mammary tissue (Gambhir et al., 2012). HCA_2 is activated by the endogenous ketone body β-OHB (Gambhir et al., 2012) and butyrate, which belongs to the short-chain fatty acids (SCFA) produced by bacterial fermentation in the colon (Donohoe et al., 2011). In addition to the endogenous agonist, several other pharmacological ligands have been described, such as niacin, known as vitamin B3 or nicotinic acid (NA). The beneficial effects of NA were first discovered by Dr Rudolf Altschul in 1955, in which he observed significant reductions in serum triglyceride

and cholesterol levels (Bobileva et al., 2014, Altschul et al., 1955). In 2003, HCA_2 activation was linked to the anti-lipolytic effect of niacin (Tunaru et al., 2003). However, the action of niacin is associated with several side effects, one of the most common of which is skin redness due to HCA_2 activation on keratinocytes and dermal dendritic cells (Hanson et al., 2010). Other exogenous HCA_2 receptor agonists include the fumaric acid ester (FAE) DMF and its metabolite, MMF, which, similar to niacin, induce redness during treatment due to prostaglandin D2 (PGD2) and E2 (PGE2) formation (H. Tang et al., 2008).

HCA_2 is expressed by neutrophils, which are one of the first cell infiltrating the CNS during first stage of MS development contributing to the increased severity and neuroinflammation. It has been shown that effect of DMF treatment is mediated by HCA_2 contributing to improved neuro score by lowering the number of infiltrating neutrophils (Chen et al., 2014).

1.7. Neutrophils

Neutrophils, also known as polymorphonuclear cells, are the most abundant leukocytes circulating in the blood, accounting for about 10-15 % of all leukocytes in mice and 50-70 % in humans (Mestas & Hughes, 2004). Neutrophils are short-lived myeloid cells with a half-life of 8-12.5 hours in mice and 5-5.4 days in humans (Pillay et al., 2010) with an estimated cell number of 10^7 and 10^11 cells, respectively (Basu et al., 2002). The development of neutrophils occurs in the bone marrow in a process called granulopoiesis and begins with granulocyte-monocyte progenitors (GMPs) (Ng et al., 2019). It is a multi-step process characterized by three main stages: (1) a pool of undifferentiated stem cells, such as hematopoietic stem cells and pluripotent progenitors; (2) a mitotic pool, including actively proliferating myeloblasts, promyelocytes and myelocytes, (3) a postmitotic pool, representing fully differentiated, mature neutrophils (Summers et al., 2010). Granulopoiesis is regulated by numerous cytokines and growth factors that are released from hematopoietic and stromal cells, such as granulocyte colony-stimulating factor (G-CSF), granulocyte-macrophage colony-stimulating factor (GM-CSF), stem cell factor (SCF), interleukin 3 (IL-3), IL-6, FMS-like tyrosine kinase ligand 3 (FLT3-L), as well as ROS (Rossi et al., 2020; Zhu et al., 2017). Under physiological conditions, G-CSF

regulates neutrophil release from the bone marrow into the blood through the pores of sinusoidal endothelial cells (Burdon et al., 2008). As neutrophils gain maturity, expression of L-selectin, also known as CD62L, is lost, while expression of CD11b and CXCR4 is gained (Silvestre-Roig et al., 2019). Neutrophils are characterized by the expression of a vast number of receptors on the cell surface, divided into several classes, including members of seven transmembrane GPCR families, Fc receptors, adhesion molecules such as selectin and integrin ligands, cytokine receptors, and innate immune receptors. GPCR receptors are the primary receptors that activate neutrophils and mediate chemoattractant signaling, neutrophil polarization, as well as triggering ROS production and exocytosis of granules and vesicles (Futosi et al., 2013). Activation of GPCR leads to dissociation of the Gα subunit from the Gβγ dimer resulting in inhibition of adenylyl cyclase activity and decrease in cytoplasmic cAMP levels (Lehmann et al., 2008). Furthermore, activation of phospholipase C (PLC) β proteins leads to the release of intracellular Ca^{2+} and activation of protein kinase C (PKC) isoforms; in addition, Phosphoinositide 3 kinase (PI3K) γ activation contributes to phosphatidylinositol (3,4,5)-trisphosphate (PIP3) production and guanosine diphosphate (GDP)/Akt activation (Mócsai et al., 1997). The PI3Kγ pathway plays an essential role in neutrophil chemotaxis. At the same time, ERK and p38 MAP kinases, which are activated by GPCRs and N-Formylmethionyl-leucyl-phenylalanine (fMLP)-induced c-Jun N-terminal kinase (JNK) activation, are necessary for neutrophil migration (Mócsai et al., 2000). In a steady state, neutrophils rapidly respond and migrate to bacterial or fungal infection sites. However, neutrophils can also create an inflammatory environment, cause additional recruitment of other leukocytes, and contribute to tissue destruction. Recent studies provided evidence that, especially during the peak of the disease, infiltration of large numbers of neutrophils in the area of vascular leakage, demyelination, and axonal damage have been observed, suggesting their destructive role in promoting inflammation. Intense infiltration of neutrophils into active lesions is observed in areas of BBB leakage, suggesting the involvement of BBB damage by cytokine secretion, ROS production, and proteases such as matrix metalloproteinase-9 (MMP9) and NET. Therefore, neutrophils present a key factor in MS pathology, contributing to more severe disease development (Rossi et al., 2020; Steinbach et al., 2013).

1.8. Experimental autoimmune encephalomyelitis (EAE) mouse model

Animal studies are critical to understand the mechanism of autoimmune MS better and assess the effectiveness of available treatments for patients. Experimental autoimmune encephalomyelitis (EAE) is an animal model resembling MS and is widely used to study disease pathogenesis, inflammation, demyelination, cell motility, and tolerance induction, as well as to investigate potential new drug candidates and their side effects, analyze pharmacokinetics and predict effective dose for humans (’t Hart et al., 2011). Over 75 years ago, EAE was described for the first time and over a decade later, it was successfully induced in mice as a model (Rivers et al., 1933, Rivers & Schwentke, 1935; Yager, 1949). EAE can be induced in several ways, including immunization by proteo-lipid-protein (PLP), myelin basic protein (MBP), or encephalitogenic epitopes of PLP (PLP139–151, PLP178–191), myelin oligodendrocyte protein (MOG92–106), or MBP (MBP84–104) in an emulsion with complete Freund's adjuvant (CFA) (Robinson et al., 2014). To study chronic RRMS, chronic EAE is developed in C57BL/6 mice by immunization with an emulsion of MOG35-55/CFA or MOG1-125/CFA followed by injection of pertussis toxin (PTX). Administration of the emulsion leads to the expansion and differentiation of MOG-specific T-cells, such as $CD4^+$ and $CD8^+$, while PTX increases T-cell entry into the CNS. EAE is characterized by CNS inflammation, demyelination, immune cell infiltration, and paralysis. The first symptoms of EAE are observed within 8-18 days after immunization, and disease progression is usually followed for 4 weeks after immunization. The onset of the disease is observed within 3-4 days after the beginning of the initial EAE symptoms, and maximum severity persists for several days, followed by partial improvement. In some cases, mice may remain at maximum severity until the end of the study, most likely caused by axonal damage during the phases of extensive inflammation. A relapse and worsening of symptoms follow partial recovery. During the disease, the anticipated weight loss is observed, reaching approximately 20 % of the mice's body weight, which can most likely be explained by the paralysis and consequently a reduced food intake, as well as increased production of pro-inflammatory TNF-α in the blood during the peak of the disease. During recovery, the mice gain weight, while clinical performance does not improve (Kits et al., 2014).

1.9. Aim of the study

Dimethyl fumarate and its metabolite monomethyl fumarate are among the most effective drugs used to treat MS. However, not all patients respond to DMF treatment. One of the explanations may be the influence of the diet. In this study I investigated the effect of the high-fiber diet (HFbD) compared to diet rich in fat (lauric acid diet, LAD) on DMF efficacy in the EAE mouse model. The aim was to determine how diet modulates the response to DMF mediated by hydroxycarboxylic receptor 2 (HCA_2), which is highly expressed by neutrophils. I hypothesized that deletion of *Hca2* in neutrophils abolish protective effects of DMF. Therefore, I investigated not only how diet influences neutrophils biology, but how therapeutic effects of DMF in EAE depend on HCA_2 on neutrophils.

2. Materials

2.1. Chemicals

Name	Vendor
4',6-diamidino-2-phenylindole (DAPI)	Thermo Fisher Scientific (Waltham, USA)
4-(2-hydroxyethyl)-1-Piperazineethanesulfonic acid (HEPES)	Sigma-Aldrich (St. Louis, USA)
Accutase	Geyer Th. GmbH & Co. KG (Renningen, Germany)
Agarose (low melt)	Carl Roth GmbH & Co. KG (Karlsruhe, Germany)
Agarose (NEEO Ultraquality)	Carl Roth GmbH & Co. KG (Karlsruhe, Germany)
Betaisodona	Mundipharma GmbH (Cambridge, Great Britan)
Bovine serum albumin (BSA)	Sigma-Aldrich (St. Louis, USA)
Calcein AM	Thermo Fisher Scientific (Waltham, USA)
Calcium chloride ($CaCl_2$)	Merck KGaA (Darmstadt, Germany)
Carbachol	Sigma-Aldrich (St. Louis, USA)
Chloroform	Sigma-Aldrich (St. Louis, USA)
D (+) Glucose Monohydrate	Merck KGaA (Darmstadt, Germany)
Dimethyl fumarate (DMF)	Sigma-Aldrich (St. Louis, USA)
Dimethylsulfoxid (DMSO)	Sigma-Aldrich (St. Louis, USA)
dNTP Mix 10 mM	Thermo Fisher Scientific (Waltham, USA)
Dulbecco′s Modified Eagle′s Medium (DMEM)	Gibco/Thermo Fisher Scientific (Waltham, USA)
Eosin	J.T. Baker (Deventer, The Netherlands)
Erythrocyte's lysis (EL) buffer	Qiagen ((Venlo, The Netherlands)
Ethanol (absolute)	Carl Roth GmbH & Co. KG

	(Karlsruhe, Germany)
Ethylenediaminetetraacetic acid dihydrate (EDTA)	Sigma-Aldrich (St. Louis, USA)
Eukitt	
Fetal calf serum (FCS)	Sigma-Aldrich (St. Louis, USA)
Fluo-4 AM	Thermo Fisher Scientific (Waltham, USA)
Fibronectin	Sigma-Aldrich (St. Louis, USA)
Fixable Viability Dye eFluor™ 780	eBioscience™ (California, USA)
Fluorescent mounting medium	Dako (Glostrup, Denmark)
Forskolin	Sigma-Aldrich (St. Louis, USA)
Hanks' Balanced Salt Solution (HBSS)	Gibco/Thermo Fisher Scientific (Waltham, USA)
Hematoxylin	Sigma-Aldrich (St. Louis, USA)
Isoflurane	Baxter (Deerfield, USA)
Ketamine 100 mg/ml	Dr. E. Graeub AG (Bern, Switzerland)
L-Glutamine 200 mM	Gibco/Thermo Fisher Scientific (Waltham, USA)
Magnesium chloride ($MgCl_2$)	Sigma-Aldrich (St. Louis, USA)
Magnesium chloride (MgCl2) 50 mM	Thermo Fisher Scientific (Waltham, USA)
Methanol	Th. Geyer GmbH & Co. KG (Renningen, Germany)
Methyl cellulose (Methocel)	Sigma-Aldrich (St. Louis, USA)
Monomethyl fumarate (MMF)	Sigma-Aldrich (St. Louis, USA)
Nicotinic acid (NA)	Sigma-Aldrich (St. Louis, USA)
N-Formylmethionine-leucyl-phenylalanine (fMLP)	Sigma-Aldrich (St. Louis, USA)
Paraformaldehyde (PFA)	Sigma-Aldrich (St. Louis, USA)
Penicillin/Streptomycin	Merck KGaA (Darmstadt, Germany)

(Penicillin G 10.000 E/ml and Streptomycin 10 mg/ml, 100 x)	
Percoll	Cytiva (Marlborough, USA)
Phorbol-12-myristat-13-acetat (PMA)	Sigma-Aldrich (St.Louis, USA)
Pluronic	Thermo Fisher Scientific (Waltham, USA)
Potassium chloride (KCl)	Sigma-Aldrich (St.Louis, USA)
Potassium dihydrogen phosphate (KH_2PO_4)	Merck KGaA (Darmstadt, Germany)
Potassium hydroxide (KOH)	Merck KGaA (Darmstadt, Germany)
Probenecid	Thermo Fisher Scientific (Waltham, USA)
Qiazol Lysis Reagent	Qiagen (Venlo, The Netherlands)
Ringer's solution	Berlin-Chemie AG (Berlin, Germany)
RPMI-1640 medium (without phenol red)	GibcoTM/Thermo Fisher Scientific (Waltham, USA)
Sodium azide (NaN_3)	Sigma-Aldrich (St. Louis, USA)
Sodium bicarbonate ($NaHCO_3$)	Sigma-Aldrich (St. Louis, USA)
Sodium butyrate	Cayman Chemical (Michigan, USA)
Sodium chloride (NaCl)	Sigma-Aldrich (St. Louis, USA)
Sodium chloride solution 0.9 %	Berlin-Chemie AG (Berlin, Germany)
Sodium dihydrogen phosphate monohydrate ($NaH_2PO_4 \cdot H_2O$)	Sigma-Aldrich (St. Louis, USA)
Sytox Green	Thermo Fisher Scientific (Waltham, USA)
Xylazine (Rompun®) 2 %	Bayer Vital GmbH (Leverkusen, Germany)
Xylene	J.T. Baker (Deventer, The Netherlands)
Tumor necrosis factor (TNF)	Thermo Fisher Scientific (Waltham, USA)

2.2. Kits

Name	Vendor
Hooke Kit™ MOG35-55/CFA Emulsion PTX (cat.no. EK-2110)	Hooke Laboratories (Massachusetts, USA)
GeneJET NGS Cleanup Kit	Thermo Fisher Scientific (Waltham, USA)
NEBNext® Library Quant Kit for Illumina®	New England Biolabs (Frankfurt, Germany)
MagSi-NGS^{PREP}- PLUS beads	Steinbrenner Laborsysteme (Wiesenbach, Germany)
Qubit™ High Sensitivity Quantification Assay Kits	Thermo Fisher Scientific (Waltham, USA)
MiSeq Reagent Nano Kit v2 (300-cycles)	Illumina (California, USA)
MiSeq Reagent Kit v3	Illumina (California, USA)
RNeasy Plus Mini Kit	Qiagen (Venlo, The Netherlands)

2.3. Enzymes

Name	Vendor
Dream Taq DNA Polymerase 5 U/µl	Thermo Fisher Scientific (Waltham, USA)
Proteinase K 20 mg/ml, genotyping	Carl Roth GmbH & Co. KG (Karlsruhe, Germany)
Phusion Taq II	Thermo Fisher Scientific (Waltham, USA)

2.4. Solutions and Buffers

Name	Vendor
10x Phosphate buffered saline (PBS)	89 g $Na_2HPO_4 \times 2H_2O$ 12 g KH_2PO_4 400 g NaCl 10 g KCl The pH of 10X is approximetely 6.8 but when diluted to 1X PBS the pH should change to 7.4
Blocking solution (for free-floating sections)	5 % BSA in 1x PBS 0.3 % Triton-X-100
Control solution (for Ussing chamber)	145 g NaCl 0.4 g KH_2PO_4 1.6 g K_2HPO_4 5 g glucose 1 g $MgCl_2$ 1.3 mM Ca-gluconate Adjusted to pH 7.4
DEPC water	1 g/l Diethyl pyrocarbonate (w/v) in aqua bidest
FACS buffer	0.5 % BSA in PBS
Lysis buffer gDNA preparation	20 mM Tris-HCl in aqua bidest 5 mM EDTA (pH 8.0) 400 mM NaCl 1 % SDS 400 µg/m Proteinase K
Paraformaldehyde fixation buffer 4 %	4 % PFA in 1x PSA 200 µl 5M KOH per 100 ml 1x PBA

	dissolved by heating up to 60 °C, filtered by Whatman filter paper and adjusted to pH 7.4 by KOH
Ringer's solution with heparin	10 U/ml heparin in Ringer's solution
Tamoxifen	100 mg Tamoxifen (w/v) 500 µl Ethanol (abs.) 4.5 ml Miglyol 812

2.5. Reagents

Name	Type	Vendor
Beaker glasses	10-5000 ml	Schott Duran (Wertheim, Germany)
Cell culture plates	Cellstar® (6-, 24-, 96- Well)	Greiner AG (Kremsmünster, Austria)
Cell scraper	28 cm	Greiner AG (Kremsmünster, Austria)
Cell strainer	40 µm	Becton Dickinson (New Jersey, USA)
Coverslips	24x40mm ⌀ 12 mm	Carl Roth GmbH & Co. KG (Karlsruhe, Germany)
Falcon tubes	15 ml, 50 ml	Greiner AG (Kremsmünster, Austria)
Filter paper	MN 615 1/4 (Ø 240 mm)	Macherey-Nagel (Düren, Germany)
	FINO PAUL	HARTMANN AG, (Heidenheim, Germany)
Individually ventilated 500 cm2 green line cages		Tecniplast (Buguggiate, Italy)

PCR-96-well plate		SARSTEDT AG & Co. KG (Nümbrecht, Germany)
Petri dishes		Schott Duran (Wertheim, Germany)
Razor blades		Wilkinson Sword (London, UK)
Reaction tube	0.2 ml, 0.5 ml, 1.5 ml, 2 ml	Eppendorf AG (Hamburg, Germany)
Scalpel	FeatherTM disposable scalpel No 10, 11, 22	Electron Microscopy Sciences (Hatfield, USA)
Slides	SUPERFROST®PLUS	ThermoScientific (Braunschweig, Germany)
Syringes	1 mL, Luer 2 mL, 5 mL, 10 mL, 20 mL DiscarditTM II	Becton Dickinson (New Jersey, USA)

2.6. Devices

Name	Type	Vendor
Autoclave	Systec V-65	Systec GmbH (Linden, Germany)
Bench	SAFE 2020	Thermo Fisher Scientific (Waltham, USA)
Centrifuges	Universal 320R	Andreas Hettich GmbH & Co. KG (Tuttlingen, Germany)
	Micro200R	Andreas Hettich GmbH & Co. KG (Tuttlingen, Germany)

CLARIOstar® Microplate reader	CLARIOstar®	BMG LABTECH GmbH (Ortenberg, Germany)
Confocal Laser Scanning Microscopes	Leica TCS SP5	Leica Microsystems AG (Wetzlar, Germany)
Fluorescence microscope	Leica DMI6000 B	Leica Microsystems AG (Wetzlar, Germany)
Freezer -20 ºC	LGex 3410-22A 001	Liebherr Hausgeräte Lienz GmbH (Germany)
Freezer -80 ºC	Hera Freeze HFU T Series	Thermo Fisher Scientific (Waltham, USA) or other
Fridge 4 ºC	LKUexv 1610-23A-001	Liebherr Hausgeräte Lienz GmbH (Germany
Gel electrophoresis system	Sub-Cell GT Cell	Bio-Rad Laboratories (München, Germany)
Heating block	Thermomixer compact	Eppendorf AG (Hamburg, Germany)
PipetBoy	Pipetus®	Hirschman Laborgeräte GmbH & CO. KG, Eberstadt Germany
Pipettes	Variable volume air displacement single-channel	Eppendorf AG (Hamburg, Germany) or Gilson (Middleton, USA) or other
Scales	MC1 LC220S	Sartorius AG (Göttingen, Germany)
	LC 4200 S	Sartorius AG (Göttingen, Germany)
Surgery tools	Scissors, tweezers etc.	Fine Science Tools (Heidelberg, Germany)
Thermocycler	2720 Thermal Cycler	Thermo Fisher Scientific (Waltham, USA)

	Analytikjena Flexcycler or TGradient or TADVANCED	Biometra GmbH (Göttingen, Germany)
Vibratome	VT 1200S	Leica Microsystems AG (Wetzlar, Germany)
Vortex	REAX 200	Heidolph Instruments (Schwabach, Germany)
Water purification system	Milli-Q® Integral System	Merck Millipore (Billerica, USA)

2.7. Software

Name	Version	Vendor
Adobe Illustrator		Adobe Inc. (California, USA)
BioRender		BioRender (Toronto, Canada)
FlowJo	v10.10	FlowJo™ Software (Oregon, USA)
GraphPad Prism	8.0	GraphPad Software (La Jolla, USA)
Grammarly	v.1.2.94.1468	Grammarly (San Francisco, USA)
ImageJ	1.51s (Fiji) Java 1.8.0_66 (64-bit)	NIH (Bethesda, USA)
Leica application suite advanced fluoresence software	2.5.1.6757	Leica Microsystems AG (Wetzlar, Germany)
Mendeley	1.19.8	Elsevier (Amsterdam, The Netherlands)

2.8. Antibodies

2.8.1. Primary antibodies

Target	Host	Vendor (Cat. Nr)	Final concentration	Type	Research resource identifier (RRID)
Red Fluorescent Proteins (RFP)	Rat	ChromoTek (5F8)	1:500/ 1 µg/mL	Monoclonal	AB_2336064

2.8.2. Secondary antibodies

Target	Host	Vendor (Cat. Nr)	Final concentration	Type	Research resource identifier (RRID)
Rat IgG	Donkey	ThermoFisher (A-21208)	1:500/ 1 µg/mL	Polyclonal	AB_25357

2.8.3. FACS antibodies

Antibody name	Final concentration	Catalog number	Supplier
Brilliant Violet 650 anti-mouse/human CD11b	2 µg/ml	101239	BioLegend
Brilliant Violet 510 anti-mouse CD45	2 µg/ml	103138	BioLegend
PerCP/Cyanine 5.5 anti-mouse Ly-6G	2 µg/ml	127616	BioLegend
PE/Cyanine 7 anti-mouse Ly-6C	0.1 µg/ml	128018	BioLegend
FITC anti-mouse CD3ε	2 µg/ml	100326	BioLegend
Brilliant Violet 650 anti-mouse/human CD11b	2 µg/ml	101239	BioLegend

3. Methods

3.1. Animals

3.1.1. Housing

All mouse lines were established on a C57BL/6 background. Unless stated differently, mice were 8-12 weeks old and age- and sex-matched between experimental groups. Mice were housed in groups of 3-4 animals in ventilated Green Line cages (Tecniplast) under controlled conditions (temperature 22 ± 1 °C, light-dark cycle: 12:12 h, lights on 7:00 am, relative humidity 55 ± 10 %). Experimental procedures were approved by the local animal ethics committee (Ministerium für Landwirtschaft, Umwelt und ländliche Räume, Kiel, Germany).

For investigation of the influence of microbiota during DMF therapy in EAE as well as during investigation of how diet modulates the sensitivity of neutrophils to MMF stimulation, C57BL/6N wild-type mice were derived from Charles River Europe. Mice were fed with a diet rich in fiber (35 % fiber, Cat. C1000 modified, #100213, Altromin), a diet rich in fat (30 % fat, Cat. C1000 modified, #100212, Altromin) and standard laboratory chow (18 % Fat, 27 % Protein, 55 % Carbohydrates, Cat. #1314M, Altromin) *ad libitum*.

To study the changes in *Hca2* expression in EAE on different diets, the *Hca2*^{mRFP} mouse line was used (Hanson et al., 2010) and fed with a diet rich in fiber and a diet rich in fat *ad libitum.*

To explore the effects of HCA_2 function, the *Hca2*$^{-/-}$ mouse line was used (Hanson et al., 2010), and compared to C57BL/6NCtrl wild-type mice that were ordered from Charles River Europe. Mice were fed with a diet rich in fiber (35 % fiber, Cat. C1000 modified, #100213, Altronim) *ad libitum*.

For the conditional knockout of *Hca2* in neutrophils, we generated *Ly6G-Cre*; *Hca2*$^{Fl/Fl}$ mice (Hasenberg et al., 2015).

To examine the role of the influence of the diet on neutrophils sensitivity to MMF stimulation, animals were fed with high-fiber diet (HFbD), lauric-acid-rich diet (LAD) and normal chow (NCD) for 4 weeks. The animals' weight was checked twice per week,

unless stated differently. After the dietary intervention, mice were terminated by the decapitation under isoflurane anesthesia. The bone marrow was collected from murine tibia and femur and within the same day, neutrophils were isolated and prepared for further investigation.

3.1.2. EAE experiments

3.1.2.1. EAE induction

Prior to EAE induction, mice were acclimated in the animal facility for at least 10 days. Because stress greatly influence EAE development, on the day of injection, mice were gently handled and were treated without the anesthesia. To induce EAE, mice were immunized with ready-to-use pre-filled syringes with an emulsion of MOG_{35-55} with complete Freund's adjuvant (CFA) (Kit information; stored and used as indicated by manufacturer at 4 °C). The administration of the emulsion was performed by subcutaneous injections at two sites with a total volume of 200 µl, upper and lower back with a volume of 100 µL per site. After 2 hours of waiting, mice were injected with the first intraperitoneal injection of pertussin toxin (PTX) diluted with ice-cold PBS in a dosage of 100 ng /100 µL per mouse. This step was repeated 24 hours later. PTX solution was prepared freshly on each day under sterile conditions and was used within 2 hours after preparation and kept on ice until injected.

3.1.2.2. EAE evaluation

To evaluate neurological symptoms and progression of EAE development, starting on the 7th day post-immunized mice were scored according to the detailed scoring table provided by the Hooke lab (Table 2):

Score	Clinical observation
0.0	**No obvious changes in motor function compared to non-immunized mice**. When picked up by base of tail, the tail has tension and is erect. Hind legs are spread apart. When the mouse is walking, there is no gait or head tilting.
0.5	**Tip of tail is limp**. When picked up by base of tail, the tail has tension except for the tip. Muscle straining is felt in the tail, while the tail continues to move.

1.0	**Limp tail**. When picked up by base of tail, instead of being erect, the whole tail drapes over finger. Hind legs are usually spread apart. No signs of tail movement are observed.
1.5	**Limp tail and hind leg inhibition**. When picked up by base of tail, the whole tail drapes over finger. When the mouse is dropped on a wire rack, at least one hind leg falls through consistently. Walking is very slightly wobbly.
2.0	**Limp tail and weakness of hind legs**. When picked up by base of tail, the legs are not spread apart but held closer together. When the mouse is observed walking, it has a clearly apparent wobbly walk. One foot may have toes dragging, but the other leg has no apparent inhibitions of movement. Mouse appears to be at score 0.0, but there are obvious signs of head tilting when the walk is observed. The balance is poor.
2.5	**Limp tail and dragging of hind legs**. Both hind legs have some movement, but both are dragging at the feet (mouse trips on hind feet). No movement in one leg/completely dragging one leg, but movement in the other leg. EAE severity appears mild when picked up (as score 0.0-1.5), but there is a strong head tilt that causes the mouse to occasionally fall over.
3.0	**Limp tail and complete paralysis of hind legs (most common)**. Limp tail and almost complete paralysis of hind legs. One or both hind legs are able to paddle, but neither hind leg is able to move forward of the hind hip. Limp tail with paralysis of one front and one hind leg. In addition, all of: severe head tilting, walking only along the edges of the cage, pushing against the cage wall, and spinning when picked up by base of tail.
3.5	**Limp tail and complete paralysis of hind legs**. In addition: mouse is moving around the cage, but when placed on its side, is unable to right itself. Hind legs are together on one side of body. Mouse is moving around the cage, but the hind quarters are flat like a pancake, giving the appearance of a hump in the front quarters of the mouse.
4.0	**Humane point**. Mice should be terminated

Table 2**: **EAE scoring guideline.

Animals were evaluated according to a 4-point scale (adapted from Hooke's lab protocol) during a 4-week experiment. When a mouse's symptoms were rated between 0 and 2, the symptoms could be described as mild. Conversely, when the mice were scored between 2.5 and 3.5, the symptoms could be described as acute. When the mouse reached a score of 4, it was killed humanely.

To obtain a reliable scoring and avoid any bias, mice were scored blind to the treatment and the genotype.

During EAE development, most of the mice showed initial neurological signs of disease between 9 and 14 days. However, individual mice had a different course of EAE depended on the genotype, treatment, or sex. On occurrence of the first symptoms food and so-called "gel pads" (0.5 % agarose mixed with water) were placed on the cage floor. During the worsening period of the disease progression, additionally a mash of food and water was prepared placed on the cage floor to help mice eat.

3.1.2.3. Body weight measurements

In EAE development, changes in the body weight reflected the disease progression and severity. During the ongoing experiment mice were weight every day in the morning. Weight loss of more than 10 % of initial body weight was supported with subcutaneous injections of 0.9 % sodium chloride (NaCl) (10 µl/g) twice per day every 12 hours. The injections were given until mice gained enough weight to reach a value of below 10 % weight loss.

3.1.2.4. Treatment of side effects due to EAE induction

Expected side effect of EAE induction that were developed by all mice include obvious bumps of emulsion at the site of the injection approximately 2- 4 days after induction. These bumps retained until the termination on day 28 post-immunization (pi) and do not require any treatment. Another common side effect (approximately 10-40 % of mice) is the development of small ulcers (5 mm or less in diameter) at the injection sites causing an emulsion leaking. The ulcers were carefully treated with Betaisodona twice per day, every 12 hours during oral dimethyl fumarate (DMF) treatment by gavaging (see paragraph 3.1.2.5.). Within a few days ulcers were healed, and scars were formed. The development of these side effects did not influence the EAE development.

3.1.2.5. DMF preparation

To administer DMF, first suspension of 0.8 % methyl cellulose (Methocel) solution had to be prepared. The measured amount of powder was added to a 1/3 of the total volume, pre-heated (80 ^{o}C) water and was continuously stirred until the mixture was evenly dispersed. The remaining water (2/3 of the total volume) was kept on ice and was combined with the mixture subsequently. The solution was then stirring on the heater for another 30 min until it became a clear solution. Afterwards, the Methocel solution was stored at 4 ^{o}C.

DMF had to be prepared freshly every day with a concentration of 5 mg/mL. DMF (about 0.5 g) was added to a mortar bowl and was suspended in a small amount of methocel solution (0.5 mL of the total volume). The mixture was grinded until it became a cloudy and viscous solution and transferred into a 50 mL Falcon tube. Remaining DMF suspension in the mortar was rinsed by the rest of the methocel into the falcon tube and properly mixed together by using vortex. Since DMF easily settles down over the time, the suspension had to be stored on the roller at 4 ^{o}C during the gavage.

From day 3 pi onwards, mice are given DMF (50 mg/kg body weight) or vehicle (Methocel) orally by gavage every 12 hours. The treatment lasted until the termination day of the ongoing experiment.

3.1.3. Perfusion of mice and organ collection

Before perfusion, the mice received an i.p. injection of Ketamine/Xylazine anesthetic solution (Ketamine 100-120 mg/kg, Xylazine 10-24 mg/kg in 0.9 % NaCl) followed by the assessment of the pedal reflex (firm toe pinch) and if necessary, administration of an additional dose of anesthetic. Afterwards, the chest of the mouse was opened, and the perfusion needle was inserted into the left ventricle of the heart while the right atrium was cut.

Mice were perfused with 20 ml Ringer's solution with 10 U/mL heparin followed by the organ collection. Carefully, the small intestine was cut, and gently cleared out of the remaining feces by flushing them out with Ringer's solution. Then, the gut was transferred into a 2 mL Eppendorf tube and snap frozen in the liquid nitrogen (N_2). After decapitation,

the brain was gently dissected from the skull and placed on dry ice. Lastly, by using fine scissors, the spinal cord was removed and transferred to dry ice. All collected organs were stored at -80 °C.

3.1.4. Ussing chamber

The Ussing chamber was used to investigate changes in the permeability of ions such as Na^+, Cl^- and K^+ across the intestinal mucosa caused by the administration of 10 µM nicotinic acid (NA) or 100 µM monomethyl fumarate (MMF). For the experiments, C57Bl/6 mice were sacrificed and the distal colon and parts of the small intestine, including the duodenum, jejunum, ileum were dissected and stripped of mucosa. The freshly prepared samples were mounted into the removable insert and placed into the chamber. Subsequently, the tissue was perfused with a solution containing 145 NaCl, 0.4 KH_2PO_4, 1.6 K_2HPO_4, 5 glucose, 1 $MgCl_2$, 1.3 Ca-gluconate [mM]. The pH of the solution was 7.4 and the temperature was kept at 37 °C. On the basolateral side of the tissue, 200 µM forskolin (FSK) and 100 µM carbachol (CCH) were applied as stimuli of cAMP and Ca^{2+} levels. Under control conditions and after stimulation, the transepithelial voltage (V_{te}) was measured in the open-circuit voltage mode. To calculate the transepithelial resistance (R_{te}), short current pulses were applied and according to Ohm's law, the equivalent short-circuit current (I'_{sc}) was calculated as V_{te}/R_{te}. Additionally, in the distal colon, on the luminal side of the tissue, amiloride was applied to distinguish reabsorpative currents caused by its inhibitory effect on ENaC channels.

3.1.5. FACS measurement

Prior to the blood collection, to prevent the blood from clotting, syringes were filled with 200 µL of 0.5 mM EDTA. First, the animal was deeply anaesthetized via intraperitoneal injection of Ketamine/Xylazine (Ketamine 120 mg/kg, Xylazine 24 mg/kg in 0.9 % NaCl), followed by a right ventricle puncture of the heart and drawing blood volume between 700 and 1000 µL per animal. The blood samples were transferred into 15 mL falcon tube and placed on ice. Then, to remove the erythrocytes, the erythrocytes lysis (EL) buffer was added, gently mixed, and incubated for 5 min at room temperature (RT). To stop the lysis reaction, 10 mL of PBS were added, followed by centrifugation for 5 min at 400 g at 4 °C. This step was repeated twice. After the second lysis, the supernatant was removed, and

the cell pellet was resuspended in FACS buffer (0.5 % bovine serum albumin (BSA) in PBS). To avoid non-specific binding of immunoglobulins to the Fc receptor, the cell suspensions were incubated with Fc-block (Anti-Mouse CD16/CD32, 1:100) for 15 minutes at 4 °C in the dark. The reaction was stopped by adding FACS buffer and the samples were centrifuged for 5 min at 400 g at RT. The supernatant was aspirated, and cells were resuspended in FACS buffer and subsequently incubated with viability dye (eBioscience Fixable Viability Dye eFluor™ 780, 1:2000) for 10 minutes at 4 °C in the dark. By adding 1 volume of FACS buffer to the sample, the incubation was stopped, and centrifugation was performed. Following the procedure, samples were incubated with an antibody cocktail (Table 3) for 20 minutes at 4 °C and in the dark.

Antibody name	Final concentration	Catalog number	Supplier
Brilliant Violet 650 anti-mouse/human CD11b	2 µg/ml	101239	BioLegend
Brilliant Violet 510 anti-mouse CD45	2 µg/ml	103138	BioLegend
PerCP/Cyanine 5.5 anti-mouse Ly-6G	2 µg/ml	127616	BioLegend
PE/Cyanine 7 anti-mouse Ly-6C	0.1 µg/ml	128018	BioLegend
FITC anti-mouse CD3ε	2 µg/ml	100326	BioLegend

Table 3: Antibody cocktail for FACS measurement.

To distinguish between cell populations in the blood, samples were incubated with a cocktail of antibodies to allow subsequent counting and analysis of the cell populations of interest.

Cells were washed with FACS buffer, centrifuged, and resuspended in 400 µL FACS buffer. Samples were ready for measurement by the Cytek Aurora placed in CAnaCore. Gating and quantification were performed using the FlowJo 10.9.0 software.

3.2. Cultivation of bEND.3 cells

The commercially available cell line bEND.3 was used. The cells were cultivated in DMEM supplied with 10 % fetal calf serum (FCS) and 1 % Penicillin/Streptomycin at 37 °C in a T75 culture flask. When cells reached a confluence of approximately 90 %, they were trypsinized and resuspended at 120 000 cells/mL. Subsequently, 40 000 cells were plated into a 48-well plate and incubated until they became 100 % confluent. When the bEND.3 cells were ready for the treatment, they were washed once with pre-warmed PBS buffer followed adding fresh medium. Each bEND.3 cell monolayer was stimulated with 10 ng/mL TNF for 6 hours at 37 °C prior to the neutrophils binding assay.

3.3. Neutrophil analysis

3.3.1. Neutrophil isolation

Neutrophils were isolated from the bone marrow (flushed from the murine tibia and femur). First, mice were anaesthetized with isoflurane and sacrifice by decapitation. In order to get a single cell suspension, the bone marrow was passed through a 23-gauge needle and the cells were centrifuged for 10 min at 1500 rpm and 4 °C. By using a Percoll gradient with a density of 52, 69 and 78 %, neutrophils were centrifuged using an ultracentrifuge for 30 min at 2000 g at RT. The cells were collected from the layer of 69/78 and 78 % and purified from remaining erythrocytes by adding erythrocytes lysis (EL) buffer. After 2 minutes, incubation was stopped by adding 10 mL HBSS buffer. The cells were centrifuged for 10 minutes at 350 g at RT and afterwards, the supernatant was discarded. The cell pellet was resuspended in 1 mL HEPES buffer and used within the same day. The neutrophil's purity (< 90 %) was assessed by multiple histological techniques: Wright-Giemsa and Hematoxylin & Eosin (H&E) staining, along with FACS measurement.

3.3.1.1. Neutrophil's purity evaluation

3.3.1.1.1. CytoSpin

To perform CytoSpin, the 6-places swing-out rotor in the UNIVERSAL 320 R centrifuge was used and prior to the centrifugation, a complete cyto-insert had to assemble. For that purpose, a filter card no. 1696 together with the Polysine slide was placed into the cyto-

slide carrier. Then, on top, the 1 mL one-funnel chamber was inserted and secured by the clamping ring. This prepared cyto-insert was placed into the bucket and into the rotor. Prior to the spinning down, cells with the dilution ratio at the ratio of 1:40 were prepared in 200 µL of HBSS buffer. Subsequently, the cell suspension was loaded into the chambers and centrifuged for 5 min at 1000 rpm at RT. Next, the cyto-insert was disassembled, and the slide dried at RT until there was no remaining liquid.

3.3.1.1.2. Wright – Giemsa staining

After drying, the slides were placed into the staining cuvette filled with Wright – Giemsa dye for 1 min followed by the washing in water for 1 min. The slides dried at RT as long until there was no remaining liquid and sealed with coverslip using the Eukitt mounting medium.

3.3.1.1.3. Hematoxylin & Eosin staining

After the cells were spun down by CytoSpin, they were fixed in ice-cold methanol for 5 min. The slides were incubated in hematoxylin for 1 min and washed under running tap water for 1 min followed by an incubation in eosin for 30 sec. Subsequently, the slides were incubated in 95 % followed by 100 % ethanol for 1 min each. The last step was an incubation in Xylene for 2 min and afterwards cells were sealing with a coverslip using the Eukitt mounting medium.

3.3.1.1.4. FACS measurement

For FACS measurement, neutrophils were centrifuged down for 5 min at 1500 rpm at RT, and the supernatant was discarded. The cell pellet was resuspended in 400 µL of FACS buffer (0.5 % bovine serum albumin (BSA) in PBS). In order to avoid non-specific binding, cells were incubated with Fc-block (Anti-Mouse CD16/CD32, 1:100) for 10 min at 4 ^{o}C, in the dark, without shaking. To stop the reaction, 1 volume of FACS buffer was added and cells were spun down. After aspiration of the supernatant, the cells were incubated in an antibody cocktail: CD11b (1:100) and Ly6-G (1:100), in 300 µL of FACS buffer for 30 min at 4 ^{o}C, in the dark, without shaking. Subsequently, 1 volume of FACS buffer was added and cells were spun down followed by the supernatant aspiration and resuspension of the cells in 400 µL of FACS buffer.

3.3.2. Neutrophil biology assays

3.3.2.1. Adhesion Assay

3.3.2.1.1. Neutrophil's preparation

After the isolation of neutrophils from the bone marrow and cell counting, in total, 8 x 10^6 cells were prepared for each mouse in phenol-free RPMI-1640 medium. Following this procedure, a cell concentration of 4 x 10^6 cells/mL was labeled with 3 µM Calcein AM for 30 min at 37 °C. To stop the reaction, 10 mL of PBS was added, and cells were spun down for 5 min at 450 g at RT. Then, the cell pellet was resuspended to the concentration of 4 x 10^6 cells/mL and subsequently divided into two conditions: one group was treated with 200 µM MMF and the second group was treated with the respective vehicle (Methocel) for 30 min at 37 °C. Afterwards, the cells were washed once with medium, centrifuged, and resuspended to the concentration of 2 x 10^6 cells/mL in phenol-free RPMI-1640 medium in separate vials for each condition.

3.3.2.1.2. Neutrophil's binding assay

After bEND.3 cells were incubated for 6 hours of with 10 ng/mL TNF, the cells were washed three times with filter-sterilized phenol-free RPMI-1640 medium containing 3 % BSA. After the last washing step, medium was aspirated, and 5 x 10^5 neutrophils were added to each well. After 20 min at 37 °C, the fluorescence intensity was measured by the Plate reader followed by gentle washing with PBS supplied with Mg^{2+} and Ca^{2+} and carful aspiration of the remaining liquid. Medium was added and again, the fluorescence intensity was measured by the Plate Reader. Afterwards, cells were fixed with 4 % PFA and stored in the dark at 4 °C. The absolute number of cells in each condition was calculated by analyzing images taken at the fluorescence microscope.

3.3.2.2. NET formation assay

3.3.2.2.1. Preparation of fibronectin-coated 24-well plate

On the same day prior to the assay, the 24-well plate had to be prepared. To each well, 12 mm cover slips were transferred and incubated with freshly prepared 10 µg/mL fibronectin solution for 30 min at 37 °C. Afterwards, the solution was discarded, and the plate was incubated at 37 °C until used.

3.3.2.2.2. Neutrophil's preparation

After the isolation of neutrophils from the bone marrow from individual mice, and cell counting, 3 x 10^6 cells were suspended, per mouse in phenol-free RPMI-1640 medium. Subsequently, cells were primed with 2 ng/mL TNF for 15 min at 37 °C followed by centrifugation for 5 min at 450 g at RT. The supernatant was discarded, and the cell pellet was resuspended to the concentration of 3 x 10^6 cells/mL in a phenol-free RPMI-1640 medium. Afterwards, cells were divided into three groups (5 x 10^5 neutrophils per group) for further treatment as follows:

1. Neutrophils + 5 µM Sytox Green
2. Neutrophils + 5 µM Sytox Green + 100 nM phorbol 12-myristate 13-acetate (PMA)
3. Neutrophils + 5 µM Sytox Green + 100 nM PMA + 200 µM MMF

Cells of each condition were incubated for 6 hours at 37 °C in the dark. Subsequently, the supernatant was carefully aspirated, and cells were fixed with 4 % PFA for 15 min at RT. The solution was discarded, and cells were gently washed with phenol-free RPMI-1640 medium. Afterwards, the cover slips were mounted on Polysine slides using Dako fluorescence mounting medium. Protected from the light, slides were stored at 4 °C. The assessment of NETosis was performed by the analysis of images taken using the fluorescence microscope.

3.3.2.3. Calcium measurement

On the day prior to the assay, fibronectin-coated cover slips in a 24-well plate were prepared and placed at 37 °C until used. First, between 8 and 12 x 10^6 neutrophils were isolated from murine bone marrow and suspended in RPMI 1640 medium supplemented with L-glutamine, 2.32 g/L sodium bicarbonate, 1 % penicillin/streptomycin and 10 % FBS. Then, approximately 2 x 10^5 cells were plated into one well and incubated for 3 hours at 37 °C. Afterwards, the supernatant was carefully discarded, and cells were loaded with 2 µM Fluo-4 with 0.5 % DMSO and 0.05 % Pluronic™ F-127 in artificial cerebrospinal fluid (aCSF, 130 mM NaCl, 26.5 mM $NaHCO_3$, 1.25 mM NaH_2PO_4, 3 mM KCL, 2 mM $CaCL_2$, 2 mM $MgCL_4$, 10 mM D-glucose) for 30 min at 37 °C. This step was followed by the aspiration of the dye solution and incubation with 2.5 mM Probenecid in aCSF for another

30 min at 37 °C. To detect changes in $[Ca^{2+}]_i$ in response to nicotinic acid (NA) or MMF, and investigate whether it is HCA_2-dependet, neutrophils were placed in the flow chamber and measured using a high-speed calcium imaging setup (Till Photonics) mounted on the Axio Examiner D1 upright fluorescent microscope (Zeiss) coupled to the polychrome V monochromator and a high-speed CCD camera (Retiga EXi-blue, QImaging). Data acquisition and quantification was done using life acquisition and offline analysis software. In the first minute of the experiment, cells were in the measurement buffer (aCSF, 5 % CO_2, 95 % O_2, 7.4 pH, flow rate of 2 ml min^{-1}) and then the stimuli: 100 μM NA or 100 μM MMF were applied for 60 seconds followed by the recovery in the measurement buffer for another 3 minutes. 100 μM fMLP was used as a positive control.

3.4. Microbiota study

3.4.1. Feces collection

During the EAE experiment, feces were collected at three different time points for each mouse: one day before diet change (14 days prior to the immunization), one day before immunization and one day before termination. For that purpose, an autoclaved and empty cage was used. Prior to the collection, 2 mL Eppendorf tubes were sterilized and labeled. Each autoclaved cage was used for one group housed cage of mice to avoid a cage effect. An individual animal was placed in the cage and was allowed to defecate without any stress factors. The feces were collected and snap frozen in N_2. The cage was cleaned with 70 % ethanol after each mouse from the same group of mice and afterwards one group housed cage was tested, changed to a new autoclaved cage. The collected feces were stored at -80 ˚C.

3.4.2. Sequencing

The first step in the preparation of the feces samples for sequencing was a DNA extraction by using a MO Bio Power Soil DNA Isolation KIT. The feces samples were placed to the Power Bead Tubes and pre-heated Solution C1 together with Proteinase K were added followed by the briefly vortexed. After 30 min incubation samples were homogenized for 30 min at 50 ˚C using the SpeedMill and centrifuged for 30 sec at 10 000 g at RT (except for the length of time, in all steps, conditions of centrifugation are the same). Carefully, the supernatant was collected and transferred into a clean 2 mL

Collection Tube. Solution C2 was added, and the samples incubated for 10 min at 4 °C. After centrifugation for 2 min, the supernatant was transferred to the new 2 mL collection Tube and solution C3 was added, and the step was repeated. Afterwards, the supernatant together with solution C4 was loaded onto the Spin filter and centrifuged for 1 min and the step was repeated twice followed by adding solution C5 and subsequent centrifugation for 30 sec. Finally, in the last step by adding solution C6, DNA was collected and stored at -20 °C until used. Afterwards, the samples were prepared for the PCR reaction. Prior to the PCR run, the samples were diluted at a ratio of 1:10 and combined with the Master Mix (Table 4). Then, 4 µL of the according reverse and forward primers were added to the sample well. The same step was performed for the control wells, including Mock community with known bacteria composition serving as a positive control, the water control, and the primer control.

Master Mix	**µL/well**
H_2O	10.25
5x Buffer	5
dNTP's 10mM	0.5
Phusion Taq II	0.25
DNA	1
Total	16µL + 1 µL DNA

***Table 4: Master Mix composition**.*

The diluted samples were combined with the Master Mix necessary for a successful PCR reaction.

Afterwards, the PCR plate was sealed and spun down followed by the PCR run (Table 5).

CYCLE STEP	TEMP, TIME	CYCLES
Initialization	98°C, 30 sec	1
Denaturation	98 °C, 9 sec	30
Annealing	55 °C, 30 sec	
Elongation	72 °C, 45 sec	
Final Elongation	72 °C, 10 min	1
Final hold	4 °C, ∞	

Table 5: PCR program.

The PCR run begins with initialization and proceeds through the steps of denaturation, annealing and elongation (the colored area indicates the repeated steps). The entire process ends with final elongation.

The products of the PCR run were evaluated by gel electrophoresis on 1.5 % agarose gel. The electrophoresis was running for 5 min at 120V followed by 70 min at 110V and the quantification of the PCR bands was performed by using the image software Quantum Capt.v16.04. As the internal standard for the band intensity, the measurement marker was used with a known concentration of DNA (1 µL marker = 0.5 µg DNA – 500 bp marker lane = 80 ng). According to the calculation, each sample was expected to contain 80 ng DNA. From each PCR plate, subpools were created and then purified by using GeneJET NGS Cleanup Kit. The purification procedure started by adding 5 volumes of Binding Buffer to 1 volume of DNA fragments sample and 1 volume of 100 % ethanol followed by mixing. The mixture was transferred into the DNA Purification Micro Colum and centrifuged for 30 sec at 10 000 g at RT. Following the washing steps by adding Prewash Buffer and Wash Buffer, respectively. Then, the empty DNA Purification Micro Colum was placed in a clean 1.5 mL Eppendorf tube and 40 µL of DNA was eluted and stored at -20 °C. Quantitive PCR (qPCR) was performed by using NEBNext® Library Quant Kit for Illumina®. Prior to the qPCR run, the subpools were diluted at the ratio of 1:100000 and then, 16 µL of NEBNext Library quant Primer Mix (with primers) was added to 4 µL of

DNA. Afterwards, the PCR plate was sealed and spun down, followed by the qPCR run (Table 6).

CYCLE STEP	TEMP, TIME	CYCLES
Initialization	95 °C, 1 min	1
Denaturation	95 °C, 15 sec	35
Elongation	63 °C, 45 sec	
Final hold	4 °C, ∞	

Table 6: qPCR program.

The qPCR run begins with initialization and proceeds through the steps of denaturation and elongation (the colored area indicates the repeated steps). The entire process ends with final elongation.

Based the obtained data, I calculated the amount of each subpool which had to be collected into the one final library followed by its purification by using MagSi-NGS^{PREP}-PLUS beads. Prior to the purification process, fresh 75 % ethanol had to be prepared, and the Agencourt AMPure XP bottle had to equilibrate to RT for 30 min. Additionally, before usage, it was vigorously shaken to resuspend any magnetic particles. Then, 1.8 volume of beads was added to the sample and mixed by pipetting. After 10 min incubation at RT, the reaction plate was placed onto an AgencourtSPRI Plate 96 Super Magnet Plate for 2 min to separate beads from the solution. Subsequently, the supernatant was discarded, and the beads were washed twice in 75 % ethanol followed by the incubation for 5 min at RT. The reaction plate was removed from the magnetic plate and the elution buffer was added. After 2 min of incubation at RT, the plate was placed onto the magnetic plate again to separate the beads and collect the eluate into a new autoclaved 1.5 mL Eppendorf tube. The samples were stored at -20 °C. The concentration the prepared and purified library was checked by using Qubit Fluorometer. At first, the library was diluted at the ratio of 1:200 in working solution, and additionally, standard 1 and 2 were prepared. After Qubit measurement, the library size was assessed using a Bioanalyzer and diluted to the concentration of 4 nM DNA. Subsequently, by using the MiSeq Reagent Kit v3, the DNA was denatured into single strands followed by the dilution of the library to the final

concentration of 10 pM by adding pre-heated HT1 buffer. Following the procedure, the same steps were performed to prepare a 10 pM PhiX library as a reliable control for the Illumina sequencing run. Then, the denatured sample library was spiked with 10 % PhiX control and loaded onto the chip together with the following primers: combined 27F Primer and 10 % read1primer Mix, Index Primer and 338R Primer. The chip was inserted into the cartridge and the sequencing run started. The set up was fixed for 302 reads.

3.5. Histological staining

3.5.1. PFA fixation of vibratome sections

Each mouse was perfused with 10 mL of Ringer's solution with 10 U/ mL heparin followed by the perfusion with 10 mL of 4 % paraformaldehyde (PFA). From each mouse, organs were collected as follows: aorta, brain, brown adipose tissue (BAT), cochlea, colon, eye, gall bladder, heart, kidney, lung, liver, pancreas, skin, skeletal muscle, small intestine, spinal cord, spleen, stomach. Organs were postfixed with 4 % PFA overnight at 4 °C. Afterwards, the PFA solution was discarded, and organs were stored in PBS with 0.02 % sodium azide (NaN_3, as an antibacterial agent) at 4 °C until staining.

3.5.2. Immunohistological staining on free-floating sections

To perform immunohistochemistry staining, organs were sectioned. Firstly, organs were embedded in 4 % low melt agarose and then, glued to the specimen plate that was inserted into the vibratome tray filled with PBS. The razor blade was carefully adjusted. Organs sections with the thickness of 50 µm and a speed between 0.2 - 0.5 mm/s according to the organ. Free floating sections were stored in PBS with 0.02 % NaN_3 in 48-well plates covered with aluminum foil at 4 °C. Prior to the staining procedure, sections were washed one time in TRIS buffered saline (TBS) for 5 min at RT followed by washing twice in TBS with 0.3% Triton-x 100 (TBS-Tx) for 5 min at RT. Then, the washing solution was discarded, and sections were incubated in a blocking buffer (5 % BSA in TBS-Tx) for 2 hours at RT. Following the procedure, the blocking solution was exchanged against the primary antibody, anti-mRFP (1:500) in a blocking buffer incubated over night at 4 °C. Subsequently, sections were washed three times in TBS-Tx for 5 min at RT followed by Alexa488-conjugated secondary donkey anti-rat antibodies (1:500) and with DAPI (1 µg/ml) at RT for 2 hours. After three times washing in TBS-Tx for 5 min at RT, sections

were mounted on SUPERFROST slides and sealed with coverslips using Mowiol with DABCO fluorescent mounting medium. Protected from the light, slides were stored at 4 °C, and then analyzed using a confocal microscope.

3.6. Imaging and image analysis

3.6.1. Fluorescence microscopy

A Leica DMI6000 B fluorescence microscope equipped with a DFC360FX camera was used for imaging, using LAS software to adjust the appropriate image settings. For qualitative tile scans a 10x objective was used by utilizing the filter cube: L5 according to the Alexa488 fluorochrome respectively.

3.6.1.1. Adhesion assay

All wells were analyzed by using the ImageJ software. A macro was created to calculate the number of cells attached to bEND.3 cells. Subsequently, the statistical analysis was performed using GraphPad Prism.

3.6.1.2. NET formation assay

The entire sample was analyzed using ImageJ. In order to quantify the area of NET formation, a macro was created that calculated the entire area encompassing the NETs, the number of cells and the corresponding cell area. The cell area was then subtracted leaving only the area of NETs presented in mm^2.

3.6.2. Confocal microscopy

3.6.2.1. HCA_2 expression in mouse organs

After immunohistochemical staining, the organs were sectioned and mounted on slides. Images were then taken using a Stellaris 5 confocal microscope. To achieve optimal pixel saturation of the organs and cells of interest, laser intensity and gain settings were adjusted. As well as the emission and excitation spectra of the fluorochromes. The images were prepared in ImageJ software.

3.7. Genotyping gDNA extraction

The tail biopsies were collected and placed into 1.5 mL tube and incubated with the lysis buffer overnight at 56 °C. The following day, the samples were shortly mixed and spun

down for 3 min at 16 000 g at RT. Subsequently, the supernatant was transferred into the new 1.5 mL tube and incubated for 10 min at 4 °C followed by the addition of ice-cold absolute ethanol. The samples were gently mixed 6-8 times and centrifuged for 8 min at 14 000 g at 4 °C. The supernatant was discarded, and the cell pellet was washed with 70% ethanol and again spun down for 8 min at 14 000 g at 4 °C. The remaining supernatant was aspirated, and the cell pellet was dried for 10 min at 56 °C. Afterwards, the cell pellet was resuspended in 200 µL aqua bidest.

4. Results

4.1. DMF treatment contribute to the adverse effects

DMF is rapidly converted to its active metabolite MMF, which is HCA_2 receptor agonists. Numerous studies have demonstrated a therapeutic effect of MMF in the treatment of MS. HCA_2 mediates not only neuroprotective effects but has also adverse drug reactions (ADRs) that range from mild to moderate and more severe. Among the most common adverse symptoms are flushing, gastrointestinal disorders, such as severe diarrhea, vomiting, nausea, abdominal pain, as well as lymphopenia (Dubrall et al., 2021). In addition to DMF and MMF, nicotinic acid (NA), known for its anti-lipidemic effects, is another HCA_2 receptor agonist with beneficial effects accompanied by side effects.

In order to detect the expression of HCA_2 in organs that might be affected by the ADRs of DMF and NA, the reporter mouse line *Hca2*^{mRFP} that expresses the mRFP reporter under the control of the *Hca2* locus was used (Hanson et al., 2010) (Figure 8a). Analysis of fluorescence microscope images was performed in selected organs collected from the *Hca2*^{mRFP} reporter mice. Wild-type (WT) mice served as controls. RFP that served as proxy of HCA_2 expression was detected in spinal cord, lung, small intestine, colon, liver, kidney, spleen, and brown adipose tissue (BAT) of *Hca2*^{mRFP} mice. However, in WT mice *Hca2* was not expressed (Figure 8b).

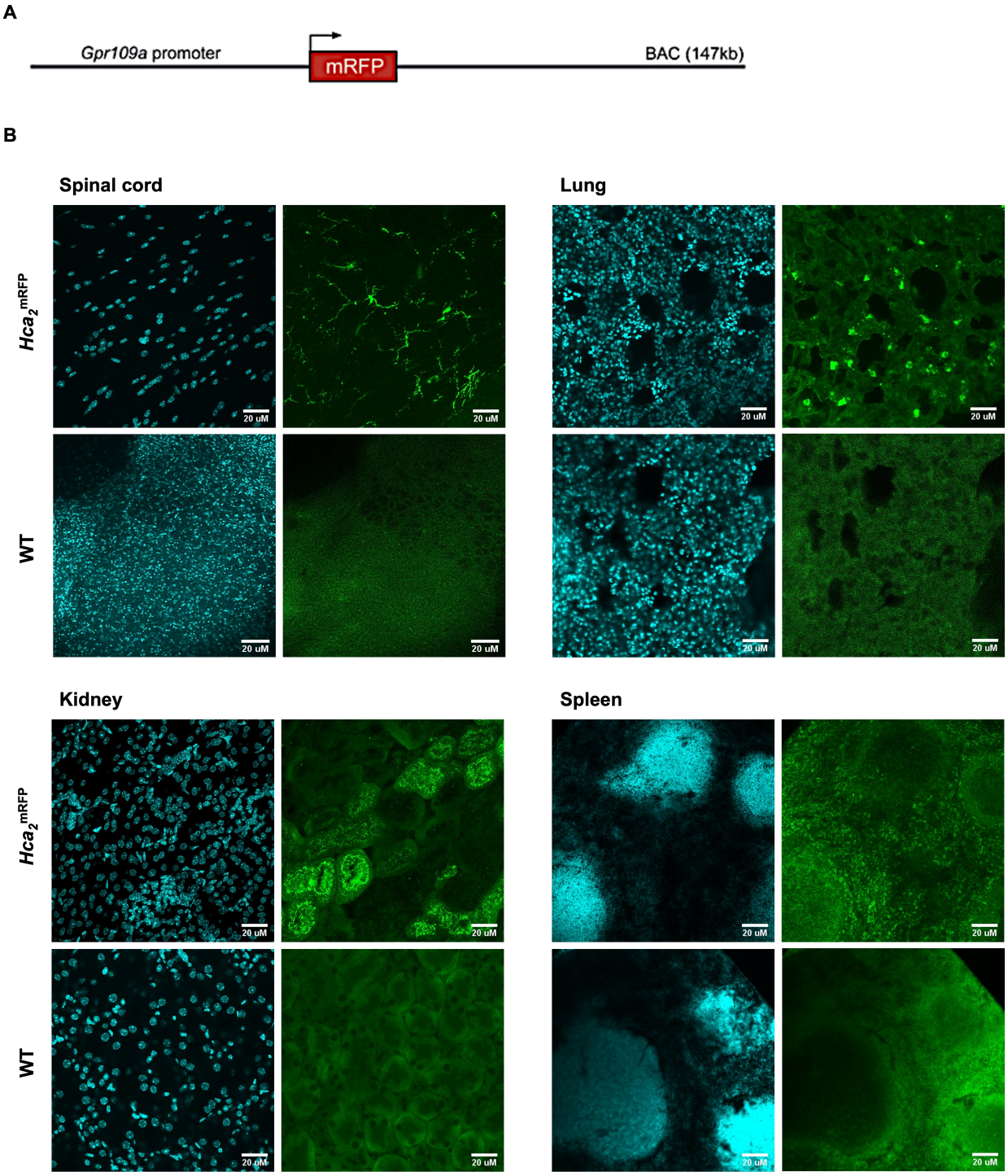
A
Gpr109a promoter
mRFP
BAC (147kb)
B
Spinal cord
Lung
Kidney
Spleen
Hca2mRFP
WT
20 uM

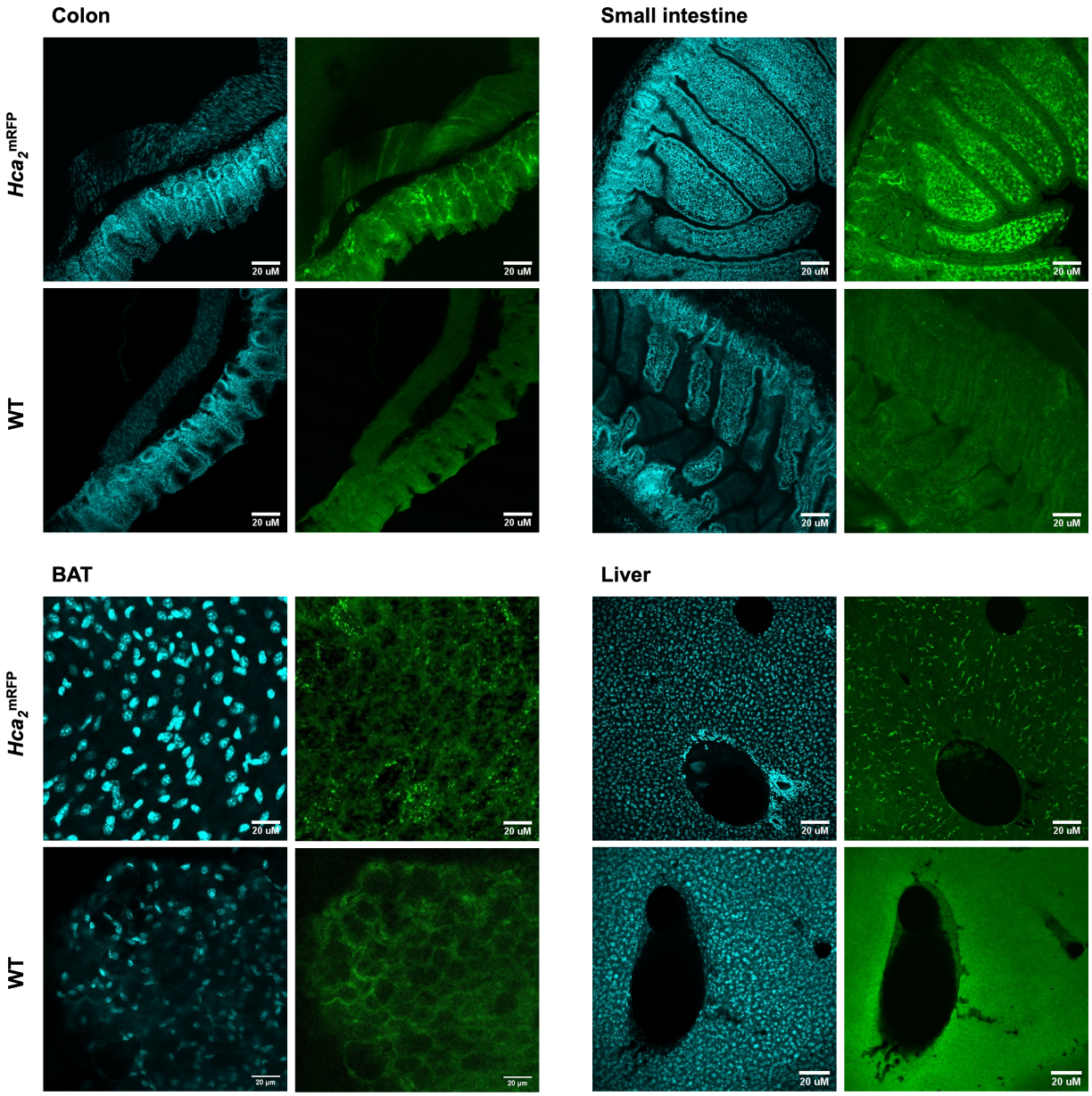

Figure 8: Expression of HCA_2 in selected organs.

(A) Representation of BAC transgene expressing mRFP under the control of Gpr109a gene promotor (Hanson et al., 2010)*.*

(B) Immunostainings of RFP as a reporter of Hca2 expression in the organs collected from Hca2^{mRFP} reporter, and wild-type (WT). Images were obtained by fluorescence microscopy. Blue staining, DAPI, green staining, mRFP reflecting Hca2 expression.

Scale bars, 20 µm.

These findings suggest the involvement of the receptor *Hca2* in possible side effects of NA and DMF treatment, one of the most common of which is diarrhea. In order to

investigate the involvement of HCA_2 in DMF or NA-induced diarrhea further, I used an Ussing chamber (Figure 9a) to evaluate whether the drug treatment might have effect on the electrogenic trans-epithelial transport. The control of keeping the body fluid homeostasis is carried out by the epithelial cells that are joined by junctional proteins, such as the zona occludens (tight junctions), zona adherens, macula adherens, and gap junctions (Saint-Criq & Gray, 2017). Salt and fluid can move through the cell in two ways: between cells (paracellular pathway) or through the cells (transcellular) by absorption and secretion. Absorption is mediated by the uptake of Na^+ via the apically located epithelial Na^+ channel (ENaC). At the same time, efflux is due to the Na^+/K^+-ATPase in the basolateral membrane, resulting in the passive creation of paracellular Cl^- transport. The water uptake is either paracellular or through the aquaporins (Saint-Criq & Gray, 2017). Secretion occurs in the apical membrane via cystic fibrosis transmembrane conductance regulator (CFTR). However, it is reported that numerous other Cl^- channels, such as calcium-activated chloride channels (CaCC), might be involved. On the other hand, the basolateral Cl^- channels, such as Na^+ K^+ $2Cl^-$ cotransporter (NKCC1) and Na^+-bicarbonate cotransporter (NBC), lead to the accumulation of Cl^- within the cells. The driving force for the Na^+ paracellular pathway is created by the active Cl^- secretion, and as for absorption, water transport happens through the paracellular pathway or the aquaporins (Ramalho et al., 2022) (Figure 9b). The occurrence of diarrhea is caused by the secretion of chloride and bicarbonate ions, with the simultaneous secretion of sodium into the intestinal lumen, resulting in the movement of water into the intestines (Cottreau et al., 2012) (Figure 9c).

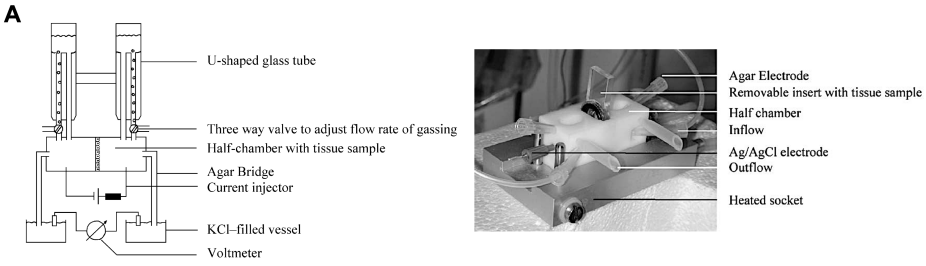

B

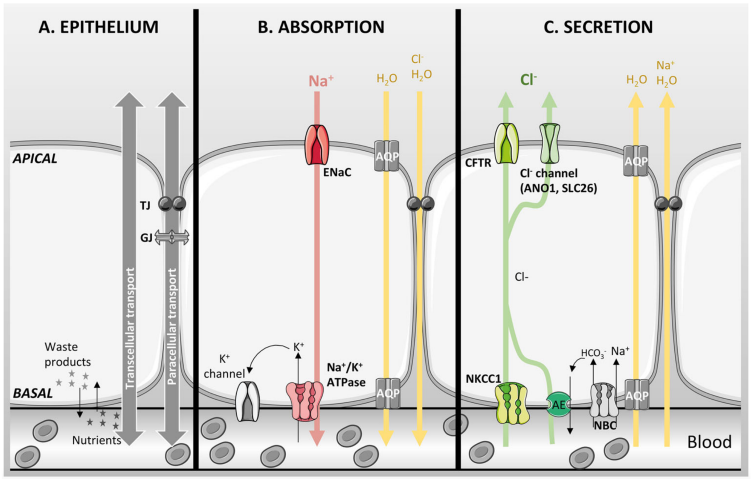

C

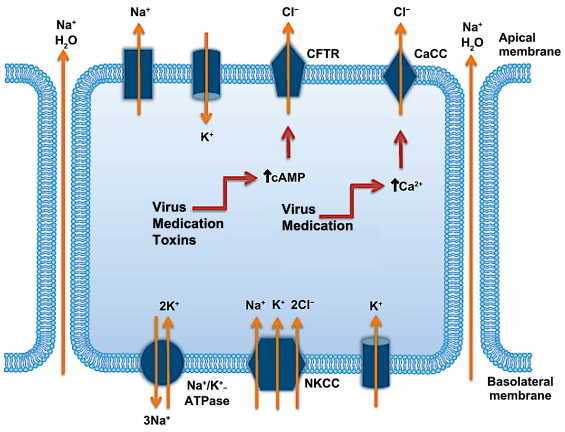

Figure 9: **Fluid *absorption and secretion.***

(A) Representative scheme demonstrating circulating Ussing chamber, which consists of U-shaped tubes, to which experimental substances are added. Tissue samples are placed in the half-chamber connected to the electrical circuity that measures resistance (R), voltage (V) and current (I) (H. Li et al., 2004).

*(B) In epithelium, cells are connected by tight junctions (TJ) and gap junctions (GJ). Salts and fluids are transported via para and transcellular pathways. During absorption an active transport of Na^+ occurs (indicated by **red arrow**) via ENaC on the apical side and Na^+/K^+-ATPase in the basolateral side creating force for passive transport for Cl^- (indicated by **yellow arrow**). During secretion, an active secretion (indicated by **green arrow**) of Cl^- via CFTR and other Cl^- channels is a main driver, that also creates the passive movement of Na^+ and H_2O into the gastrointestinal tracks (GI) (Saint-Criq & Gray, 2017).*

(C) Representation of secretory diarrhea caused by the hyperactivation of Cl^- channels leading to the increase in the secretion of Cl^- and other fluid into the intestinal lumen (adapted from Patel et al., 2013).

In order to understand the possible mechanism of drug-induced diarrhea, I investigated the mucosa in the colon of mice. Firstly, to the increase in cAMP and Ca^{2+} release I applied 200 µM forskolin (FSK) and 100 µM carbachol (CCH) on the basolateral side of the tissue as controls. The chart shows the positive current response to both control stimuli. Subsequently, applying either 10 µM NA or 100 µM MMF did not affect transepithelial transport in the colon. To check whether drugs might affect Na^{+} imbalance on the luminal side of the tissue, I applied amiloride, which acts as an inhibitor of the ENaC channel (Figure 10a). However, the statistical analysis revealed no significant differences in the action of either NA or MMF (Figure 10b). These findings suggest that other mechanisms causing diarrhea might be involved.

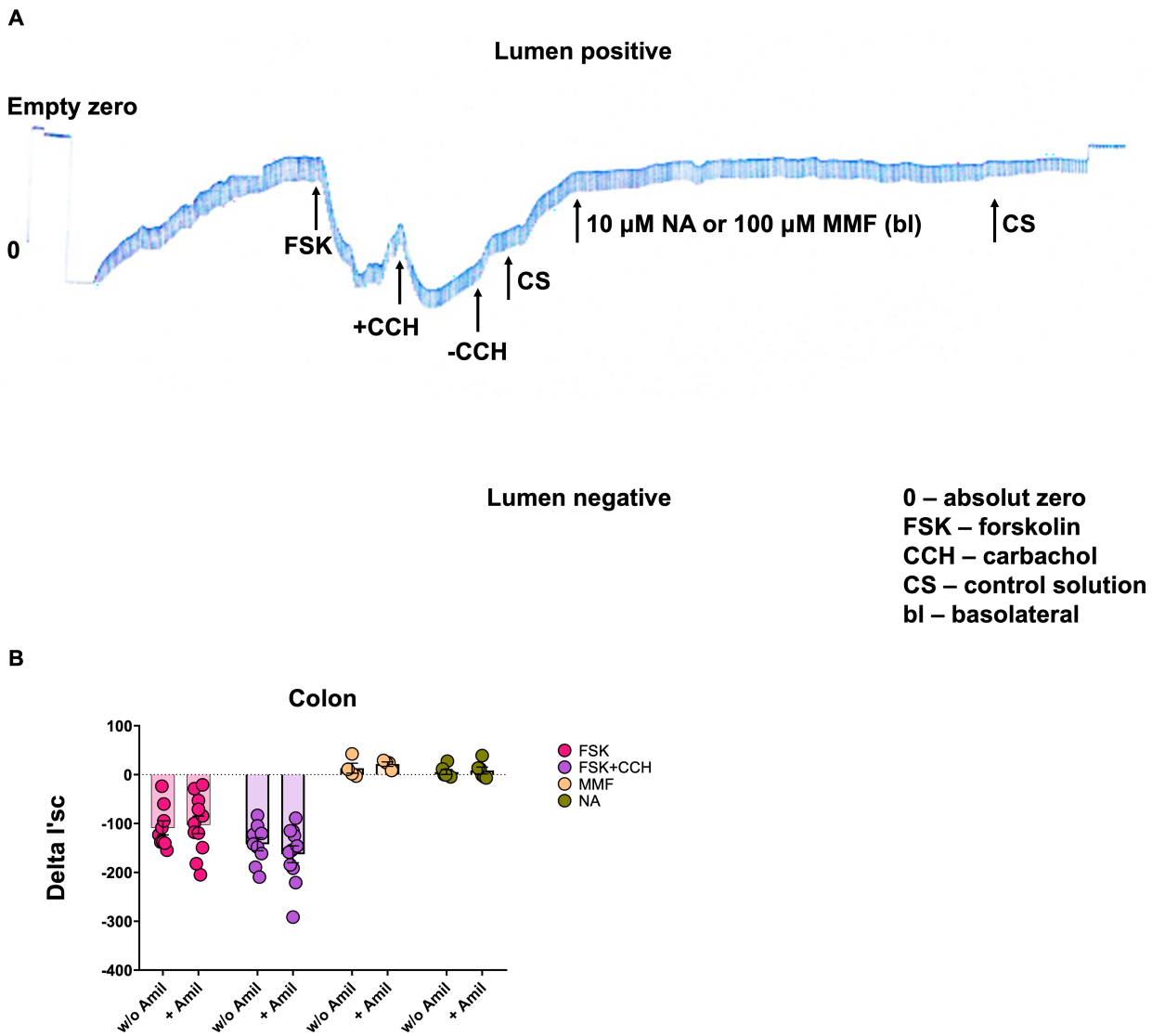

Figure 10: Ussing chamber results of colon tissue stimulated with 100 µM MMF and 10 µM NA.

(A) Graph *showing the reading obtained from the Ussing chamber measurement. Basolateral application of 200 µM forskolin (FSK) and 100 µM carbachol (CCH)* modulated transport. *However, treatment with NA (10 µM) or MMF (100 µM) had no effect, which was later confirmed by* additional experiments.

(B) Statistical analysis of the graph measurement showed no observed effect of NA or MMF on the ion transport in colonic tissue. Additional application of amiloride (Amil) on the lateral side did not result in a difference in drug effect.

4.2. Diet modulates response to DMF treatment

The gastrointestinal microbiota has a vital role in the normal functioning of organisms as well as during diseases. The gut microbiota takes part in the immune system development, as well as in the modulation of the CNS; it is involved in the synthesis and

secretion of essential vitamins, such as vitamin K, nicotinic acid, biotin, or riboflavin, and supports endothelial growth (Chu et al., 2018a). One of the most essential classes of bacteria are the producers of short-chain fatty acids (SCFAs), including butyrate, metabolites are derived from fermented products of indigestible carbohydrates, including dietary fiber (Portincasa et al., 2022). During MS development, a dysbiosis with increases in bacteria has been observed, such as *Methanobrevibacter Akkermansia, Actinobacteria, Bifidobacterium, Streptococcus, Firmicutes, or Ruminococcus,* and decreases in bacteria, including *Butyricimonas, Lachnospiraceae, Ruminococcaceae, Faecalibacterium, Prevotella, Bacteroidaceae.* During DMF treatment, a reshaping of the gut microbiota in MS patients has been observed, suggesting microbiota involvement in a better tolerance and response to the treatment and decreased severity of the disease (Ferri et al., 2023a).

4.2.1. Diet affects neutrophil's function

It has been reported that SCFAs have a positive impact on immune responses, such as enhancement of the production of IL-10 and IL-4, reduction of the adherence of leukocytes to the vascular endothelium, promotion of the remyelination and modulation of the response of cell populations via GPCRs, including HCA_2 (Kasper et al., 2019). One of the cell populations susceptible to modulation by SCFA are neutrophils expressing HCA_2.

4.2.1.1. Measurement of neutrophils adherence by Adhesion Assay

I investigated the effect of diet on neutrophil response to DMF treatment and whether it is HCA_2-dependent. To evaluate this hypothesis, mice were fed 3 different diets: a high fiber diet (HFbD), a lauric acid diet (LAD) - high in fat content (30 %), and a normal chow diet (NCD) as a control diet for 4 weeks each (Figure 11a). Subsequently, the primary neutrophils were collected from the bone marrow of each mouse from each diet. One of the crucial steps in CNS infiltration is the adhesion of neutrophils to activated brain endothelial cells. To investigate this step, an adhesion assay was performed, that consists of two steps. Prior to the first step of the assay almost confluent brain endothelial (bEND.3) cells were incubated with 10 ng/ml TNF. In parallel, 5 x 10^5 neutrophils were labelled with 3 µM Calcein AM and treated either with 200 µM MMF or vehicle for 30

minutes in the presence of carbenoxolone (100 µM) to inhibit calcein efflux through hemichannels. Finally, calcein was measured by Plate Reader. Binding of neutrophils to activated bEND.3 cells occured in the second step (Figure 11b). Fluorescent microscopy images and quantification showed a significant inhibition of neutrophil adherence into the bEND.3 cells in the DMF treated group in comparison to the vehicle treated group in the HFbD mouse group, while I did not find this effect of MMF either in neutrophils prepared from the LAD or NCD group (Figure 11c).

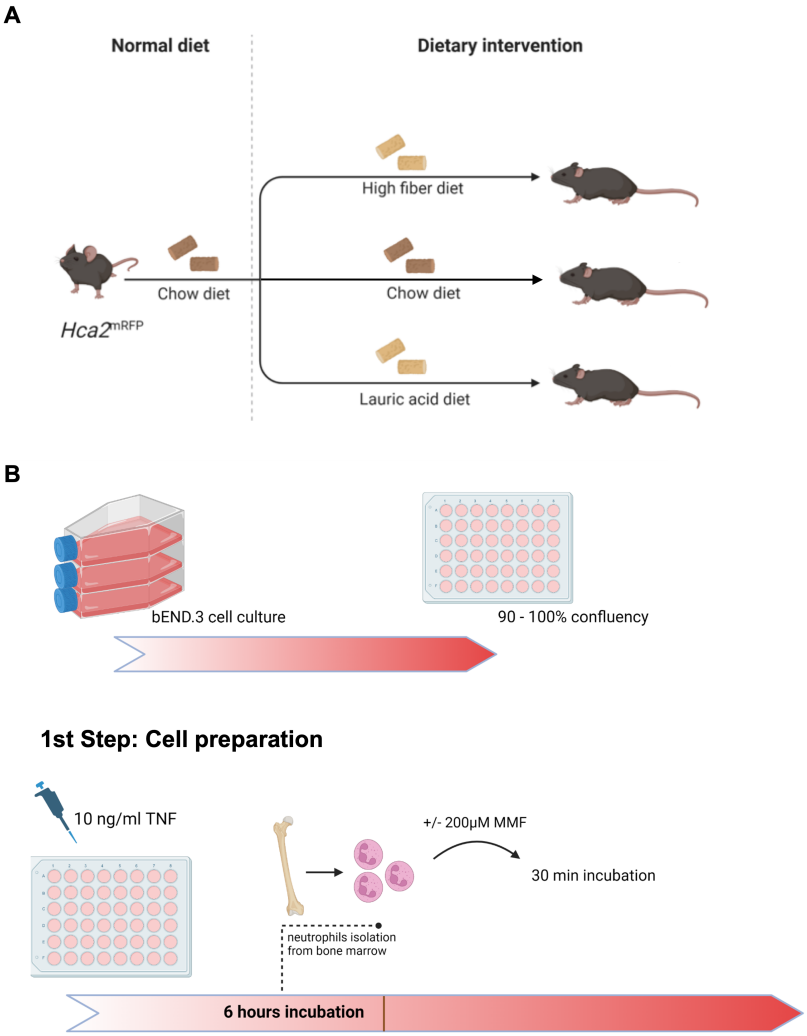

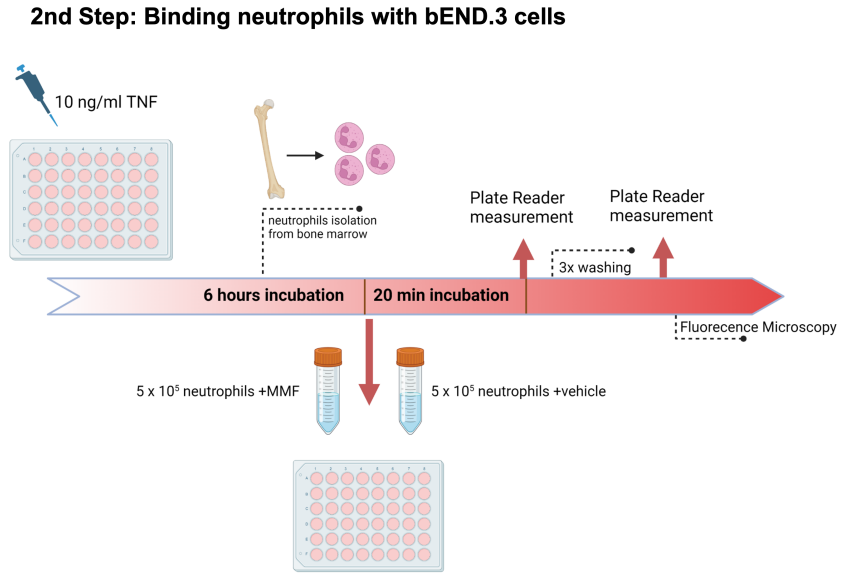

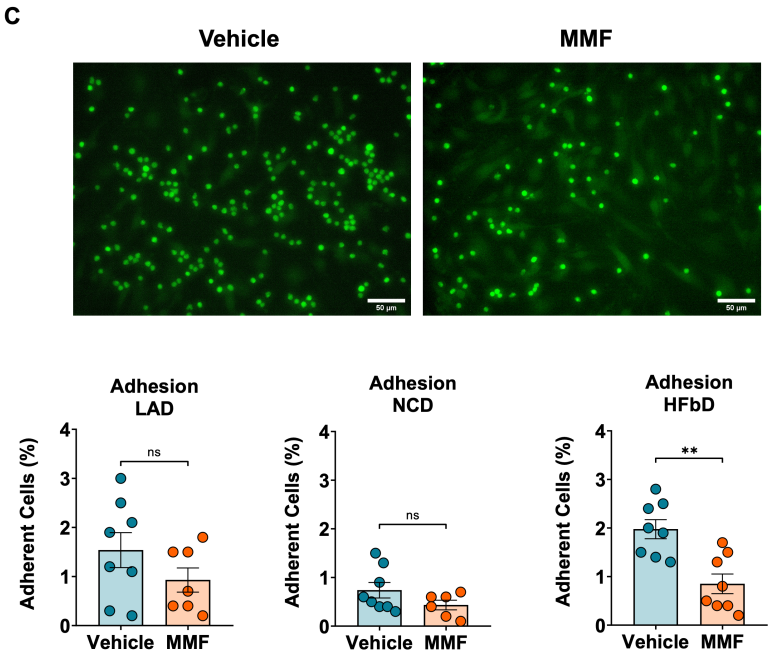

***Figure 11:* Pronounced effect of *HFbD* on neutrophils response to MMF treatment.**

(A) Three groups of mice were fed LA, NC and HFb diets for 4 weeks.

(B) Confluent brain endothelial cells bEND.3 cells were incubated with 10 ng/ml TNF for 6 hours. Meanwhile, Calcein-labelled neutrophils (green) were stimulated with 200 µM MMF and incubated with bEND.3 cells during the second stage of the assay. Between two measurements with a plate reader, cells were washed three times.

(C) As a final step, cells were fixed, and microscopic images were analyzed. Quantification of the cells showed a significant inhibition of neutrophil adhesion induced by MMF treatment in mice fed the HFb diet compared to the LA and NC diets. MMF significantly inhibited neutrophils adhesion to activated bEnd.3

when neutrophils were isolated from mice fed HFbD, while in mice fed with LAD or NCD no effects were observed. In the left panels, representative images from the HFbD group are shown.
** P < 0.05, **P < 0.05. Means ± S.E.M. are shown. Points represent cultures from individual mice. Scale bars, 50 µm. Detailed information on the exact test statistics, sidedness and values is provided in Supplementary Table 1.*

These results suggest that HFb diet promoting an increase in butyrate production results in a better response of neutrophils to DMF treatment in an HCA_2-dependent manner. To confirm these findings, I performed another experiment in which I proved that diet increases the effect of DMF treatment on neutrophils.

4.2.1.2. Quantification of NET formation by NETosis Assay

I performed a NETosis Assay in which I investigated another hallmark of neutrophil activation, the production of neutrophil extracellular traps (NETs), which consist of a network of extracellular DNA chains accompanied by the release of granule proteins and histones. During EAE and MS, the BBB becomes damaged, to which NETs neutrophils may contribute. In addition, the release of neutrophil's granules contributes to increased ROS production, leading to aggravated disease symptoms (Woodberry et al., 2018). DMF treatment has been shown to impair neutrophil function and inhibit NET production (Müller et al., 2016).

As for the Adhesion Assay, primary neutrophils were collected from the bone marrow. In order to investigate the MMF effects on Netosis, TNF-primed neutrophils were divided into 3 distinct groups: 1) only Sytox Green (SG)-labeled neutrophils to assess the simultaneous NET release; 2) SG-labeled neutrophils stimulated by the phorbol myristate acetate (PMA), a well-known inducer of NETosis, without MMF treatment and 3) SG-labeled neutrophils stimulated by the 100 µM PMA and treated with 200 µM MMF (Figure 12a). The analysis of the fluorescence microscopy images enabled the quantification of the NETs area and showed a significant reduction of NETosis in MMF-treated neutrophils obtained from the HFbD group. Neither in the LAD nor NCD group a similar effect of MMF was found (Figure 12b). This data set suggest that the HCA_2-mediated effect of MMF is enhanced by the HFb diet, reflecting protective effects in EAE.

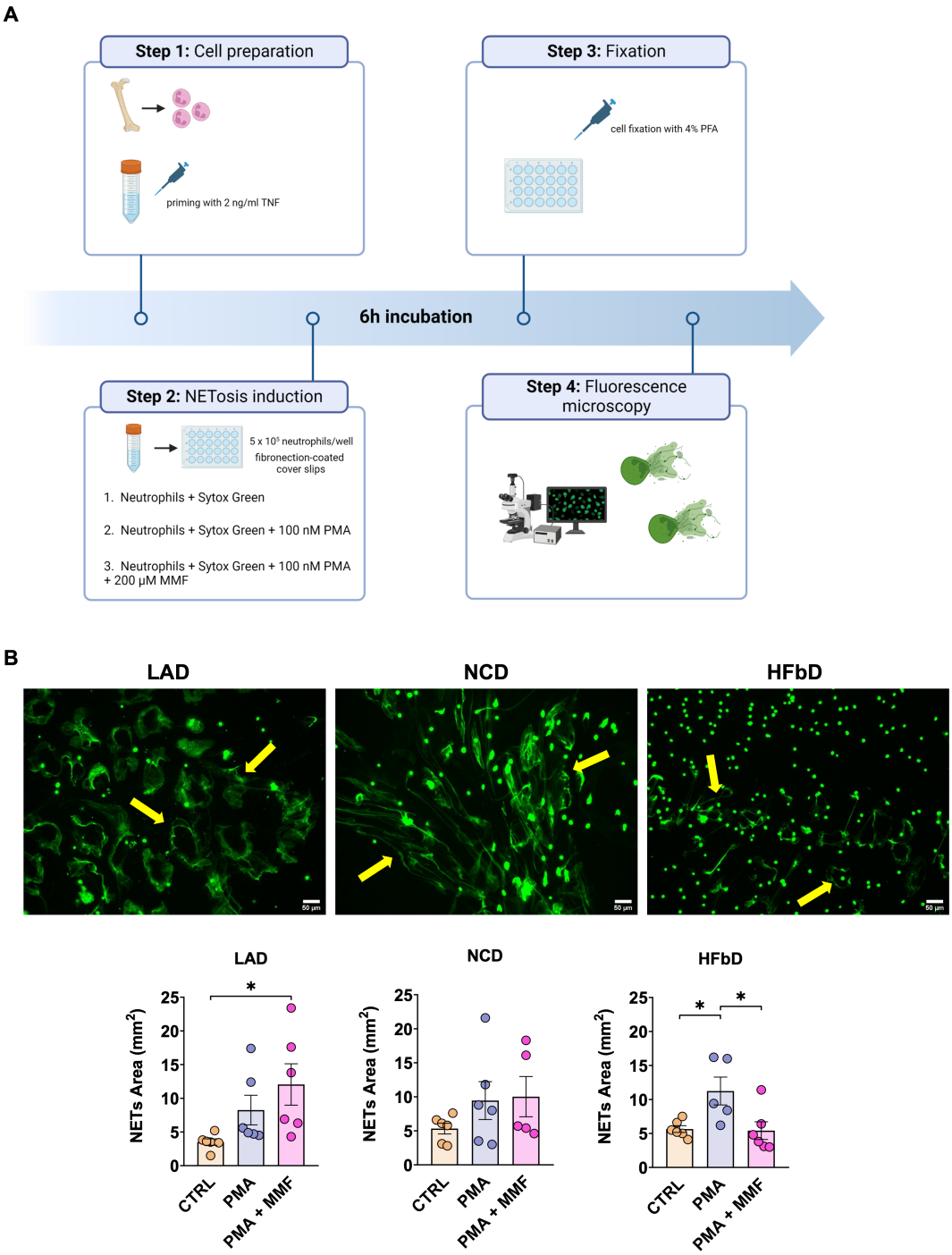

Figure 12: **Pronounced effect of HFbD on reducing NET formation in the MMF-treated group.**

(A) Neutrophils collection from bone marrow from three groups of mice fed LA, NC and HFb diets. Subsequently neutrophils were divided into 3 different group either treated with or without 200 µM MMF. Followed by cell fixation and quantification.

(B) MMF treatment significantly reduced release of neutrophil extracellular traps (NETs, yellow arrows) in the HFbD-fed mice, while in LAD and NCD groups, MMF had no effect. In the left panels, representative images of neutrophils treated with PMA + MMF of the three diets are shown.
** P < 0.05, **P < 0.05. Means ± S.E.M. are shown. Points represent cultures from individual mice. Scale bars, 50 µm. Detailed information on the exact test statistics, sidedness and values is provided in Supplementary Table 1.*

4.2.2. Diet modulates DMF efficacy in an EAE mouse model

DMF treatment has shown high efficacy in patients with RRMS, but unfortunately, some patients have not responded to treatment (Havrdova et al., 2017). Therefore, it is essential to investigate factors that may contribute to treatment response. During the study of neutrophil biology, I showed an enhancement of DMF effects in the HFb diet compared to the fat-rich LA and control NC diets.

4.2.2.1. Diet intervention during DMF treatment

To study the influence of the diets on the improved protective effects of DMF in EAE, *in vivo* studies using an EAE mouse model was performed. 14 days prior to the immunization, and later during the whole time of the experiment, mice were fed fat-rich LAD, HFbD or NCD. On the 3rd day post-immunization (dpi), mice received an oral DMF treatment (50 mg/kg, twice per day) or vehicle until the last day of the experiment (28th dpi) (Figure 13a). An increase in body mass in mice on LAD, NCD, and HFbD has been observed; nevertheless, at the onset of the first neurological symptoms between 8 and 10 dpi, there was a drop in body mass. DMF treatment showed a notable effect in HFbD, while it had a moderate effect in NCD and LAD (Figure 13b). The weight loss reflected the neurological score obtained by mice. Depending on the diet, an effect of DMF on the neuroscore was observed. The scoring started on the 7th dpi, showing the lack of DMF effects in the LAD group, while in NCD, there was a moderate improvement of neuroscore in the treated group. A prominent neurological deficit improvement was observed in the DMF-treated group on HFbD (Figure 13c), which was also reflected by the significantly lower area under the curve (AUC) and the maximal neuroscore. First neuro-symptom onset was significantly delayed under DMF treatment in HFbD group (Figure 13d).

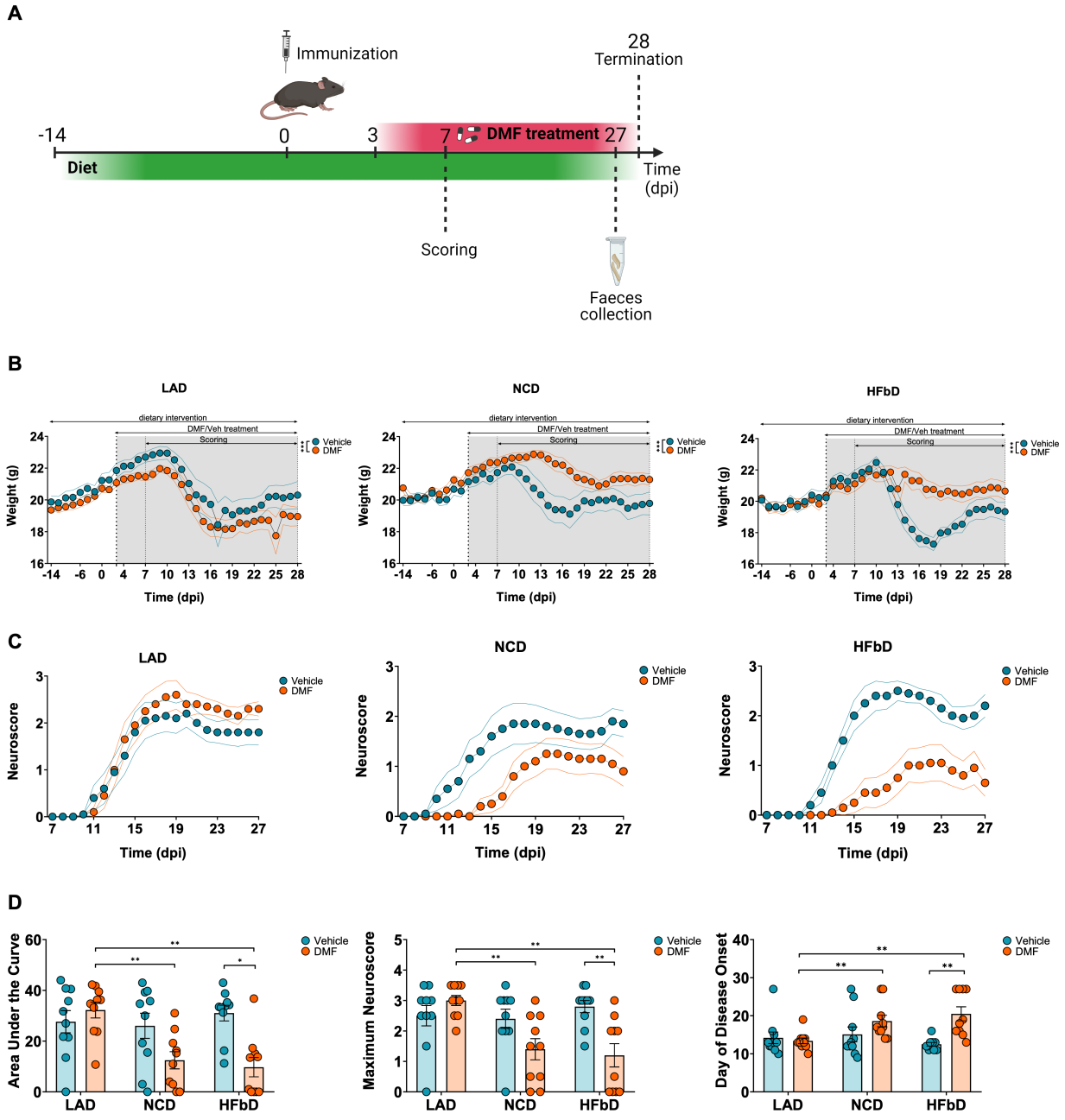

Figure 13: DMF efficacy* is modulated by the diet *in EAE.

(A) 14 days before immunization diet intervention started and was followed by DMF treatment (dpi 3) and scoring (dpi 7), feces collection one day before termination (dpi 28).

(B) Body weight of mice on lauric acid diet (LAD), normal chow diet (NCD), and high fiber diet (HFbD) during EAE. DMF reduced weight loss in mice on NCD and HFbD, while the effect was lost in the LAD group.

(C) Neuroscores in wild-type mice treated orally with vehicle or DMF (50 mg/kg body weight, twice daily).

(D) Area under the curve (AUC) of neuroscores, maximum scores, and the day of disease onset in mice on the three diets with or without DMF treatment.

*Dpi, day post immunization. *P < 0.05, **P < 0.01. Means ± S.E.M. are shown. Points represent individual mice (D). Detailed information on the exact test statistics, sidedness and values is provided in Supplementary Table 1.*

The experiment was performed by Julian Assmann, a previous PhD student at the Institute.

4.2.2.2. Effect of the diet and DMF treatment on microbiota and metabolism

Previous findings showed an interaction between the diet and the response to the treatment. They suggest that the microbiota influences the resorption of MMF, a prodrug formed from oral DMF administration. I further investigated and measured the concentrations of MMF in the plasma 20 minutes after applying DMF by oral gavage. However, there was no significant difference between the diets (Figure 14a), in addition, the analysis of the plasma concentrations of the SCFA, such as acetic acid and propionic acid, did not show significant changes due to the DMF treatment or between the diets (Figure 14b). These findings did not support the idea that the microbiota influence a better response to DMF treatment. However, I checked the effect of the diet on the gut microbiota by analyzing data obtained from the sequencing of the feces collected on the 28th dpi. The hallmark of EAE is the presence of gut dysbiosis, and both treatment and diet lead to a reshaping of the gut microbiota. The analysis of β-diversity of operational taxonomic unit (OTU) level abundances demonstrated significant differences between the diets; however, no effects in regard to DMF treatment were found. Moreover, α-diversity analysis showed a significantly lower diversity of microbiota species in HFbD compared to LAD and NCD, while there were no effects of DMF treatment within the diet group (Figure 18c). The data showed a notable change within the microbiota niche at the phylum and genus level. Compared to LAD and NCD in HFbD, an increased level of SCFA and butyrate producers has been demonstrated, simultaneously decreasing the level of pro-inflammatory microbiota (Figure 14d). At the genus level, a significant change has been observed in numerous bacteria, such as the butyrate-producer *Parabacteriodes*, for which relative abundance was elevated in HFbD compared to LAD and NCD. A similar effect in HFbD was also observed in another bacteria genus, including *Acetatofactor* or *Prevotellamasilla*. Conversely, in LAD, there was an increase in the pro-inflammatory bacteria *Streptococcus*, while in NCD and HFbD, it was significantly

decreased (Figure 18e). These data suggest that the metabolites of those bacteria might modulate the efficacy of DMF treatment.

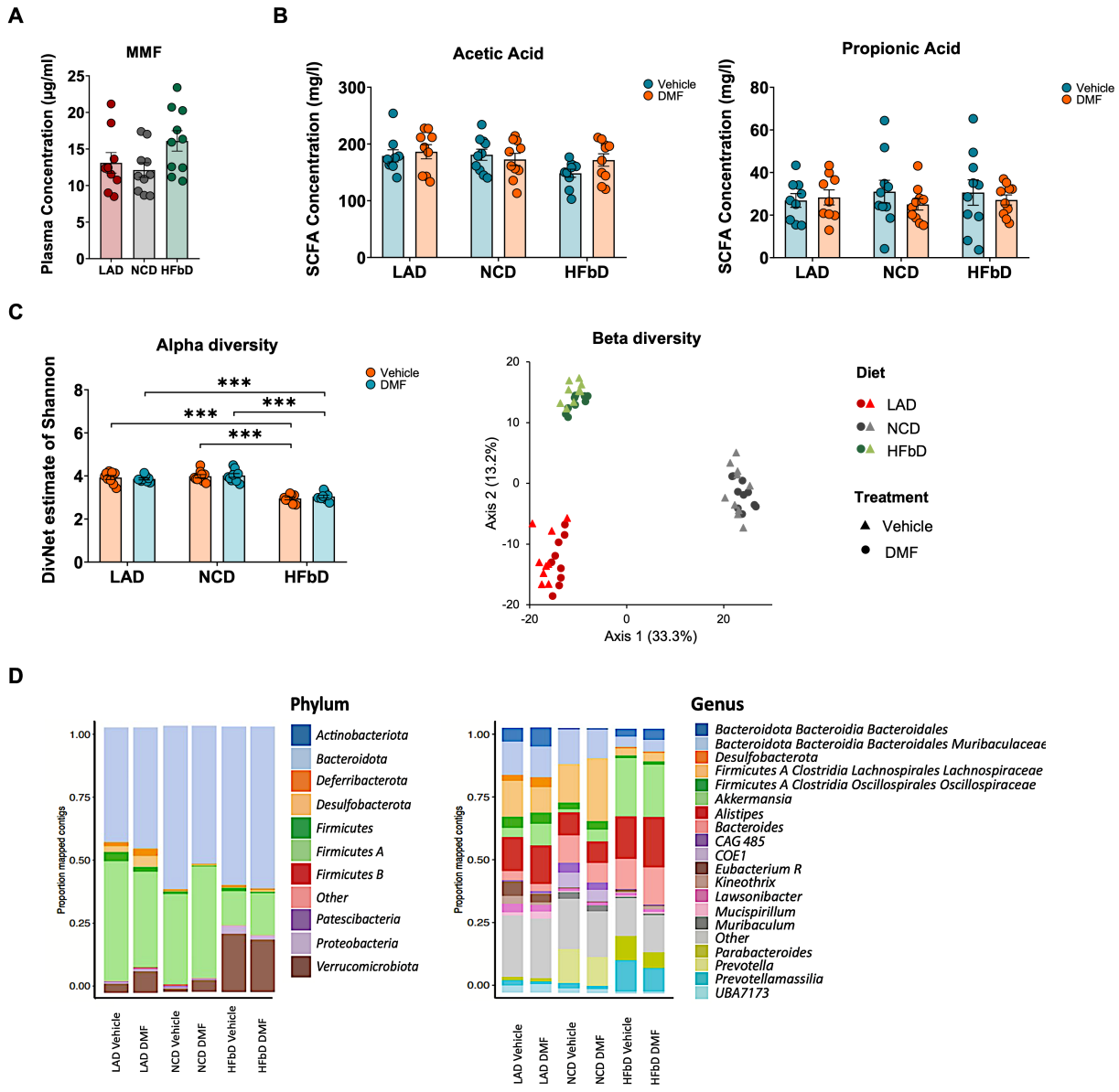

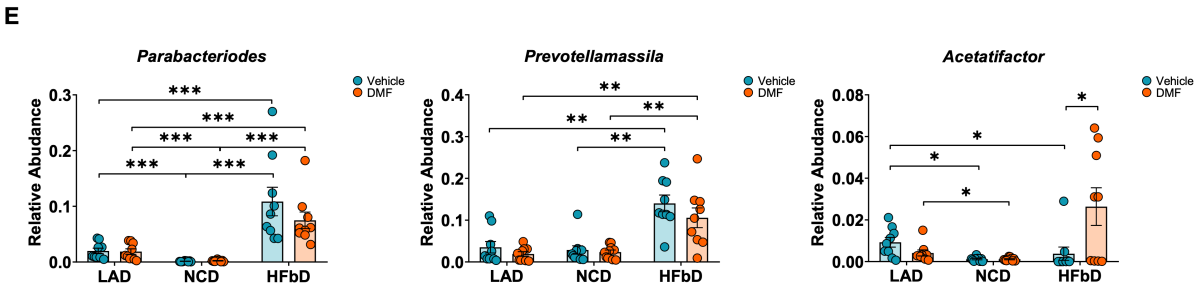

Figure 14: Effect of diet and DMF treatment on microbiota and metabolism.

(A) MMF plasma concentration collected from mice fed LAD, NCD and HFbD.

(B) Concentrations of acetic and propionic acid in plasma did not differ between the diets nor treatments.

(C) Alpha diversity was significantly reduced by the HFb diet compared to LA and NC diets, but DMF treatment had no effect. Similarly, only diet, not treatment affected beta diversity as shown by principal coordinates analysis and PERMANOVA.

(D) Diet intervention and DMF treatment affected the gut microbiota at the phylum and genus level. HFbD increased the relative abundance of short-chain fatty acids (SCFAs) producers, while in LAD I observed elevation of pro-inflammatory bacteria.

(E) The abundance of SCFAs producers such as Prevotellamassila or Parabacteriodes and Acetatifactor was increased in DMF-treated mice fed HFbD.

*Fecal samples were obtained from the experiment shown in Fig. 1 at dpi 28. *P < 0.05, **P < 0.01, ***P < 0.001. Means ± S.E.M. are shown. Points represent individual mice. Detailed information on the exact test statistics, sidedness and values is provided in Supplementary Table 1.*

4.2.2.3. HCA_2 mediate the effect of DMF treatment in EAE mice fed HFbD

Previous *in vivo* experiments have shown that HCA_2 is required to reduce neurological deficits and decrease the spinal cord's immune cell infiltration and demyelination. However, in mice lacking HCA_2, the efficacy of DMF treatment was lost, when mice received NCD (Chen et al., 2014). As the previous results indicated the enhanced protective effect of DMF on HFb diet, I decided to conduct the EAE experiment to confirm that HCA_2 is required to mediate a neuroprotective effect of DMF treatment. Thus, 14 days before immunization and during the experiment, *Hca2*$^{-/-}$ mice and *Hca2*$^{+/+}$ littermate controls were fed with HFbD. On the 3rd dpi, oral DMF (50 mg/kg, twice per day) or vehicle was administrated by oral gavage until the last day of the experiment (28th dpi). The scoring started on the 7th dpi, and the onset of the first neurological symptoms manifested between 14 and 16 dpi. *Hca2*$^{+/+}$ mice receiving DMF treatment showed significantly decreased disease severity and improved neurological deficit compared to the vehicle

group (Figure 15a). However, the effect of DMF treatment was lost in *Hca2*$^{-/-}$ mice Moreover, DMF treatment contribute to a significant reduction in AUC in *Hca2*$^{+/+}$ mice, while in *Hca2*$^{-/-}$ mice there is no significant difference (Figure 15b). These findings confirm that DMF improves the neurological deficit in the HCA2 manner when mice are on HFbD.

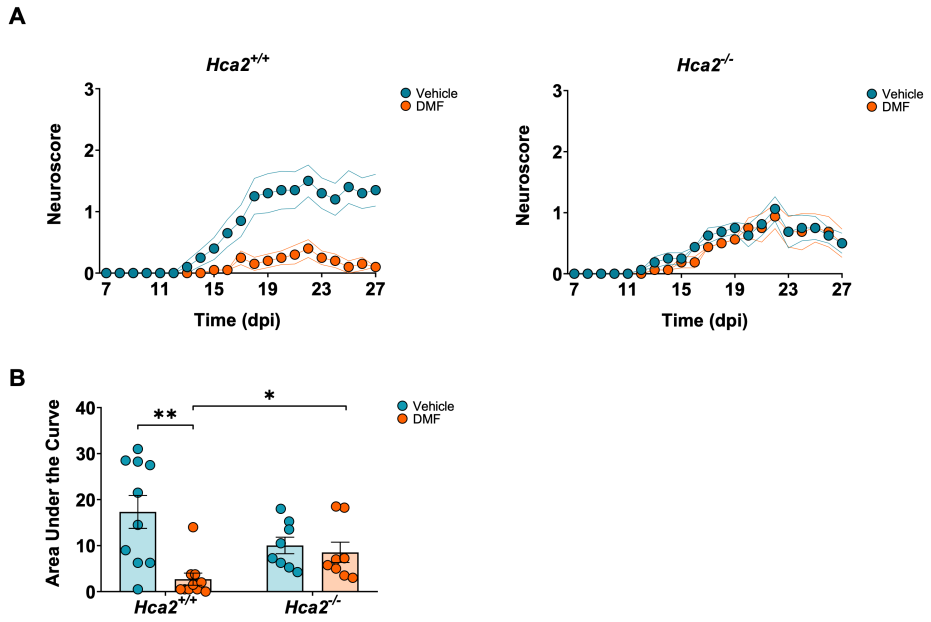

Figure 15: HCA$_2$ mediates the effect of DMF treatment in EAE when mice were fed HFbD.

(A) DMF significantly improved the neuroscore in Hca2$^{+/+}$ *mice, while the effect was lost in Hca2*$^{-/-}$ *mice, confirming our previous results.*

(B) Area under the curve (AUC) of neuroscores in Hca2$^{+/+}$ *mice and Hca2*$^{-/-}$ *mice treated with vehicle or DMF.*

**P < 0.05, **P < 0.01. Means ± S.E.M. are shown. Points represent individual mice (B). Detailed information on the exact test statistics, sidedness and values is provided in Supplementary Table 1.*

4.2.2.4. *Hca2* expression is not influenced significantly by treatment or diet.

As shown in a previous experiment, HCA$_2$ mediates a therapeutic effect of DMF in EAE mice. I wondered which Hca2-expressing cell population contributes to enhanced DMF treatment on HFbD. For this purpose, I used *Hca2*^{mRFP} mice fed either HFbD or LAD. As in previous EAE experiments, mice were on the diet 14 days before the immunization, as well as during the whole experiment until the 16th dpi. On the 3rd dpi, mice received the oral DMF treatment (50 mg/kg, twice per day) or vehicle by gavage, and the scoring started on the 7th dpi until termination day (16 dpi). At the end of the experiment, I performed FACS measurement to assess the RFP^{+} cell population in the blood. The

quantitative analysis was based on the gating strategy (Figure 16a). In both diets, HFbD and LAD, over 95 % of $Ly6G^{+}Ly6C^{-}$ neutrophils were RFP^{+}. However, neither diet nor treatment led to a significant difference in HCA2 expression per cell, which is already very high in untreated neutrophils (Figure 16b). Among the monocyte populations, regardless of diet, almost all pro-inflammatory $Ly6C^{high}$ monocytes did not express HCA_2 (Figure 16c), while about 20-40 % of $Ly6C^{int}$ and $Ly6C^{low}$ monocytes were RFP^{+} positive. As I observed, in both diets, HFbD and LAD, no significant difference in expression per cell (Figures 16d and 16e). However, HFbD moderately upregulated the expression of *Hca2* in $Ly6C^{int}$ monocytes (Figure 16d), which might suggest its possible contribution to improved efficacy of DMF treatment in mice. These data demonstrate that the highest expression of *Hca2* was found in neutrophils, which might suggest their most significant role in improving disease severity. In addition, DMF had no effect on the number of neutrophils as well as $Ly6C^{int}$ and $Ly6C^{low}$ monocytes regardless of the diet. However, HFb diet led to a reduction of $Ly6C^{high}$ monocytes in comparison to LAD group.

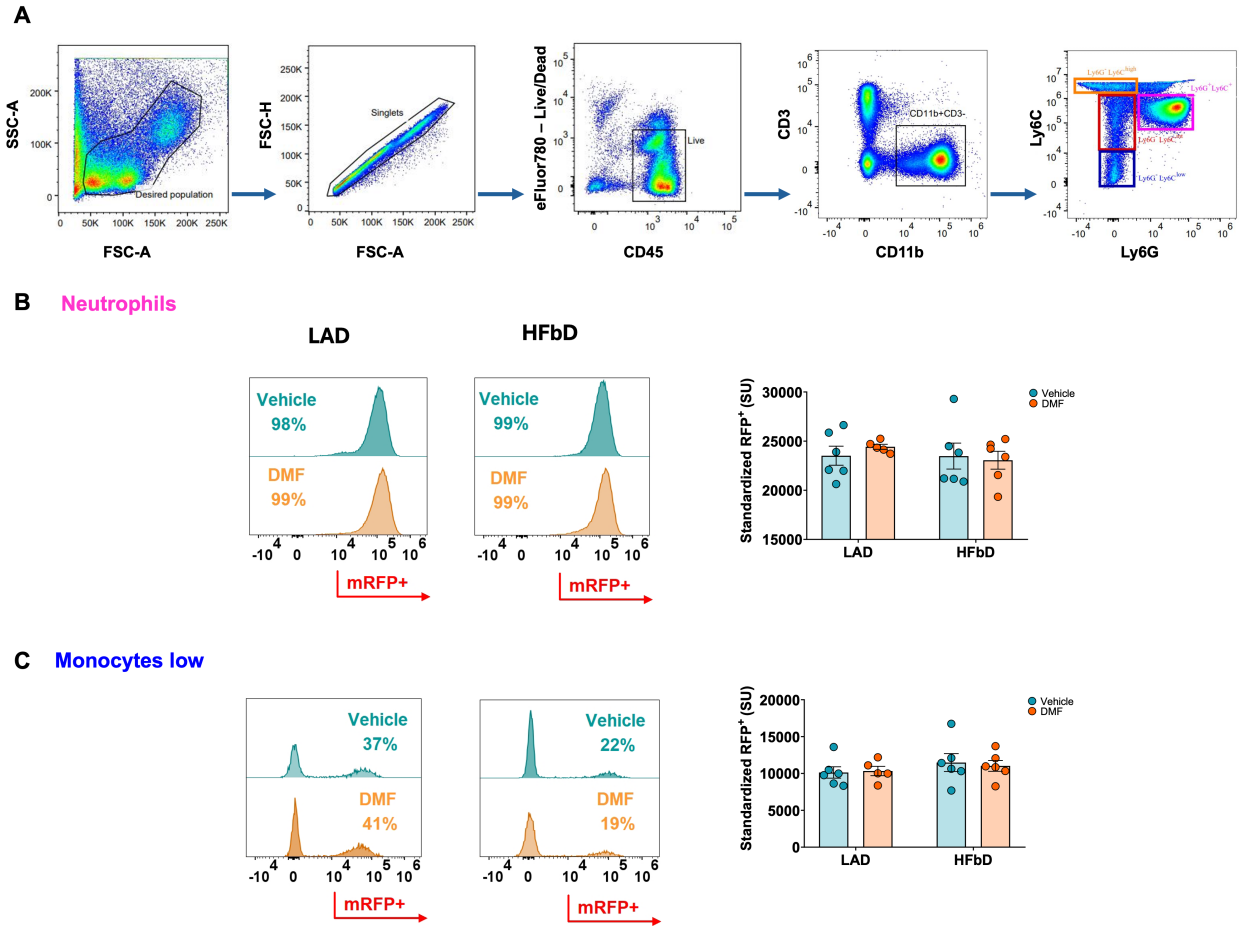

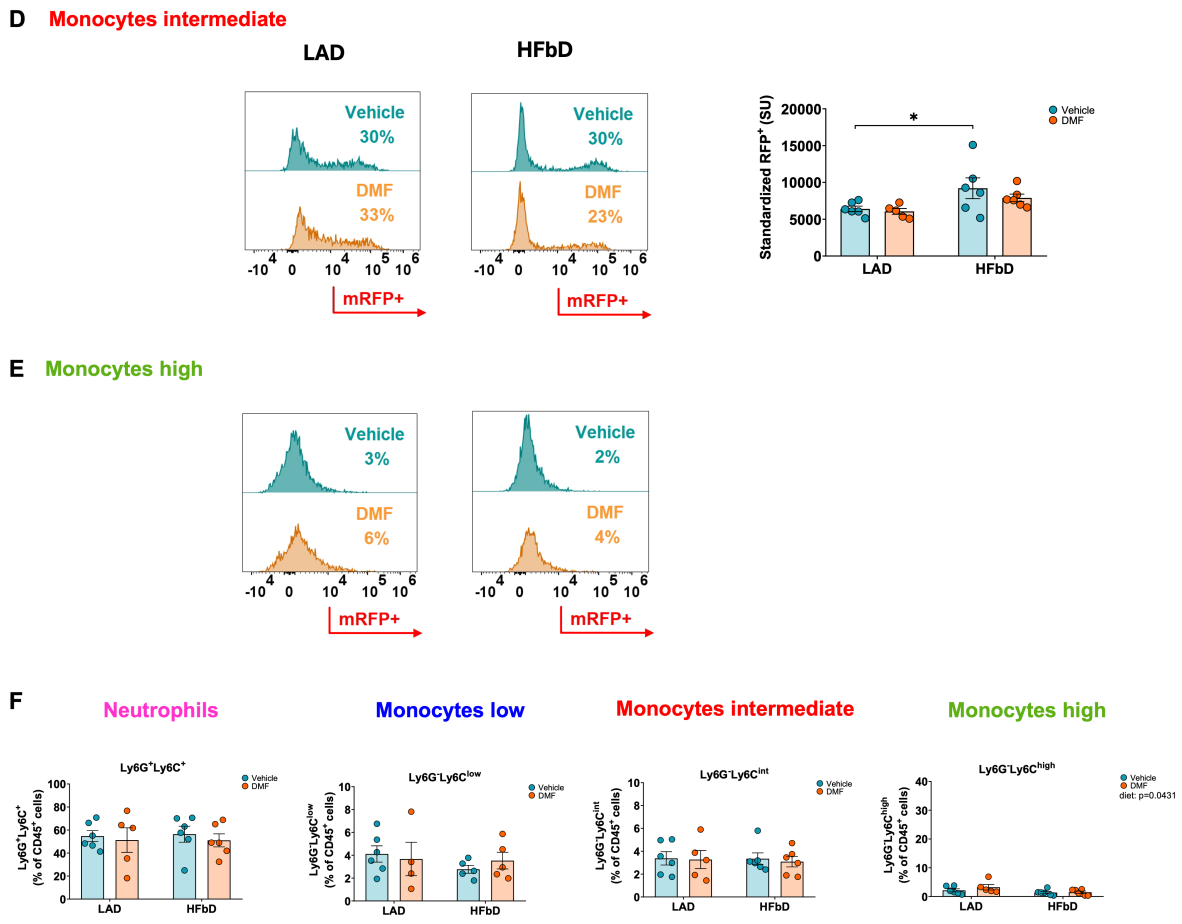

Figure 16: Hca2 expression is not influenced significantly by treatment or diet.

(A) Blood cells were gated into viable and CD45-positive cells. Subsequently, the leukocyte population was gated into $CD45^+CD11b^+Ly6G^+Ly6C^-$ neutrophils, $CD45^+CD11b^+Ly6G^-Ly6C^{hi}$, $CD45^+CD11b^+Ly6G^-Ly6C^{int}$ and $CD45^+CD11b^+Ly6G^-Ly6C^{low}$ monocytes.

(B) Histogram demonstrating that over 95 % of neutrophils are RFP^+ regardless of the diet and the treatment. The Hca2 expression per neutrophil, represented as standardized unit (SU) of $mRFP^+$ was not affected by DMF or the diet.

(C) and (D) Histogram demonstrating that $Ly6C^{int}$ and $Ly6C^{low}$ monocytes expressed mRFP at intermediate levels and Hca2 expression per cell was not changed by DMF. However, DMF led to the mild increase of mRFP expression in $Ly6C^{int}$ monocytes.

(E) Histogram demonstrating that almost all pro-inflammatory $Ly6C^{hi}$ monocytes were mRFP-negative.

(F) Neither treatment or diet significantly reduced the number of infiltrating neutrophils, monocytes low and intermediate. However, diet did reduce the number of high monocytes in HFbD-fed mice compared to LAD-fed mice.

**P < 0.05. Means ± S.E.M. are shown. Points represent individual mice. Detailed information on the exact test statistics, sidedness and values is provided in Supplementary Table 1.*

4.2.2.5. HCA_2 mediate effects of DMF in neutrophils cell-specific manner.

In the following, to investigate a mediating role of HCA_2 in neutrophils in a cell-specific manner during DMF treatment, the *Hca2*$^{Fl/Fl}$ mouse line was generated and subsequently was crossed with the mouse line termed Catchup, which is the neutrophil-specific Ly6G-Cre driver with the expression of the fluorescent protein tdTomato (Hasenberg et al., 2015). To assess the effectiveness of recombination, I used primary neutrophils collected from the bone marrow. I stimulated them with 100 µM MMF (Figure 17c), as a product of intestinal DMF metabolism along with 100 µM NA (Figure 17a, which are *Hca2* receptor agonists and elevate intracellular Ca^{2+} ($[Ca^{2+}]_i$) release in neutrophils. Cells were collected from four different genotypes of mice: wild-type *Hca2*$^{+/+}$, *Hca2* $^{-/-}$, *Hca2*$^{FL/FL}$ and *Hca2*^{nKO} (Figure 17a). Stimulation with the drugs resulted in HCA_2–mediated increase in $[Ca^{2+}]_i$ in wild-type *Hca2*$^{+/+}$ neutrophils, but the effect was lost in neutrophils from *Hca2*$^{-/-}$ mice. The measurement has shown a similar effect of NA and MMF in *Hca2*$^{Fl/Fl}$ as in wild-type *Hca2*$^{+/+}$ neutrophils, suggesting that the artificial intron that was inserted into the floxed locus does not interfere with *Hca2* expression and, thereby, response to an agonist. Interestingly, in comparison to *Hca2*$^{Fl/FL}$ neutrophils, I could observe a significant drop in the rate of responsive cells to the stimuli from 75 % to approximately 40 % in neutrophils from *Hca2*^{nKO} mice (Figure 17b). These findings suggest that Ly6G-Cre-mediated recombination in neutrophils is a successful way to inhibit the HCA_2 activation.

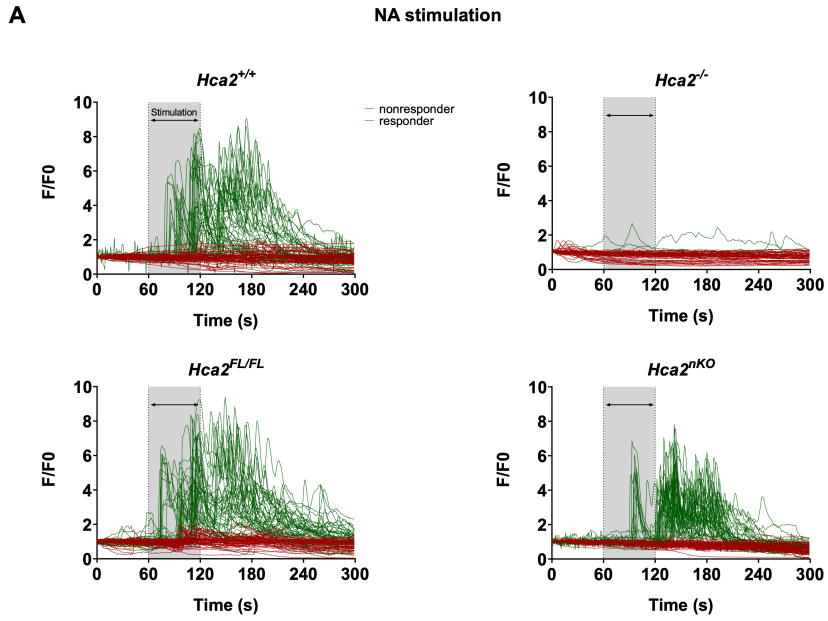

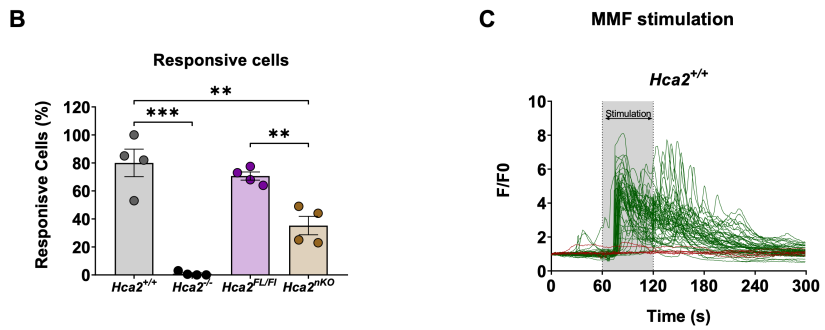

Figure 17: Conditional knockout of Hca2 in neutrophils (Hca2^{nKO}) decreases HCA$_2$-stimulated increase in intracellular Ca^{2+} concentrations ([Ca^{2+}]$_i$).

(A) Stimulation with nicotinic acid (NA, 100 µM, 60 sec) increased [Ca^{2+}]$_i$ concentrations in a majority of Hca2$^{+/+}$ neutrophils, while it had no effect in Hca2$^{-/-}$ neutrophils. Hca2$^{Fl/Fl}$ neutrophils responded in a similar manner to NA stimulation as Hca2$^{+/+}$ cells. The amplitude of [Ca^{2+}]$_i$ stimulated by nicotinic acid was lower in Hca2^{nKO} neutrophils.

(B) The number of neutrophils responsive to MMF treatment was significantly reduced in the Hca2^{nKO} genotype compared to Hca2$^{Fl/Fl}$ genotype.

(C) Stimulation with MMF (100 µM) increased [Ca^{2+}]$_i$ in neutrophils.

***P < 0.05. Means ± S.E.M. are shown. Points represent individual mice. Detailed information on the exact test statistics, sidedness and values is provided in Supplementary Table 1.*

Due to a successful knockout of the *Hca2* receptor in neutrophils, I induced EAE in *Hca2$^{Fl/FL}$* and *Hca2^{nKO}* mice. During this experiment, all mice were fed with HFbD, starting two weeks before immunization and continuing until the last day (28 dpi). Mice received oral DMF or vehicle treatment on the 3rd dpi, followed by the scoring from 7th dpi onwards. As I observed, DMF treatment significantly reduced neurological symptoms in *Hca2$^{Fl/Fl}$* mice, while in *Hca2^{nKO}* mice, this effect was lost (Figure 18a). Neurological improvement in DMF-treated *Hca2$^{Fl/Fl}$* mice was also supported by the reduction of the AUC of neuroscores (Figure 18b).

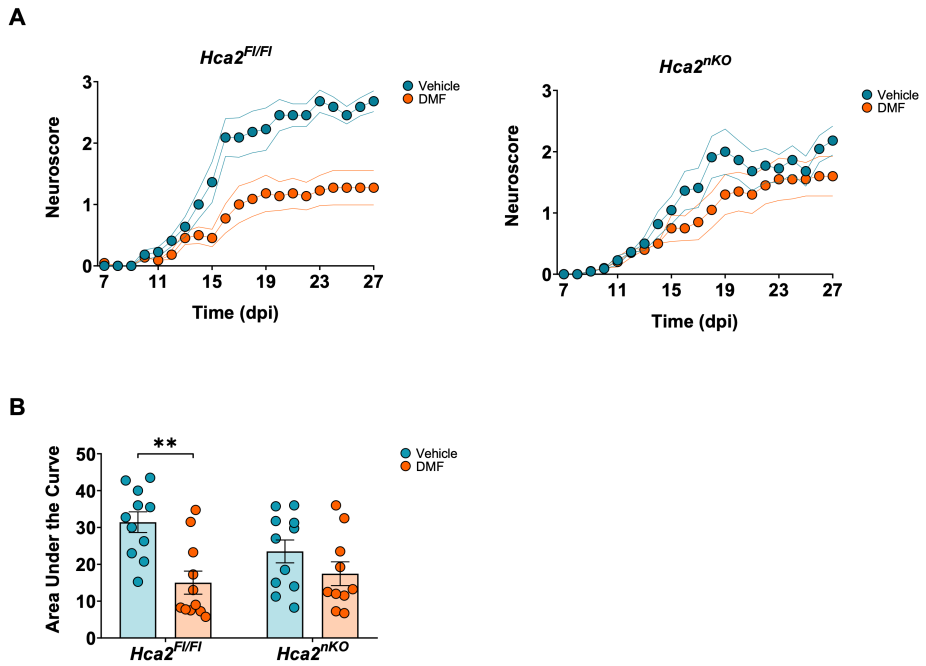

Figure 18: The therapeutic effect of DMF in EAE depends on HCA_2 in neutrophils.

(A) Neuroscores of $Hca2^{FL/FL}$ and $Hca2^{nKO}$ mice fed HFb diet and treated orally with vehicle or DMF (50 mg/kg body weight, twice daily). DMF treatment significantly improved the neurological deficit in $Hca2^{FL/FL}$ mice, while the effect was lost in $Hca2^{nKO}$ mice, indicating that HCA_2 mediates the protective effect of DMF in neutrophils.

(B) DMF treatment significantly reduced the area under the curve (AUC) of neuroscores in $Hca2^{FL/FL}$ but not in $Hca2^{nKO}$ mice.

***P < 0.05. Means ± S.E.M. are shown. Points represent individual mice (B). Detailed information on the exact test statistics, sidedness and values is provided in Supplementary Table 1.*

In summary, our data indicate that HCA_2 is required for mediating the protective effect of DMF treatment in EAE mice.

5. Discussion

In 2013, DMF was approved as an oral medication in patients with relapsing-remitting multiple sclerosis (RRMS) and showed great improvement in delaying relapses and patient disability. A recent long-term follow-up studies demonstrated a favorable benefit-risk profile of DMF treatment. More than 70 % of patients receiving DMF treatment did not experience an increased number of relapses or disease worsening. In addition, other patients became relapse-free for more than 10 years (Gold et al., 2022). However, not all patients have benefited from DMF treatment (Havrdova et al., 2017), therefore, further research is needed to improve the current treatment strategy. In this study, I focused on the impact of diet on the therapeutic effect of DMF in EAE, a mouse model of MS. The data showed that in mice fed an HFb diet, the efficacy of DMF treatment was most pronounced and resulted in increased improvement in neurological deficits. It has been shown that the protective effect of DMF depends on HCA_2, a GPCR which is activated by DMF and its active prodrug MMF, NA, as well as ketone body β-OHB and butyrate (Taing et al., 2023). Furthermore, recent studies demonstrated the importance of neutrophils, as a key factor contributing to MS development and neuroinflammation (Shi et al., 2021). It has been reported that *Hca2* is expressed by neutrophils (Tunaru et al., 2003) whose infiltration into the CNS is reduced after DMF treatment (Chen et al., 2014). In this study, I showed that the HFb diet intervention altered neutrophil biological functions and upregulated cell activation genes, which may have contributed to a more robust response to MMF treatment.

In this study, I investigated the relationship between microbiota and the efficacy of DMF and its effects on neutrophil function in a model of EAE. In addition, I demonstrated the importance of the MMF-HCA_2 axis in improving neurological deficits.

5.1. Adverse effects caused by DMF treatment

DMF a globally used drug in the treatment of MS, has demonstrated promising outcomes in reducing the EDSS score, a key measure of disability and disease progression. However, clinical tests on its safety profile have revealed adverse effects (AE) in patients, with the most common being flushing or gastrointestinal issues like diarrhea, vomiting, or abdominal pain (Bomprezzi, 2015). Some of those AE might be mediated by HCA_2

(Dubrall et al., 2021) a receptor expressed in the cell membrane of various tissues and cell types (Taing et al., 2023).

To examine which tissues express *Hca2*, I investigated cryosections of a reporter mouse model, *Hca2*^{mRFP} (Hanson et al., 2010) enhanced by an antibody staining. Ilocalized HCA_2 in selected organs, focusing mostly on the mucosa of the colon. Using the Ussing chamber, I have shown that the diarrhea in patients with MS might not occur due to changes in transepithelial transport caused by DMF or NA treatment, and another mechanism may explain/cause the AE. One explanation may involve prostanoids, such as prostaglandin D_2 (PGD_2) and PGE_2. Mediated by HCA_2, they may contribute to the secretory diarrhea and flushing reaction. Hanson and colleagues demonstrated that mice lacking the *Hca2* receptor did not experience DMF or NA-induced flushing in a well-established mouse model for flushing. Moreover, keratinocytes and Langerhans cells expressing HCA_2 were involved in the flushing mechanism (Hanson et al., 2010). Another study provided evidence for the essential role of Langerhans cells in HCA_2-mediated vasodilation. After activation of the receptor, an increase in $[Ca^{2+}]_i$ was observed followed by activation of phospholipase A_2, and subsequent release of PGD_2 and PGE_2, resulting in flushing (Benyó et al., 2006). Furthermore, it has been reported that prostaglandins are involved in inducing diarrhea and one study showed effective prevention of diarrhea mediated by PGE_2 using prostaglandin-synthetase inhibitors (Lange et al., 1977). However, during this study I did not characterize the cell type of the selected organs or further investigate other mechanisms of potential HCA_2-mediated diarrhea. Overall, our data showed that the DMF-HCA_2 axis did not affect transepithelial transport in the colon. To understand how DMF affects the occurrence of increased diarrhea in patients, further detailed studies are needed.

5.2. Diet modulates the efficacy of DMF treatment in EAE

The gut microbiota plays a primary role in maintaining human well-being by promoting immune cell maturation and normal immune function regulation and being in symbiosis with the host, contributing to homeostasis (Clemente et al., 2012). Under healthy conditions, the microbiome has tremendous taxonomic diversity and high microbial gene richness, providing host stability and resilience (Fan & Pedersen, 2021). However,

microbiota dysbiosis and its interaction with the host immune system contribute to dysregulations and disease development. Numerous studies indicate that dysbiosis of the microbiota may be considered a potential factor for MS as well as other autoimmune and neurodegenerative diseases. They reported that specific gut bacteria are associated with a pro-inflammatory environment and contribute to the pathogenesis of MS and increased disease severity (Mirza & Mao-Draayer, 2017).

The main families of bacteria in the gut are the Bacteroidetes, Firmicutes, Proteobacteria and Actinobacteria, as well as other phyla. Recent studies conducted by several groups demonstrated the profile of specific gut bacteria in MS compared to healthy control groups. SCFA or butyrate producers, such as *Bacteroides, Parabacteroides, Prevotella,* which display protective and anti-inflammatory effects, were shown to be reduced in MS. On the other hand, there is an increase in pro-inflammatory bacteria such as *Ruminococcus*, or *Methanobrevibacter* in RRMS patients (Altieri et al., 2023; Shahi et al., 2017). Moreover, Cekanaviciute et al. identified that certain bacteria, *Akkermansia muciniphila* and *Acinetobacter calcoaceticus*, which are significantly increased in MS patients are linked to pro-inflammatory responses and a more severe course of disease (Cekanaviciute et al., 2017). Interestingly, the genus *Akkermansia* has been reported to exert both inflammatory and regulatory properties. It can convert mucin into SCFAs but is also involved in the breakage of the gut barrier, which consequently results in elevated exposure to microbial antigens (Jangi et al., 2016).

Other factors that have a major impact on altering the gut microbiota are the commonly used drugs in MS, one of which is DMF (Zhou et al., 2022). Significant changes in the gut microbiota were found in DMF-treated MS patients. Several clinical trials demonstrated a beneficial effect of DMF in decreasing pro-inflammatory bacteria taxa, such as *Akkermansia muciniphila, Coprococcus eutactus, Streptococcus* or some members of the Clostridia families, such as *Lachnospiraceae*. These bacteria taxa were associated with impaired myelination and differentiation of oligodendrocytes. However, DMF resulted in a significant increase in the relative abundance of beneficial bacteria from the Bacteroidetes family, such as *Bacteroides* or *Prevotella*, which are linked to ameliorating EAE and MS symptoms (Chu et al., 2018b; Del Negro et al., 2024; Diebold et al., 2022; Ferri et al., 2023b; Katz Sand et al., 2019). In this experiment, I observed a significant

impact of the diet on DMF treatment efficacy. I observed that the HFb diet greatly increased the relative abundance of butyrate and SCFAs producers at the phylum and genus level, such as *Bacteroidota,* and *Bacteroides, Parabacteroides,* and *Prevotella,* respectively. Simultaneously, the HFb diet reduced the abundance of pathological bacteria. Moreover, I showed a pronounced effect of DMF treatment in the reduction of disease severity compared to the untreated group, indicating the contribution of the HFb diet in a better host response to the DMF treatment mediated by HCA_2. On the contrary, the LA diet promoted increased relative abundance of pro-inflammatory bacteria, such as *Lachnospiraceae* and *Streptococcus,* while beneficial bacteria were reduced. The possible consequence of the elevated levels of those bacteria might be their contribution to the loss of the protective effect of DMF treatment and progressed disease course. However, there might be several ways the diet impacts the host and immune cells, such as neutrophil functions decreasing susceptibility to DMF treatment.

One reason for the ineffective effect of DMF mediated by HCA_2 on neutrophils in the mice fed the LA diet may be the blocking effect of the medium- and long-chain fatty acids and saturated lipids. It has been reported that diets high in fat, as well as fatty acids and polyphenols, may contribute to the inflammatory cascade and production of TNF, prostaglandins, or interleukins, leading to oxidative stress and inflammation (Stoiloudis et al., 2022). It has been demonstrated that two of the most abundant saturated fatty acids (SFA), palmitic and stearic acids affect neutrophil functions. They significantly increased the production of ROS without any neutrophil stimuli, which indicates the pro-inflammatory action and contribution to the damage of the tissue. Moreover, palmitic acid promoted the migration of neutrophils by increasing IL-8 production, a key chemoattractant for neutrophils (Rodrigues et al., 2016). So far, very few studies have investigated the effect of lauric acid on neutrophils. However, the effect of lauric acid was investigated on cancer colonic cells and was greatly associated with a significant increase in their apoptosis, while butyrate did not induce apoptosis. Similarly, ROS generation was significantly elevated by lauric acid, while butyrate reduced the levels of ROS (Fauser et al., 2014). A recent study demonstrated that exposure to a high-fat diet rich in SFA is linked to inflammation and immune system dysregulation. Moreover, they showed that SFA contributed to a robust release of neutrophils from the bone marrow into the

bloodstream. It has been known that the increased number of neutrophils is linked to many inflammatory illnesses, including autoimmune diseases. Moreover, they showed an increased induction of neutrophils apoptosis and bone marrow inflammation (Ortega-Gomez et al., 2022). Interestingly, lauric acid which belongs to medium-chain fatty acids promotes differentiation of Th-1 and Th-17 cells, causing EAE to worsen. One of the studies observed an elevated influx of Th-17 cells into the small intestine in a group of mice fed the LA diet which contributed to a more severe course of EAE (Haghikia et al., 2015).

On the contrary, SCFAs suppress the induction of Th-17 and promote T-reg cells, ameliorating disease severity (Haase et al., 2018). SCFAs are mainly produced from the dietary fiber fermentation in the colon and are promptly absorbed by the colonocytes. However, SCFAs are not metabolized in colonocytes but in the liver, and eventually only a tiny fraction of acetate, propionate and butyrate derived from the colon reaches the systemic circulation (Boets et al., 2015). Moreover, it has been shown in a cell culture model that SCFAs are able to cross the BBB, reach the brain and promote CNS histone crotonylation modulating this way brain functions (Fellows et al., 2018; Mitchell et al., 2011). More importantly, the *Hca2* receptor is not only expressed by the adipocytes or immune cells but also by the colonocytes, which are activated by the butyrate (Thangaraju et al., 2009). Evidence suggests the SCFAs are a strong candidate in mediating the effect of the HFb diet in a HCA_2-dependent manner. In this experiment, I observed a great impact of dietary intervention on DMF treatment efficacy, demonstrating a pronounced effect of DMF in HFb diet-fed mice. Even though butyrate was not detected in the plasma and all other SFACs did not differ between the treatment groups in the HFb diet, butyrate might exert a local effect in the gut wall by improving the intestinal barrier. The expression of tight junction proteins may be affected and consequently prevents bacteria from translocating (Dalile et al., 2019). Butyrate has been shown to have a beneficial effect mediated by HCA_2 in the intestinal wall. Butyrate promoted the production of IL-10, resulting in the inhibition of pro-inflammatory Th-17 cells and converting naïve T-cells into regulatory T-cells (Offermanns, 2017). The enhanced effect of DMF treatment in the HFb diet observed in our EAE model might be mediated by SCFAs, including butyrate, which

stimulates the *Hca2* receptor, resulting in reduced disease severity and a significant delay of the onset.

5.3. Influence of the microbiota on neutrophil function

As mentioned before microbiota play a key role in the formation and development of the immune system and play an important role in mediating communication along the gut-brain axis (Fung, 2020). The gut microbiota modulates the function of cell populations such as neutrophils, which play significant roles in neurodegeneration in MS.

Here I demonstrated that during dietary intervention, the neutrophils response to the MMF treatment was modulated by the diet. I showed that the HFb diet regulates some neutrophil activities and contributes to their pronounced response to MMF treatment. I found no significant effect of MMF treatment in mice fed the LA or NC diets. One explanation for how a fiber-rich diet increases neutrophil susceptibility to treatment is that SCFAs to which propionate, acetate, and butyrate belong exert a modulating role. SCFAs modulate several processes, such as recruitment, differentiation, gene expression and activation of many immune cells, including neutrophils, monocytes, and macrophages, as well as DCs and T-cells. SCFAs affect neutrophil recruitment by influencing the production of pro-inflammatory mediators, such as TNF- α and IL-17 which activate the endothelial cells, as well as regulate the neutrophil-chemoattractants such as CXCL1 and CXCL8 produced by different cells (Corrêa-Oliveira et al., 2016). Moreover, another study has demonstrated an inhibitory effect of SCFAs on the production of pro-inflammatory cytokines, such as TNF-α and NO (Vinolo et al., 2011). In addition, a dual role of SCFAs in ROS production was reported. ROS are essential for antimicrobial activity, while on the other hand, the overproduction of ROS led to tissue destruction. However, SCFAs contributed to a healthy balance in ROS generation (Kamp et al., 2016). Moreover, one study on inflammatory bowel disease (IBS), in which dysbiosis of the intestinal microflora occured like in MS, found that butyrate inhibited NET production and effectively suppresses neutrophil migration (G. Li et al., 2021). One of the key steps in inflammation is the migration and adhesion of leukocytes to the tissue. During this process, adhesion molecules such as vascular cell adhesion molecule-1 (VCAM-1) or intercellular cell adhesion molecule-1 (ICAM-1) expressed by endothelial cells play a key role. Butyrate

has been shown to effectively reduce the induction of adhesion molecules, and consequently contribute to the reduced adhesiveness of leukocytes to the TNF-α stimulated endothelial cells (Zapolska-Downar et al., 2004). Another study also provided evidence showing an inhibitory effect of butyrate treatment on leukocyte adhesion to endothelial cells due to a reduced expression of VCAM-1 and ICAM-1 (Menzel et al., 2004). Additionally, it has been reported that DMF treatment affected the expression of the surface expression of different activation markers and adhesion molecules of leukocytes (Rubant et al., 2008), subsequently leading to reduced neutrophil adherence to endothelial cells. In this study, I showed that the strongest effect of MMF on reduced neutrophil adhesion to stimulated bEND.3 cells was observed in the presence of HFb diet. These results may indicate that butyrate not only has a beneficial effect on the pronounced effect of MMF treatment, but also modulates adhesion molecules independent of treatment. Similarly, I could also observe this potent effect of MMF in the group of mice fed HFb diet during PMA-induced NETosis in neutrophils. Activated neutrophils release neutrophil extracellular traps (NETs) that are net-like DNA fibers decorated with histones and proteases (Masucci et al., 2020). Butyrate has been found to have an inhibitory effect on NET development, leading to an amelioration of mucosal inflammation (G. Li et al., 2021). One of the newest studies has also shown that butyrate inhibited release of NETs by inhibiting neutrophils autophagy (Y. Li et al., 2022). In addition, many studies have demonstrated that DMF treatment impaired neutrophils' function and reduced NET formation (Hoffmann et al., 2018; Müller et al., 2016). In this study, I showed that the effect of MMF treatment was not observed in either the LA or NC diet-fed group of mice, and MMF did not significantly inhibit NET release if neutrophils were isolated from mice fed these diets. However, a significant reduction in NET formation was observed in a group of mice fed an HFb diet. Whether SCFAs modulate the action of MMF remains still unclear and further studies are needed.

5.4. HCA_2 is required for DMF efficacy

In patients suffering from MS, DMF significantly improved their clinical parameters and provided beneficial protective effect. One of the immunomodulatory effects of DMF action is the reduction of immune cells immigrating into the CNS. Several follow-up studies on the effect of DMF on cell population abundance have shown that the number of $CD8^+$ and

$CD4^+$ T-cells was reduced, as was the number of $CD19^+$ B-cells, $CD56^{dim}$ NK cells and plasmacytoid DCs. In addition, *in vitro* studies showed that DMF decreased infiltration of monocytes/macrophages and neutrophils in a HCA2-dependet manner (Yadav et al., 2019).

A previous study in this institute carried out by Chen et al. demonstrated a neuroprotective effect of DMF in the EAE model of mice mediated by HCA_2. To investigate this effect, he used wild-type (WT), *Hca2*$^{+/+}$ and *Hca2*$^{-/-}$ mice. The results showed a decreased infiltration of neutrophils in the spinal cord of WT mice, and lowered number of $CD4^+$ T-cells, macrophages and $CD11c^+$ cells. However, the DMF effect was lost in *Hca2*$^{-/-}$ mice. Moreover, during *in vitro* culture he observed that MMF increased number of neutrophils adherent to bEND.3 cells in WT mice but in *Hca2*$^{-/-}$ mice MMF had no effect. Those results strongly indicate that HCA2 is essential in mediating neuroprotective effects of DMF treatment (Chen et al., 2014). Interestingly, the protective effect of DMF mediated by HCA_2 was also observed in a model of another neutrophils-driven disease, pemphigoid disease (PD). A reduction of the number of infiltrating neutrophils and monocytes into the skin was observed, as well as decreased number of skin lesions, which significantly lowered the disease severity. To test whether the therapeutic effect is mediated by HCA_2, authors of the latter study compared the DMF efficacy in *Hca2*$^{+/+}$ and *Hca2*$^{-/-}$ mice. They reported that a protective effect of DMF, which in *Hca2*$^{-/-}$ mice was lost. Those results strongly indicate that HCA_2 is required for the protective effect of DMF treatment (Wannick et al., 2018). As observed previously in Chen's experiments, DMF significantly improved neurological deficits and disease parameters in mice fed NC diet via HCA_2 (Chen et al., 2014) .

I investigated whether the DMF effect is influenced by the diet. Therefore, I induced EAE in *Hca2*$^{+/+}$ and *Hca2*$^{-/-}$ mice, both fed HFb diet. I provide evidence that DMF reduced the neurological score and improved disease severity in *Hca2*$^{+/+}$ mice, however DMF was ineffective in *Hca2*$^{-/-}$ mice. A key finding was that the DMF effect depends on HCA_2.

It has been reported that diet greatly influences DMFs mode of action. The therapeutic effect is mediated by the *Hca2* receptor. Many immune cells, such as monocytes or T-cells, are involved in the disease pathology, but recent studies suggest a growing role of

neutrophils in MS (Rumble et al., 2015; Shi et al., 2021). I wanted to investigate which immune cells express *Hca2* and mediate the DMF effect, and whether the diet influences the receptor expression. For this purpose, I immunized *Hca2*^{mRFP} mice (Hanson et al., 2010) fed either LA or HFb diet. A key finding of the study was that almost all neutrophils expressed *Hca2* at the very high level regardless of the diet and the treatment. The finding was consistent with other studies (H. Tang et al., 2008; von Glehn et al., 2018). While in monocyte populations, only Ly6C^{int} and Ly6C^{low} were mRFP-positive, almost all Ly6C^{hi} monocytes were mRFP-negative. I could observe a DMF effect on the expression per cell in Ly6C^{int} in HFb diet compared to LA diet. The upregulation of *Hca2* receptor might be associated with a better response to DMF treatment and clinical outcome. Another study showed that human CD14^{+}CD16^{+} monocytes, which resembles murine Ly6C^{int} monocytes adhere to the brain microvasculature contributing to the breakage of the BBB by promoting trafficking of CD4^{+} T-cells into CNS and consequently increase severity (Waschbisch et al., 2016). Another study, in which MS patients were divided into those who responded to DMF treatment and those who did not show that DMF influenced lymphocytes and monocytes subpopulations and had mild transcriptional effect on gene expression in responders compared to non-responders. In both groups the population of monocytes intermediate was decreased, but in non-responders the reduction was more pronounced. After one year of treatment, downregulation of genes related to pro-inflammatory cytokines and their receptors, chemokines, T-lymphocyte regulation and the NF-kB pathway was observed in the response group, which was not present in the non-response group. However, non-responders also demonstrated a downregulation of several genes involved in pro-inflammatory response (Sánchez-Sanz et al., 2023). According to our hypothesis, diets may play a key role in a better response to DMF treatment, and therefore may explain why not all MS patients respond to the drug.

Our results showed the highest *Hca2* expression in neutrophils. Therefore, I further investigated the role of HCA_2 in neutrophils in a cell-specific manner. For that purpose, I crossed *Hca2*$^{Fl/Fl}$ mice with the mouse model called Catchup, in which the neutrophil specific locus Ly6G is modulated with a knock-in allele expressing Cre recombinase and the fluorescent protein tdTomato (Hasenberg et al., 2015). To assess whether recombination was effective, I stimulated neutrophils and measured intracellular Ca^{2+}

concentrations ($[Ca^{2+}]_i$). As mentioned before, NA is one of the agonists of HCA_2 and is a known as antidyslipidemic drug (Hanson et al., 2012). Kostylina et al. reported that in neutrophils, stimulation with NA led to the rapid increase in ($[Ca^{2+}]_i$). Peak level was observed within 1 minute (Kostylina et al., 2008). Similarly, in our experiment I could observe an instant elevation of ($[Ca^{2+}]_i$) concentration in *Hca2*$^{+/+}$ neutrophils after stimulation with NA, but this effect was lost in *Hca2*$^{-/-}$ mice, which suggests a HCA_2-mediated effect. Moreover, when I applied MMF in *Hca2*$^{+/+}$ neutrophils, I observed a prompt increase in ($[Ca^{2+}]_i$) levels as well. Another study that investigated the clinical effect of NA reported that the activation of the receptor led to the mobilization and increased release of ($[Ca^{2+}]_i$) via HCA_2 (Y. Tang et al., 2006). A study from 2020 demonstrated that *Hca2* is expressed not only in human and mice, but also is present in bovine neutrophils. The goal of this study was to investigate the mediating role of HCA_2 in those animals. The researchers showed that NA led to a rapid increase in ($[Ca^{2+}]_i$) mediated by HCA_2. However, they suggested that HCA_2 agonists play different roles in cattle compared to murine and human species (Carretta et al., 2020).

In my experiments, the quantification of cells responsive to NA stimulation showed that *Hca2*$^{Fl/Fl}$ neutrophils responded in a similar manner as *Hca2*$^{+/+}$ neutrophils. However, in Ly6G-Cre *Hca2*^{nKO} mice I observed a significant decrease in the cell number activated by NA and consequently, reduced ($[Ca^{2+}]_i$) mobilization. This data indicates the importance of HCA_2 in neutrophils function. Thus, I further investigated the role of HCA_2 in neutrophils during DMF treatment in the EAE mouse model.

In the last decade, neutrophils became of a great interest as a key player in contributing to neuroinflammation and aggravating the course of MS. They are also considered as a novel MS biomarker and therapeutic target during disease treatment (Rumble et al., 2015). Several *in vivo* studies demonstrated the infiltration of neutrophils into the CNS and lesions during the early stage of disease development and their contribution to inflammation (Christy et al., 2013; Rumble et al., 2015; Steinbach et al., 2013). Moreover, the study demonstrated a massive infiltration of neutrophils into the spinal cord and its accumulation at the sites of axonal loss, demyelinated and degenerated areas during the peak of the disease. The researchers suggested that neutrophils contribute to neuroinflammation not only during the disease onset, but also further drive the destructive

action during the acute phase and consequently leading to more severe disease progression (F. Wu et al., 2010). Similarly, in MS patients, neutrophils were present in cerebrospinal fluid (CSF) during the relapse and during the early stages. Moreover, in CSF collected from MS patients, they found a positive correlation between numbers of neutrophils and IL-17A, secreted by Th17 cells. IL-17A promotes recruitment of neutrophils and contribute to the pro-inflammatory cascade (Kostic et al., 2014). Interestingly, evidence indicated that depletion of neutrophils led to delay of disease onset and reduced EAE severity (Steinbach et al., 2013).

DMF treatment has been shown to affect neutrophil numbers infiltrating into CNS mediated via HCA2 (Chen et al., 2014). Moreover, DMF may also alert the neutrophils' function (Müller et al., 2016). In our EAE mouse model I showed that during the absence of *Hca2* in neutrophils, DMF treatment had no effect on disease improvement. However, in $Hca2^{Fl/Fl}$ animals I observed a significant effect on neurological deficits, as well as delayed disease onset. One of the explanations of a protective effect of DMF mediated by HCA_2 could be an inhibition of neutrophils' activation, by affecting the expression of surface markers, such as CD62L, reducing production of ROS, NETosis and migration (Morrison et al., 2021).

6. Supplements

Supplementary Table 1

Figure	Sample size (n)	Statistical test	Values
Fig. 11C	6-8 wells/group excluded, 2 mice found dead, HFbD	Unpaired Student t-test	HFbD MMF vs. HFbD veh: *T* (14) = 3.99, *p = 0.0013*
Fig. 12B	5-6 wells/group	One-way ANOVA with Bonferroni posthoc test	***LAD*** F (2, 15) = 3,795, *p = 0.0464* CTRL vs. MMF: *p = 0.0447* ***HFbD*** *F* (2, 14) = 5.66, *p = 0.0158* CTRL vs. PMA: *p = 0.0298* PMA vs. MMF: *p = 0.0236*
Fig. 13B	10 (f) mice/group	Two-way ANOVA for AUC with Sidak posthoc test	diet: F (2, 54) = 81.3, *p < 0.0001* treatment: F (1, 54) = 39.89, *p < 0.0001* interaction: F (2,54) = 149.5, p < 0.0001 LAD veh vs. LAD DMF: *p < 0.0001* NCD veh vs. NCD DMF: *p < 0.0001* HFbD veh vs. HFbD DMF: *p < 0.0001*
Fig. 13D, AUC	10 (f) mice/group	Scheirer-Ray-Hare test followed by targeted Mann-Whitney U test; Bonferroni-Holm corrected	diet: χ^2 (2) = 6.39, *p = 0.0268* treatment: χ^2 (1) = 6.44, *p = 0.041* interaction: χ^2 (2) = 7.24, *p = 0.0112*

			HFbD DMF vs. HFbD veh: *p = 0.0148* NCD DMF vs. LAD DMF: *p = 0.0084* HFbD DMF vs. LAD DMF: *p = 0.0095*
Fig.13D, Neuroscore	10 (f) mice/group	Scheirer-Ray-Hare test followed by targeted Mann-Whitney U test; Bonferroni-Holm corrected	diet: χ^2 (2) = 7.55, *p = 0.0229* treatment: χ^2 (1) = 4.74, *p = 0.0295* interaction: χ^2 (2) = 8.97, *p = 0.0113* HFbD DMF vs. HFbD veh: *p = 0.0092* NCD DMF vs. LAD DMF: *p = 0.005* HFbD DMF vs. LAD DMF: *p = 0.0048*
Fig. 13D, Onset	10 (f) mice/group	Scheirer-Ray-Hare test followed by targeted Mann-Whitney U test; Bonferroni-Holm corrected	diet: χ^2 (2) = 4.11, *p = 0.1281* treatment: χ^2 (1) = 13.12, *p < 0.0003* interaction: χ^2 (2) = 6.66, *p = 0.0358* HFbD DMF vs. HFbD veh: *p = 0.0012* NCD DMF vs. LAD DMF: *p = 0.006* HFbD DMF vs. LAD DMF: *p = 0.006*
Fig. 14A	9-10 (f) mice/group	One-way ANOVA	*F* (2, 26) = 22.73, *p = 0.0839*
Fig.14B,	9-10 (f) mice/group	Two – way ANOVA	diet: *F* (2, 52) = 2.59,

Acetic Acid			*p = 0.0842* treatment: *F*(1,52)= 0.7765, *p = 0.3823* interaction: *F* (2,52) = 1.21, *p = 0.3074*
Fig.14B, Propionic Acid	9-10 (f) mice/group	Two – way ANOVA	diet: *F* (2, 52) = 0.05, *p = 0.9512* treatment: *F*(1,52)= 0.6346, *p = 0.4293* interaction: *F* (2,52) = 0.40, *p = 0.6708*
Fig.14C, Alpha diversity	9-10 (f) mice/group	Scheirer-Ray-Hare test followed by targeted Mann-Whitney U test; Bonferroni-Holm corrected	diet: χ^2 (2) = 36.63, *p < 0.0001* treatment: χ^2 (1) = 0.03, *p = 0,8625* interaction: χ^2 (2) = 0.46, *p = 0,4976* HFbD DMF vs. LAD DMF: *p < 0.001* HFbD DMF vs. NCD DMF: *p < 0.001* HFbD veh vs. LAD veh: *p < 0.001* HFbD veh vs. NCD veh: *p < 0.001*
Fig.14E, Prevotellamassila	9-10 (f) mice/group	Scheirer-Ray-Hare test followed by targeted Mann-Whitney U test; Bonferroni-Holm corrected	diet: χ^2 (2) = 26.87, *p < 0.0001* treatment: χ^2 (1) = 0.74, *p = 0,3897* interaction: χ^2 (2) = 0.25, *p = 0,8825* HFbD DMF vs. LAD DMF: *p = 0.0048*

			HFbD DMF vs. NCD DMF: *p = 0.0048* HFbD veh vs. LAD veh: *p = 0.0025* HFbD veh vs. NCD veh: *p = 0.0012*
Fig.14E, *Parabacteriodes*	9-10 (f) mice/group	Scheirer-Ray-Hare test followed by targeted Mann-Whitney U test; Bonferroni-Holm corrected,	diet: χ^2 (2) = 47.08, *p < 0.0001* treatment: χ^2 (1) = 0.01, *p = 0.9203* interaction: χ^2 (2) = 0.75, *p = 0.6873* NCD DMF vs. LAD DMF: *p < 0.001* HFbD DMF vs. LAD DMF: *p < 0.001* HFbD DMF vs. NCD DMF: *p < 0.001* NCD veh vs. LAD veh: *p < 0.001* HFbD veh vs. LAD veh: *p < 0.001* HFbD veh vs. NCD veh: *p < 0.001*
Fig.14E, *Acetatifactor*	9-10 (f) mice/group	Scheirer-Ray-Hare test followed by targeted Mann-Whitney U test; Bonferroni-Holm corrected	diet: χ^2 (2) = 10.20, *p = 0.0061* *treatment:* χ^2 (1) = 1.48, *p = 0.2238* interaction: χ^2 (2) = 6.64, *p = 0.0362* NCD DMF vs. LAD DMF: *p = 0.024* NCD veh vs. LAD veh: *p = 0.0135*

			HFbD veh vs. LAD veh: *p = 0.0441* HFbD DMF vs. HFbD veh: *p = 0.0441*
Fig. 15B	8-10 (3-4f, 5-6m) mice/group; excluded, 4 mice found dead, 2 DMF and 2 Vehicle	Scheirer-Ray-Hare test followed by targeted Mann-Whitney U test; Bonferroni-Holm corrected	genotype: χ^2 (1) = 0.90, *p = 0.3428* treatment: χ^2 (1) = 8.97, *p = 0.0027* interaction: χ^2 (1) = 4.83, *p = 0.028* *Hca2*$^{+/+}$ DMF vs. *Hca2*$^{+/+}$ veh: *p = 0.0052* *Hca2*$^{-/-}$ DMF vs. *Hca2*$^{+/+}$ DMF: *p = 0.0165*
Fig.16D, monocytes intermediate	5-6 (1-4f, 3-5m) mice/group; excluded, 1 mouse terminated due to eczema, LAD/DMF	Two-way ANOVA, with Bonferroni posthoc test	diet: *F* (1,19) = 7.76, *p = 0.0118* treatment: *F* (1,19) = *0.99*, *p = 0.3325* interaction: *F* (1,19) = 0.34, *p = 0.5675* HFbD veh vs. LAD veh: *p = 0.0493*
Fig.16F, monocytes high	5-6 (1-4f, 3-5m) mice/group; excluded, 1 mouse terminated due to eczema, LAD/DMF	Two – way ANOVA with Bonferroni posthoc test	diet: *F* (1, 19) = 4.70, *p = 0.0431* treatment: *F* (1,19) = 1.07, *p = 0.3142* interaction: *F* (1,19) = 0.68, *p = 0.4181* HFbD DMF vs. LAD DMF: *p = 0.1047* HFbD veh vs. LAD veh: *p = 0.6874*

Fig. 17B	4 (1-3f, 1-3m) mice/group, 50 cells/mouse	One-way ANOVA with Bonferroni posthoc test	*F* (3,12) = 35.00, *p* < 0.0001 *Hca2*$^{Fl/Fl}$ vs. *Hca2*^{nKO}*:* *p = 0.0089* *Hca2*$^{+/+}$ vs. *Hca2*$^{-/-}$*:* *p = <0.0001* *Hca2*$^{+/+}$ vs. *Hca2*^{nKO} *p = 0.0014*
Fig. 18B, AUC	10-13 (5-7f, 4-8m) mice/group	Scheirer-Ray-Hare test followed by targeted Mann-Whitney U test; Bonferroni-Holm corrected	treatment: χ^2 (1) = 10.35, *p = 0.0013* *genotype:* χ^2 (1) = 0.39, *p = 0.5323* interaction: χ^2 (1) = 2.30, *p = 0.1294* *Hca2*$^{Fl/Fl}$ DMF vs. *Hca2*$^{Fl/Fl}$ veh: *p = 0.0038*

7. References

Altieri, C., Speranza, B., Corbo, M. R., Sinigaglia, M., & Bevilacqua, A. (2023). Gut-Microbiota, and Multiple Sclerosis: Background, Evidence, and Perspectives. *Nutrients*, *15*(4). https://doi.org/10.3390/nu15040942

Altschul, R., Hoffer, A., & Stephen, J. D. (1955). Influence of nicotinic acid on serum cholesterol in man. *Archives of Biochemistry and Biophysics*, *54*(2), 558–559. https://doi.org/10.1016/0003-9861(55)90070-9

Ascherio, A. (2013). Environmental factors in multiple sclerosis. *Expert Review of Neurotherapeutics*, *13*(sup2), 3–9. https://doi.org/10.1586/14737175.2013.865866

Attfield, K. E., Jensen, L. T., Kaufmann, M., Friese, M. A., & Fugger, L. (2022). The immunology of multiple sclerosis. *Nature Reviews Immunology*, *22*(12), 734–750. https://doi.org/10.1038/s41577-022-00718-z

Basu, S., Hodgson, G., Katz, M., & Dunn, A. R. (2002). Evaluation of role of G-CSF in the production, survival, and release of neutrophils from bone marrow into circulation. *Blood*, *100*(3), 854–861. https://doi.org/10.1182/blood.V100.3.854

Beatty, W. W., & Aupperle, R. L. (2002). Sex differences in cognitive impairment in multiple sclerosis. *Clinical Neuropsychologist*, *16*(4), 472–480. https://doi.org/10.1076/clin.16.4.472.13904

Benyó, Z., Gille, A., Bennett, C. L., Clausen, B. E., & Offermanns, S. (2006). Nicotinic acid-induced flushing is mediated by activation of epidermal langerhans cells. *Molecular Pharmacology*, *70*(6), 1844–1849. https://doi.org/10.1124/mol.106.030833

Bitsch, A., Schuchardt, J., Bunkowski, S., Kuhlmann, T., & Brück, W. (2000). Acute axonal injury in multiple sclerosis Correlation with demyelination and inflammation. In *Brain* (Vol. 123).

Bobileva, O., Bokaldere, R., Gailite, V., Kaula, I., Ikaunieks, M., Duburs, G., Petrovska, R., Mandrika, I., Klovins, J., & Loza, E. (2014). Synthesis and evaluation of (E)-2-(acrylamido)cyclohex-1-enecarboxylic acid derivatives as HCA1, HCA2, and HCA3 receptor agonists. *Bioorganic and Medicinal Chemistry*, *22*(14), 3654–3669. https://doi.org/10.1016/j.bmc.2014.05.011

Boegel, S., Löwer, M., Bukur, T., Sorn, P., Castle, J. C., & Sahin, U. (2018). HLA and proteasome expression body map. *BMC Medical Genomics*, *11*(1), 1–12. https://doi.org/10.1186/s12920-018-0354-x

Boets, E., Deroover, L., Houben, E., Vermeulen, K., Gomand, S. V., Delcour, J. A., & Verbeke, K. (2015). Quantification of in vivo colonic short chain fatty acid production from inulin. *Nutrients*, *7*(11), 8916–8929. https://doi.org/10.3390/nu7115440

Bomprezzi, R. (2015). Dimethyl fumarate in the treatment of relapsing-remitting multiple sclerosis: An overview. *Therapeutic Advances in Neurological Disorders*, *8*(1), 20–30. https://doi.org/10.1177/1756285614564152

Brownlee, W. J., Hardy, T. A., Fazekas, F., & Miller, D. H. (2017). Diagnosis of multiple sclerosis: progress and challenges. *The Lancet*, *389*(10076), 1336–1346. https://doi.org/10.1016/S0140-6736(16)30959-X

Burdon, P. C. E., Martin, C., & Rankin, S. M. (2008). Migration across the sinusoidal endothelium regulates neutrophil mobilization in response to ELR + CXC chemokines. *British Journal of Haematology*, *142*(1), 100–108. https://doi.org/10.1111/j.1365-2141.2008.07018.x

Carretta, M. D., Barría, Y., Borquez, K., Urra, B., Rivera, A., Alarcón, P., Hidalgo, M. A., & Burgos, R. A. (2020). β-hydroxybutyrate and hydroxycarboxylic acid receptor 2 agonists activate the AKT, ERK and AMPK pathways, which are involved in bovine neutrophil chemotaxis. *Scientific Reports*, *10*(1), 1–13. https://doi.org/10.1038/s41598-020-69500-2

Cekanaviciute, E., Yoo, B. B., Runia, T. F., Debelius, J. W., Singh, S., Nelson, C. A., Kanner, R., Bencosme, Y., Lee, Y. K., Hauser, S. L., Crabtree-Hartman, E., Sand, I. K., Gacias, M., Zhu, Y., Casaccia, P., Cree, B. A. C., Knight, R., Mazmanian, S. K., & Baranzini, S. E. (2017). Gut bacteria from multiple sclerosis patients modulate human T cells and exacerbate symptoms in mouse models. *Proceedings of the National Academy of Sciences of the United States of America*, *114*(40), 10713–10718. https://doi.org/10.1073/pnas.1711235114

Chen, H., Assmann, J. C., Krenz, A., Rahman, M., Grimm, M., Karsten, C. M., Köhl, J., Offermanns, S., Wettschureck, N., & Schwaninger, M. (2014). Hydroxycarboxylic

acid receptor 2 mediates dimethyl fumarate's protective effect in EAE. *Journal of Clinical Investigation*, *124*(5), 2188–2192. https://doi.org/10.1172/JCI72151

Christy, A. L., Walker, M. E., Hessner, M. J., & Brown, M. A. (2013). Mast cell activation and neutrophil recruitment promotes early and robust inflammation in the meninges in EAE. *Journal of Autoimmunity*, *42*, 50–61. https://doi.org/10.1016/j.jaut.2012.11.003

Chu, F., Shi, M., Lang, Y., Shen, D., Jin, T., Zhu, J., & Cui, L. (2018a). Gut microbiota in multiple sclerosis and experimental autoimmune encephalomyelitis: current applications and future perspectives. *Mediators of Inflammation*, *2018*. https://doi.org/10.1155/2018/8168717

Chu, F., Shi, M., Lang, Y., Shen, D., Jin, T., Zhu, J., & Cui, L. (2018b). Gut microbiota in multiple sclerosis and experimental autoimmune encephalomyelitis: current applications and future perspectives. *Mediators of Inflammation*, *2018*. https://doi.org/10.1155/2018/8168717

Clemente, J. C., Ursell, L. K., Parfrey, L. W., & Knight, R. (2012). The impact of the gut microbiota on human health: An integrative view. *Cell*, *148*(6), 1258–1270. https://doi.org/10.1016/j.cell.2012.01.035

Cohen, J. A., Barkhof, F., Comi, G., Hartung, H.-P., Khatri, B. O., Montalban, X., Pelletier, J., Capra, R., Gallo, P., Izquierdo, G., Tiel-Wilck, K., de Vera, A., Jin, J., Stites, T., Wu, S., Aradhye, S., & Kappos, L. (2010). Oral Fingolimod or Intramuscular Interferon for Relapsing Multiple Sclerosis. *New England Journal of Medicine*, *362*(5), 402–415. https://doi.org/10.1056/nejmoa0907839

Collongues, N., Patte-Mensah, C., De Seze, J., Mensah-Nyagan, A. G., & Derfuss, T. (2018). Testosterone and estrogen in multiple sclerosis: from pathophysiology to therapeutics. *Expert Review of Neurotherapeutics*, *18*(6), 515–522. https://doi.org/10.1080/14737175.2018.1481390

Compston, A., & Coles, A. (2008). Multiple sclerosis. *The Lancet*, *372*(9648), 1502–1517. https://doi.org/10.1016/S0140-6736(08)61620-7

Correale, J., & Marrodan, M. (2022). Multiple sclerosis and obesity: The role of adipokines. *Frontiers in Immunology*, *13*(November), 1–14. https://doi.org/10.3389/fimmu.2022.1038393

Corrêa-Oliveira, R., Fachi, J. L., Vieira, A., Sato, F. T., & Vinolo, M. A. R. (2016). Regulation of immune cell function by short-chain fatty acids. *Clinical and Translational Immunology*, *5*(4), 1–8. https://doi.org/10.1038/cti.2016.17

Cottreau, J., Tucker, A., Crutchley, R., & Garey, K. W. (2012). Crofelemer for the treatment of secretory diarrhea. *Expert Review of Gastroenterology and Hepatology*, *6*(1), 17–23. https://doi.org/10.1586/egh.11.87

Coyle, P. K. (2021). What can we learn from sex differences in MS? *Journal of Personalized Medicine*, *11*(10). https://doi.org/10.3390/jpm11101006

Dalile, B., Van Oudenhove, L., Vervliet, B., & Verbeke, K. (2019). The role of short-chain fatty acids in microbiota–gut–brain communication. *Nature Reviews Gastroenterology and Hepatology*, *16*(8), 461–478. https://doi.org/10.1038/s41575-019-0157-3

Dargahi, N., Katsara, M., Tselios, T., Androutsou, M. E., De Courten, M., Matsoukas, J., & Apostolopoulos, V. (2017). Multiple sclerosis: Immunopathology and treatment update. *Brain Sciences*, *7*(7), 1–27. https://doi.org/10.3390/brainsci7070078

Das Sarma, J., Ciric, B., Marek, R., Sadhukhan, S., Caruso, M. L., Shafagh, J., Fitzgerald, D. C., Shindler, K. S., & Rostami, A. M. (2009). Functional interleukin-17 receptor A is expressed in central nervous system glia and upregulated in experimental autoimmune encephalomyelitis. *Journal of Neuroinflammation*, *6*, 1–12. https://doi.org/10.1186/1742-2094-6-14

Debebe, B. J., Boelen, L., Lee, J. C., Thio, C. L., Astemborski, J., Kirk, G., Khakoo, S. I., Donfield, S. M., Goedert, J. J., Asquith, B., Sanders, E. J., Anzala, O., Kamali, A., Kaleebu, P., Karita, E., Kilembe, W., Inambao, M., Lakhi, S., Allen, S., … Tang, J. (2020). Identifying the immune interactions underlying HLA class I disease associations. *ELife*, *9*, 1–43. https://doi.org/10.7554/eLife.54558

Del Negro, I., Pez, S., Versace, S., Marziali, A., Gigli, G. L., Tereshko, Y., & Valente, M. (2024). Impact of Disease-Modifying Therapies on Gut–Brain Axis in Multiple Sclerosis. *Medicina (Lithuania)*, *60*(1). https://doi.org/10.3390/medicina60010006

Dendrou, C. A., Fugger, L., & Friese, M. A. (2015). Immunopathology of multiple sclerosis. *Nature Reviews Immunology*, *15*(9), 545–558. https://doi.org/10.1038/nri3871

Diebold, M., Meola, M., Purushothaman, S., Siewert, L. K., Pössnecker, E., Roloff, T., Lindberg, R. L. P., Kuhle, J., Kappos, L., Derfuss, T., Egli, A., & Pröbstel, A. K. (2022). Gut microbiota composition as a candidate risk factor for dimethyl fumarate-induced lymphopenia in multiple sclerosis. *Gut Microbes*, *14*(1). https://doi.org/10.1080/19490976.2022.2147055

D.M.W., B. (2015). Fumaric acid esters in the management of psoriasis. *Psoriasis: Targets and Therapy*, *5*, 9–23.

Dobson, R., Ramagopalan, S., Davis, A., & Giovannoni, G. (2013). Cerebrospinal fluid oligoclonal bands in multiple sclerosis and clinically isolated syndromes: A meta-analysis of prevalence, prognosis and effect of latitude. *Journal of Neurology, Neurosurgery and Psychiatry*, *84*(8), 909–914. https://doi.org/10.1136/jnnp-2012-304695

Donohoe, D. R., Garge, N., Zhang, X., Sun, W., O'Connell, T. M., Bunger, M. K., & Bultman, S. J. (2011). Microbiome, The Regulate, Butyrate Metabolism, Energy. *Cell Metabolism*, *13*(5), 517–526. https://doi.org/10.1016/j.cmet.2011.02.018.The

Dubrall, D., Pflock, R., Kosinska, J., Schmid, M., Bleich, M., Himmerkus, N., Offermanns, S., Schwaninger, M., & Sachs, B. (2021). Do dimethyl fumarate and nicotinic acid elicit common, potentially HCA2-mediated adverse reactions? A combined epidemiological-experimental approach. *British Journal of Clinical Pharmacology*, *87*(10), 3813–3824. https://doi.org/10.1111/bcp.14787

Fan, Y., & Pedersen, O. (2021). Gut microbiota in human metabolic health and disease. *Nature Reviews Microbiology*, *19*(1), 55–71. https://doi.org/10.1038/s41579-020-0433-9

Fauser, J. K., Matthews, G. M., Cummins, A. G., & Howarth, G. S. (2014). Induction of apoptosis by the medium-chain length fatty acid lauric acid in colon cancer cells due to induction of oxidative stress. *Chemotherapy*, *59*(3), 214–224. https://doi.org/10.1159/000356067

Fellows, R., Denizot, J., Stellato, C., Cuomo, A., Jain, P., Stoyanova, E., Balázsi, S., Hajnády, Z., Liebert, A., Kazakevych, J., Blackburn, H., Corrêa, R. O., Fachi, J. L., Sato, F. T., Ribeiro, W. R., Ferreira, C. M., Perée, H., Spagnuolo, M., Mattiuz, R., … Varga-Weisz, P. (2018). Microbiota derived short chain fatty acids promote histone

crotonylation in the colon through histone deacetylases. *Nature Communications*, *9*(1), 1–15. https://doi.org/10.1038/s41467-017-02651-5

Ferri, C., Castellazzi, M., Merli, N., Laudisi, M., Baldin, E., Baldi, E., Mancabelli, L., Ventura, M., & Pugliatti, M. (2023a). Gut Microbiota Changes during Dimethyl Fumarate Treatment in Patients with Multiple Sclerosis. *International Journal of Molecular Sciences*, *24*(3). https://doi.org/10.3390/ijms24032720

Ferri, C., Castellazzi, M., Merli, N., Laudisi, M., Baldin, E., Baldi, E., Mancabelli, L., Ventura, M., & Pugliatti, M. (2023b). Gut Microbiota Changes during Dimethyl Fumarate Treatment in Patients with Multiple Sclerosis. *International Journal of Molecular Sciences*, *24*(3). https://doi.org/10.3390/ijms24032720

Filippi, M., Bar-, A., Piehl, F., Preziosa, P., Solari, A., Vukusic, S., & Rocca, M. A. (2018). *Mulitple sclerosis*. 1–27.

Filippi, M., Preziosa, P., Banwell, B. L., Barkhof, F., Ciccarelli, O., De Stefano, N., Geurts, J. J. G., Paul, F., Reich, D. S., Toosy, A. T., Traboulsee, A., Wattjes, M. P., Yousry, T. A., Gass, A., Lubetzki, C., Weinshenker, B. G., & Rocca, M. A. (2019). Assessment of lesions on magnetic resonance imaging in multiple sclerosis: practical guidelines. *Brain*, *142*(7), 1858–1875. https://doi.org/10.1093/brain/awz144

Fung, T. C. (2020). The microbiota-immune axis as a central mediator of gut-brain communication. *Neurobiology of Disease*, *136*, 104714. https://doi.org/10.1016/j.nbd.2019.104714

Futosi, K., Fodor, S., & Mócsai, A. (2013). Neutrophil cell surface receptors and their intracellular signal transduction pathways. *International Immunopharmacology*, *17*(3), 638–650. https://doi.org/10.1016/j.intimp.2013.06.034

Gambhir, D., Ananth, S., Veeranan-Karmegam, R., Elangovan, S., Hester, S., Jennings, E., Offermanns, S., Nussbaum, J. J., Smith, S. B., Thangaraju, M., Ganapathy, V., & Martin, P. M. (2012). GPR109A as an anti-inflammatory receptor in retinal pigment epithelial cells and its relevance to diabetic retinopathy. *Investigative Ophthalmology & Visual Science*, *53*(4), 2208–2217. https://doi.org/10.1167/iovs.11-8447

Ghasemi, N., Razavi, S., & Nikzad, E. (2017). Multiple Sclerosis: Pathogenesis, Symptoms, Diagnoses and Cell-Based Therapy Citation: Ghasemi N, Razavi Sh,

Nikzad E. Multiple sclerosis: pathogenesis, symptoms, diagnoses and cell-based therapy. *Cell Journal*, *19*(191), 1–10. https://doi.org/10.22074/cellj.2016.4867

Gianfrancesco, M., & Barcellos, L. (2016). Obesity and Multiple Sclerosis Susceptibility: A Review. *Journal of Neurology & Neuromedicine*, *1*(7), 1–5. https://doi.org/10.29245/2572.942x/2016/7.1064

Gold, R., Arnold, D. L., Bar-Or, A., Fox, R. J., Kappos, L., Mokliatchouk, O., Jiang, X., Lyons, J., Kapadia, S., & Miller, C. (2022). Long-term safety and efficacy of dimethyl fumarate for up to 13 years in patients with relapsing-remitting multiple sclerosis: Final ENDORSE study results. *Multiple Sclerosis Journal*, *28*(5), 801–816. https://doi.org/10.1177/13524585211037909

Golden, L. C., & Voskuhl, R. (2017). The importance of studying sex differences in disease: The example of multiple sclerosis. *Journal of Neuroscience Research*, *95*(1–2), 633–643. https://doi.org/10.1002/jnr.23955

Grigoriadis, N., & van Pesch, V. (2015). A basic overview of multiple sclerosis immunopathology. *European Journal of Neurology*, *22*, 3–13. https://doi.org/10.1111/ene.12798

Haase, S., Haghikia, A., Gold, R., & Linker, R. A. (2018). Dietary fatty acids and susceptibility to multiple sclerosis. *Multiple Sclerosis*, *24*(1), 12–16. https://doi.org/10.1177/1352458517737372

Haghikia, A., Jörg, S., Duscha, A., Berg, J., Manzel, A., Waschbisch, A., Hammer, A., Lee, D. H., May, C., Wilck, N., Balogh, A., Ostermann, A. I., Schebb, N. H., Akkad, D. A., Grohme, D. A., Kleinewietfeld, M., Kempa, S., Thöne, J., Demir, S., … Linker, R. A. (2015). Dietary Fatty Acids Directly Impact Central Nervous System Autoimmunity via the Small Intestine. *Immunity*, *43*(4), 817–829. https://doi.org/10.1016/j.immuni.2015.09.007

Han, R., Xiao, J., Zhai, H., & Hao, J. (2016). Dimethyl fumarate attenuates experimental autoimmune neuritis through the nuclear factor erythroid-derived 2-related factor 2/hemoxygenase-1 pathway by altering the balance of M1/M2 macrophages. *Journal of Neuroinflammation*, *13*(1), 1–14. https://doi.org/10.1186/s12974-016-0559-x

Hanson, J., Gille, A., & Offermanns, S. (2012). Role of HCA2 (GPR109A) in nicotinic acid and fumaric acid ester-induced effects on the skin. *Pharmacology and Therapeutics*, *136*(1), 1–7. https://doi.org/10.1016/j.pharmthera.2012.06.003

Hanson, J., Gille, A., Zwykiel, S., Lukasova, M., Clausen, B. E., Ahmed, K., Tunaru, S., Wirth, A., & Offermanns, S. (2010). Nicotinic acid- and monomethyl fumarate-induced flushing involves GPR109A expressed by keratinocytes and COX-2-dependent prostanoid formation in mice. *Journal of Clinical Investigation*, *120*(8), 2910–2919. https://doi.org/10.1172/JCI42273

Hartung, H. P., Graf, J., Aktas, O., Mares, J., & Barnett, M. H. (2019). Diagnosis of multiple sclerosis: Revisions of the McDonald criteria 2017 - Continuity and change. In *Current Opinion in Neurology* (Vol. 32, Issue 3, pp. 327–337). Lippincott Williams and Wilkins. https://doi.org/10.1097/WCO.0000000000000699

Hasenberg, A., Hasenberg, M., Männ, L., Neumann, F., Borkenstein, L., Stecher, M., Kraus, A., Engel, D. R., Klingberg, A., Seddigh, P., Abdullah, Z., Klebow, S., Engelmann, S., Reinhold, A., Brandau, S., Seeling, M., Waisman, A., Schraven, B., Göthert, J. R., … Gunzer, M. (2015). Catchup: A mouse model for imaging-based tracking and modulation of neutrophil granulocytes. *Nature Methods*, *12*(5), 445–452. https://doi.org/10.1038/nmeth.3322

Hauser, S. L., & Cree, B. A. C. (2020). Treatment of Multiple Sclerosis: A Review. *American Journal of Medicine*, *133*(12), 1380-1390.e2. https://doi.org/10.1016/j.amjmed.2020.05.049

Havrdova, E., Giovannoni, G., Gold, R., Fox, R. J., Kappos, L., Phillips, J. T., Okwuokenye, M., & Marantz, J. L. (2017). Effect of delayed-release dimethyl fumarate on no evidence of disease activity in relapsing–remitting multiple sclerosis: integrated analysis of the phase III DEFINE and CONFIRM studies. *European Journal of Neurology*, *24*(5), 726–733. https://doi.org/10.1111/ene.13272

Hoffmann, J. H. O., Schaekel, K., Hartl, D., Enk, A. H., & Hadaschik, E. N. (2018). Dimethyl fumarate modulates neutrophil extracellular trap formation in a glutathione- and superoxide-dependent manner. *The British Journal of Dermatology*, *178*(1), 207–214. https://doi.org/10.1111/bjd.15839

Huang, W. J., Chen, W. W., & Zhang, X. (2017). Multiple sclerosis: Pathology, diagnosis and treatments (review). *Experimental and Therapeutic Medicine*, *13*(6), 3163–3166. https://doi.org/10.3892/etm.2017.4410

Huppert, J., Closhen, D., Croxford, A., White, R., Kulig, P., Pietrowski, E., Bechmann, I., Becher, B., Luhmann, H. J., Waisman, A., & Kuhlmann, C. R. W. (2010). Cellular mechanisms of IL-17-induced blood-brain barrier disruption. *The FASEB Journal*, *24*(4), 1023–1034. https://doi.org/10.1096/fj.09-141978

Ifergan, I., Kébir, H., Bernard, M., Wosik, K., Dodelet-Devillers, A., Cayrol, R., Arbour, N., & Prat, A. (2008). The blood-brain barrier induces differentiation of migrating monocytes into Th17-polarizing dendritic cells. *Brain*, *131*(3), 785–799. https://doi.org/10.1093/brain/awm295

Jacobs, L. D., Cookfair, D. L., Rudick, R. A., Herndon, R. M., Richert, J. R., Salazar, A. M., Fischer, J. S., Goodkin, D. E., Granger, C. V., Simon, J. H., Alam, J. J., Bartoszak, D. M., Bourdette, D. N., Braiman, J., Brownscheidle, C. M., Coats, M. E., Cohan, S. L., Dougherty, D. S., Kinkel, R. P., … Whitham, R. H. (1996). Intramuscular interferon beta-1a for disease progression in relapsing multiple sclerosis. *Annals of Neurology*, *39*(3), 285–294. https://doi.org/10.1002/ana.410390304

Jangi, S., Gandhi, R., Cox, L. M., Li, N., Von Glehn, F., Yan, R., Patel, B., Mazzola, M. A., Liu, S., Glanz, B. L., Cook, S., Tankou, S., Stuart, F., Melo, K., Nejad, P., Smith, K., Topçuolu, B. D., Holden, J., Kivisäkk, P., … Weiner, H. L. (2016). Alterations of the human gut microbiome in multiple sclerosis. *Nature Communications*, *7*(May). https://doi.org/10.1038/ncomms12015

Johnson, K. P., Brooks, B. R., Cohen, J. A., Ford, C. C., Goldstein, J., Lisak, R. P., Myers, L. W., Panitch, H. S., Rose, J. W., Schiffer, R. B., Vollmer, T., Weiner, L. P., & Wolinsky, J. S. (1998). Extended use of glatiramer acetate (Copaxone) is well tolerated and maintains its clinical effect on multiple sclerosis relapse rate and degree of disability. *Neurology*, *50*(3), 701–708. https://doi.org/10.1212/WNL.50.3.701

Johnson, K. P., Brooks, B. R., Cohen, J. A., Ford, C. C., Goldstein, J., Lisak, R. P., Myers, L. W., Panitch, H. S., Rose, J. W., Schiffer, R. B., Vollmer, T., Weiner, L. P., Wolinsky, J. S., Bird, S. J., Kolson, D. L., Gonzalez–scarano, F., Brennan, D., Pfohl, D.,

Mandler, R. N., … Gomolin, I. H. (1995). Copolymer 1 reduces relapse rate and improves disability in relapsing-remitting multiple sclerosis: Results of a phase III multicenter, double-blind placebo-controlled trial. *Neurology*, *45*(7), 1268–1276. https://doi.org/10.1212/WNL.45.7.1268

Kamp, M. E., Shim, R., Nicholls, A. J., Oliveira, A. C., Mason, L. J., Binge, L., Mackay, C. R., & Wong, C. H. Y. (2016). G protein-coupled receptor 43 modulates neutrophil recruitment during acute inflammation. *PLoS ONE*, *11*(9), 1–15. https://doi.org/10.1371/journal.pone.0163750

Kasper, L., Chitnis, T., Avila, M., Sconzo, N., Ashton, R., & Rametta, M. (2019). *in Multiple Sclerosis*. 82–90.

Katz Sand, I., Zhu, Y., Ntranos, A., Clemente, J. C., Cekanaviciute, E., Brandstadter, R., Crabtree-Hartman, E., Singh, S., Bencosme, Y., Debelius, J., Knight, R., Cree, B. A. C., Baranzini, S. E., & Casaccia, P. (2019). Disease-modifying therapies alter gut microbial composition in MS. *Neurology: Neuroimmunology and NeuroInflammation*, *6*(1), 1–13. https://doi.org/10.1212/NXI.0000000000000517

Kieseier, B. C. (2011). The mechanism of action of interferon-β in relapsing multiple sclerosis. *CNS Drugs*, *25*(6), 491–502. https://doi.org/10.2165/11591110-000000000-00000

Kits, H., Kit, H., Emulsion, C. F. a, Ptx, C. F. a E., & Ptxx, C. F. a E. (2014). *EAE Induction by Active Immunization in SJL Mice*. *2*(1003), 1–5.

Klineova, S., & Lublin, F. D. (2018). Clinical course of multiple sclerosis. *Cold Spring Harbor Perspectives in Medicine*, *8*(9), 1–12. https://doi.org/10.1101/cshperspect.a028928

Kornek, B., Storch, M. K., Weissert, R., Wallstroem, E., Stefferl, A., Olsson, T., Linington, C., Schmidbauer, M., & Lassmann, H. (2000). Multiple sclerosis and chronic autoimmune encephalomyelitis: A comparative quantitative study of axonal injury in active, inactive, and remyelinated lesions. *American Journal of Pathology*, *157*(1), 267–276. https://doi.org/10.1016/S0002-9440(10)64537-3

Kostic, M., Dzopalic, T., Zivanovic, S., Zivkovic, N., Cvetanovic, A., Stojanovic, I., Vojinovic, S., Marjanovic, G., Savic, V., & Colic, M. (2014). IL-17 and Glutamate

Excitotoxicity in the Pathogenesis of Multiple Sclerosis. *Scandinavian Journal of Immunology*, *79*(3), 181–186. https://doi.org/10.1111/sji.12147

Kostylina, G., Simon, D., Fey, M. F., Yousefi, S., & Simon, H. U. (2008). Neutrophil apoptosis mediated by nicotinic acid receptors (GPR109A). *Cell Death and Differentiation*, *15*(1), 134–142. https://doi.org/10.1038/sj.cdd.4402238

Kreiter, S., Vormehr, M., Van De Roemer, N., Diken, M., Löwer, M., Diekmann, J., Boegel, S., Schrörs, B., Vascotto, F., Castle, J. C., Tadmor, A. D., Schoenberger, S. P., Huber, C., Türeci, O., & Sahin, U. (2015). Mutant MHC class II epitopes drive therapeutic immune responses to cancer. *Nature*, *520*(7549), 692–696. https://doi.org/10.1038/nature14426

Lange, A. P., Secher, N. J., & Amery, W. (1977). Prostaglandin-Induced Diarrhoea Treated with Loperamide or Diphenoxylate: A Double-Blind Study. *Acta Medica Scandinavica*, *202*(1–6), 449–454. https://doi.org/10.1111/j.0954-6820.1977.tb16863.x

Lassmann, H. (2018). Multiple sclerosis pathology. *Cold Spring Harbor Perspectives in Medicine*, *8*(3), 1–16. https://doi.org/10.1101/cshperspect.a028936

Lehmann, D. M., Seneviratne, A. M. P. B., & Smrcka, A. V. (2008). Small molecule disruption of G protein βγ subunit signaling inhibits neutrophil chemotaxis and inflammation. *Molecular Pharmacology*, *73*(2), 410–418. https://doi.org/10.1124/mol.107.041780

Li, G., Lin, J., Zhang, C., Gao, H., Lu, H., Gao, X., Zhu, R., Li, Z., Li, M., & Liu, Z. (2021). Microbiota metabolite butyrate constrains neutrophil functions and ameliorates mucosal inflammation in inflammatory bowel disease. *Gut Microbes*, *13*(1), 1–19. https://doi.org/10.1080/19490976.2021.1968257

Li, H., Sheppard, D. N., & Hug, M. J. (2004). Transepithelial electrical measurements with the Ussing chamber. *Journal of Cystic Fibrosis*, *3*(SUPPL. 2), 123–126. https://doi.org/10.1016/j.jcf.2004.05.026

Li, Y., Liu, J., Cui, Y., Cao, Y., Xu, P., Kan, X., Guo, W., & Fu, S. (2022). Sodium butyrate attenuates bovine mammary epithelial cell injury by inhibiting the formation of neutrophil extracellular traps. *International Immunopharmacology*, *110*, 109009. https://doi.org/https://doi.org/10.1016/j.intimp.2022.109009

Lie, I. A., Weeda, M. M., Mattiesing, R. M., Mol, M. A. E., Pouwels, P. J. W., Barkhof, F., Torkildsen, Ø., Bø, L., Myhr, K. M., & Vrenken, H. (2022). Relationship between White Matter Lesions and Gray Matter Atrophy in Multiple Sclerosis. *Neurology*, *98*(15), E1562–E1573. https://doi.org/10.1212/WNL.0000000000200006

Linker, R. A., & Gold, R. (2013). Dimethyl fumarate for treatment of multiple sclerosis: Mechanism of action, effectiveness, and side effects. *Current Neurology and Neuroscience Reports*, *13*(11). https://doi.org/10.1007/s11910-013-0394-8

Litjens, N. H. R., Burggraaf, J., Van Strijen, E., Van Gulpen, C., Mattie, H., Schoemaker, R. C., Van Dissel, J. T., Thio, H. B., & Nibbering, P. H. (2004). Pharmacokinetics of oral fumarates in healthy subjects. *British Journal of Clinical Pharmacology*, *58*(4), 429–432. https://doi.org/10.1111/j.1365-2125.2004.02145.x

Lublin, F. D., Reingold, S. C., Cohen, J. A., Cutter, G. R., Sørensen, P. S., Thompson, A. J., Wolinsky, J. S., Balcer, L. J., Banwell, B., Barkhof, F., Bebo, B., Calabresi, P. A., Clanet, M., Comi, G., Fox, R. J., Freedman, M. S., Goodman, A. D., Inglese, M., Kappos, L., … Polman, C. H. (2014). Defining the clinical course of multiple sclerosis: The 2013 revisions. *Neurology*, *83*(3), 278–286. https://doi.org/10.1212/WNL.0000000000000560

Ma, Q. (2013). Role of Nrf2 in oxidative stress and toxicity. *Annual Review of Pharmacology and Toxicology*, *53*(1), 401–426. https://doi.org/10.1146/annurev-pharmtox-011112-140320

Martin, R., Sospedra, M., Eiermann, T., & Olsson, T. (2021). Multiple sclerosis: doubling down on MHC. *Trends in Genetics*, *37*(9), 784–797. https://doi.org/10.1016/j.tig.2021.04.012

Masucci, M. T., Minopoli, M., Del Vecchio, S., & Carriero, M. V. (2020). The Emerging Role of Neutrophil Extracellular Traps (NETs) in Tumor Progression and Metastasis. *Frontiers in Immunology*, *11*(September), 1–7. https://doi.org/10.3389/fimmu.2020.01749

Mehta, D., Miller, C., Arnold, D. L., Bame, E., Bar-Or, A., Gold, R., Hanna, J., Kappos, L., Liu, S., Matta, A., Phillips, J. T., Robertson, D., von Hehn, C. A., Campbell, J., Spach, K., Yang, L., & Fox, R. J. (2019). Effect of dimethyl fumarate on lymphocytes in

RRMS: Implications for clinical practice. *Neurology*, *92*(15), e1724–e1738. https://doi.org/10.1212/WNL.0000000000007262

Menzel, T., Lührs, H., Zirlik, S., Schauber, J., Kudlich, T., Gerke, T., Gostner, A., Neumann, M., Melcher, R., & Scheppach, W. (2004). Butyrate inhibits leukocyte adhesion to endothelial cells via modulation of VCAM-1. *Inflammatory Bowel Diseases*, *10*(2), 122–128. https://doi.org/10.1097/00054725-200403000-00010

Mestas, J., & Hughes, C. C. W. (2004). Of Mice and Not Men: Differences between Mouse and Human Immunology. *The Journal of Immunology*, *172*(5), 2731–2738. https://doi.org/10.4049/jimmunol.172.5.2731

Miclea, A., Bagnoud, M., Chan, A., & Hoepner, R. (2020). A Brief Review of the Effects of Vitamin D on Multiple Sclerosis. *Frontiers in Immunology*, *11*(May), 1–10. https://doi.org/10.3389/fimmu.2020.00781

Mirza, A., & Mao-Draayer, Y. (2017). The gut microbiome and microbial translocation in multiple sclerosis. *Clinical Immunology*, *183*, 213–224. https://doi.org/10.1016/j.clim.2017.03.001

Mitchell, R. W., On, N. H., Del Bigio, M. R., Miller, D. W., & Hatch, G. M. (2011). Fatty acid transport protein expression in human brain and potential role in fatty acid transport across human brain microvessel endothelial cells. *Journal of Neurochemistry*, *117*(4), 735–746. https://doi.org/10.1111/j.1471-4159.2011.07245.x

Mócsai, A., Bánfi, B., Kapus, A., Farkas, G., Geiszt, M., Buday, L., Faragó, A., & Ligeti, E. (1997). Differential effects of tyrosine kinase inhibitors and an inhibitor of the mitogen-activated protein kinase cascade on degranulation and superoxide production of human neutrophil granulocytes. *Biochemical Pharmacology*, *54*(7), 781–789. https://doi.org/10.1016/S0006-2952(97)00245-1

Mócsai, A., Jakus, Z., Vántus, T., Berton, G., Lowell, C. A., & Ligeti, E. (2000). Kinase Pathways in Chemoattractant-Induced Degranulation of Neutrophils: The Role of p38 Mitogen-Activated Protein Kinase Activated by Src Family Kinases. *The Journal of Immunology*, *164*(8), 4321–4331. https://doi.org/10.4049/jimmunol.164.8.4321

Morrison, P. J., Suhrkamp, I., Gerdes, S., & Mrowietz, U. (2021). Oral dimethyl fumarate induces changes within the peripheral neutrophil compartment of patients with

psoriasis that are linked with skin improvement*. *British Journal of Dermatology*, *185*(3), 605–615. https://doi.org/10.1111/bjd.19899

Mrowietz, U., Morrison, P. J., Suhrkamp, I., Kumanova, M., & Clement, B. (2018). The Pharmacokinetics of Fumaric Acid Esters Reveal Their In Vivo Effects. *Trends in Pharmacological Sciences*, *39*(1), 1–12. https://doi.org/10.1016/j.tips.2017.11.002

MSIF. (2020). Atlas of MS 3 rd edition. *The Multiple Sclerosis International Federation (MSIF), September 2020*, *September*, 1–37.

Müller, S., Behnen, M., Bieber, K., Möller, S., Hellberg, L., Witte, M., Hänsel, M., Zillikens, D., Solbach, W., Laskay, T., & Ludwig, R. J. (2016). Dimethylfumarate impairs neutrophil functions. *Journal of Investigative Dermatology*, *136*(1), 117–126. https://doi.org/10.1038/JID.2015.361

Ng, L. G., Ostuni, R., & Hidalgo, A. (2019). Heterogeneity of neutrophils. *Nature Reviews Immunology*, *19*(4), 255–265. https://doi.org/10.1038/s41577-019-0141-8

O'Connor, P., Wolinsky, J. S., Confavreux, C., Comi, G., Kappos, L., Olsson, T. P., Benzerdjeb, H., Truffinet, P., Wang, L., Miller, A., & Freedman, M. S. (2011). Randomized Trial of Oral Teriflunomide for Relapsing Multiple Sclerosis. *New England Journal of Medicine*, *365*(14), 1293–1303. https://doi.org/10.1056/nejmoa1014656

Offermanns, S. (2017). Hydroxy-Carboxylic Acid Receptor Actions in Metabolism. *Trends in Endocrinology and Metabolism*, *28*(3), 227–236. https://doi.org/10.1016/j.tem.2016.11.007

Ortega-Gomez, A., Lopez, S., Varela, L. M., Jaramillo, S., Muriana, F. J. G., & Abia, R. (2022). New evidence for dietary fatty acids in the neutrophil traffic between the bone marrow and the peripheral blood. *Food Chemistry: Molecular Sciences*, *5*(July), 100133. https://doi.org/10.1016/j.fochms.2022.100133

Patel, T. S., Crutchley, R. D., Tucker, A. M., Cottreau, J., & Garey, K. W. (2013). Crofelemer for the treatment of chronic diarrhea in patients living with HIV/AIDS. *HIV/AIDS - Research and Palliative Care*, *5*, 153–162. https://doi.org/10.2147/HIV.S30948

Patsopoulos, N. A., Baranzini, S. E., Santaniello, A., Shoostari, P., Cotsapas, C., Wong, G., Beecham, A. H., James, T., Replogle, J., Vlachos, I. S., McCabe, C., Pers, T. H.,

Brandes, A., White, C., Keenan, B., Cimpean, M., Winn, P., Panteliadis, I. P., Robbins, A., … De Jager, P. L. (2019). Multiple sclerosis genomic map implicates peripheral immune cells and microglia in susceptibility. *Science*, *365*(6460). https://doi.org/10.1126/science.aav7188

Pierrot-Deseilligny, C., & Souberbielle, J. C. (2017). Vitamin D and multiple sclerosisAn update. *Multiple Sclerosis and Related Disorders*, *14*, 35–45. https://doi.org/10.1016/j.msard.2017.03.014

Pillay, J., Den Braber, I., Vrisekoop, N., Kwast, L. M., De Boer, R. J., Borghans, J. A. M., Tesselaar, K., & Koenderman, L. (2010). In vivo labeling with 2H2O reveals a human neutrophil lifespan of 5.4 days. *Blood*, *116*(4), 625–627. https://doi.org/10.1182/blood-2010-01-259028

Pirko, I., Lucchinetti, C. F., Sriram, S., & Bakshi, R. (2007). Gray matter involvement in multiple sclerosis. *Neurology*, *68*(9), 634–642. https://doi.org/10.1212/01.wnl.0000250267.85698.7a

Ponath, G., Park, C., & Pitt, D. (2018). The role of astrocytes in multiple sclerosis. *Frontiers in Immunology*, *9*(FEB), 1–12. https://doi.org/10.3389/fimmu.2018.00217

Popescu, B. F. G., Pirko, I., & Lucchinetti, C. F. (2013). Pathology of multiple sclerosis: Where do we stand? *CONTINUUM Lifelong Learning in Neurology*, *19*(4), 901–921. https://doi.org/10.1212/01.CON.0000433291.23091.65

Portincasa, P., Bonfrate, L., Vacca, M., De Angelis, M., Farella, I., Lanza, E., Khalil, M., Wang, D. Q. H., Sperandio, M., & Di Ciaula, A. (2022). Gut Microbiota and Short Chain Fatty Acids: Implications in Glucose Homeostasis. *International Journal of Molecular Sciences*, *23*(3). https://doi.org/10.3390/ijms23031105

Ramalho, A. S., Boon, M., Proesmans, M., Vermeulen, F., Carlon, M. S., & De Boeck, K. (2022). Assays of CFTR Function In Vitro, Ex Vivo and In Vivo. *International Journal of Molecular Sciences*, *23*(3). https://doi.org/10.3390/ijms23031437

Robinson, A. P., Harp, C. T., Noronha, A., & Miller, S. D. (2014). The experimental autoimmune encephalomyelitis (EAE) model of MS. utility for understanding disease pathophysiology and treatment. In *Handbook of Clinical Neurology* (1st ed., Vol. 122). Elsevier B.V. https://doi.org/10.1016/B978-0-444-52001-2.00008-X

Rodrigues, H. G., Takeo Sato, F., Curi, R., & Vinolo, M. A. R. (2016). Fatty acids as modulators of neutrophil recruitment, function and survival. *European Journal of Pharmacology*, *785*, 50–58. https://doi.org/10.1016/j.ejphar.2015.03.098

Rossi, B., Constantin, G., & Zenaro, E. (2020). The emerging role of neutrophils in neurodegeneration. *Immunobiology*, *225*(1), 0–1. https://doi.org/10.1016/j.imbio.2019.10.014

Rubant, S. A., Ludwig, R. J., Diehl, S., Hardt, K., Kaufmann, R., Pfeilschifter, J. M., & Boehncke, W. H. (2008). Dimethylfumarate reduces leukocyte rolling in vivo through modulation of adhesion molecule expression. *Journal of Investigative Dermatology*, *128*(2), 326–331. https://doi.org/10.1038/sj.jid.5700996

Rumble, J. M., Huber, A. K., Krishnamoorthy, G., Srinivasan, A., Giles, D. A., Zhang, X., Wang, L., & Segal, B. M. (2015). Neutrophil-related factors as biomarkers in EAE and MS. *Journal of Experimental Medicine*, *212*(1), 23–35. https://doi.org/10.1084/jem.20141015

Saint-Criq, V., & Gray, M. A. (2017). Role of CFTR in epithelial physiology. *Cellular and Molecular Life Sciences*, *74*(1), 93–115. https://doi.org/10.1007/s00018-016-2391-y

Sánchez-Sanz, A., García-Martín, S., Sabín-Muñoz, J., Moreno-Torres, I., Elvira, V., Al-Shahrour, F., García-Grande, A., Ramil, E., Rodríguez-De la Fuente, O., Brea-Álvarez, B., García-Hernández, R., García-Merino, A., & Sánchez-López, A. J. (2023). Dimethyl fumarate-related immune and transcriptional signature is associated with clinical response in multiple sclerosis-treated patients. *Frontiers in Immunology*, *14*(July), 1–13. https://doi.org/10.3389/fimmu.2023.1209923

Schilling, S., Goelz, S., Linker, R., Luehder, F., & Gold, R. (2006). Fumaric acid esters are effective in chronic experimental autoimmune encephalomyelitis and suppress macrophage infiltration. *Clinical and Experimental Immunology*, *145*(1), 101–107. https://doi.org/10.1111/j.1365-2249.2006.03094.x

Schott, G., & Garcia-Blanco, M. A. (2021). MHC Class III RNA Binding Proteins and Immunity. *RNA Biology*, *18*(5), 640–646. https://doi.org/10.1080/15476286.2020.1860388

Schulze-Topphoff, U., Varrin-Doyer, M., Pekarek, K., Spencer, C. M., Shetty, A., Sagan, S. A., Cree, B. A. C., Sobel, R. A., Wipke, B. T., Steinman, L., Scannevin, R. H., &

Zamvil, S. S. (2016). Dimethyl fumarate treatment induces adaptive and innate immune modulation independent of Nrf2. *Proceedings of the National Academy of Sciences of the United States of America*, *113*(17), 4777–4782. https://doi.org/10.1073/pnas.1603907113

Serafini, B., Rosicarelli, B., Magliozzi, R., Stigliano, E., Capello, E., Mancardi, G. L., & Aloisi, F. (2006). Dendritic cells in multiple sclerosis lesions: Maturation stage, myelin uptake, and interaction with proliferating T cells. *Journal of Neuropathology and Experimental Neurology*, *65*(2), 124–141. https://doi.org/10.1097/01.jnen.0000199572.96472.1c

Shahi, S. K., Freedman, S. N., & Mangalam, A. K. (2017). Gut microbiome in multiple sclerosis: The players involved and the roles they play. *Gut Microbes*, *8*(6), 607–615. https://doi.org/10.1080/19490976.2017.1349041

Shi, X., Wan, Y., Wang, N., Xiang, J., Wang, T., Yang, X., Wang, J., Dong, X., Dong, L., Yan, L., Li, Y., Liu, L., Hou, S., Zhong, Z., Wilson, I. A., Yang, B., Yang, G., & Lerner, R. A. (2021). Selection of a picomolar antibody that targets CXCR2-mediated neutrophil activation and alleviates EAE symptoms. *Nature Communications*, *12*(1), 1–14. https://doi.org/10.1038/s41467-021-22810-z

Silvestre-Roig, C., Fridlender, Z. G., Glogauer, M., & Scapini, P. (2019). Neutrophil Diversity in Health and Disease. *Trends in Immunology*, *40*(7), 565–583. https://doi.org/10.1016/j.it.2019.04.012

Smith, M. D., Martin, K. A., Calabresi, P. A., & Bhargava, P. (2017). Dimethyl fumarate alters B-cell memory and cytokine production in MS patients. *Annals of Clinical and Translational Neurology*, *4*(5), 351–355. https://doi.org/10.1002/acn3.411

Soldan, S. S., & Lieberman, P. M. (2023). Epstein–Barr virus and multiple sclerosis. *Nature Reviews Microbiology*, *21*(1), 51–64. https://doi.org/10.1038/s41579-022-00770-5

Steinbach, K., Piedavent, M., Bauer, S., Neumann, J. T., & Friese, M. A. (2013). Neutrophils Amplify Autoimmune Central Nervous System Infiltrates by Maturing Local APCs. *The Journal of Immunology*, *191*(9), 4531–4539. https://doi.org/10.4049/jimmunol.1202613

Stoiloudis, P., Kesidou, E., Bakirtzis, C., Sintila, S. A., Konstantinidou, N., Boziki, M., & Grigoriadis, N. (2022). The Role of Diet and Interventions on Multiple Sclerosis: A Review. *Nutrients*, *14*(6). https://doi.org/10.3390/nu14061150

Summers, C., Rankin, S. M., Condliffe, A. M., Singh, N., Peters, A. M., & Chilvers, E. R. (2010). Neutrophil kinetics in health and disease. *Trends in Immunology*, *31*(8), 318–324. https://doi.org/10.1016/j.it.2010.05.006

't Hart, B. A., Gran, B., & Weissert, R. (2011). EAE: Imperfect but useful models of multiple sclerosis. *Trends in Molecular Medicine*, *17*(3), 119–125. https://doi.org/10.1016/j.molmed.2010.11.006

Taggart, A. K. P., Kero, J., Gan, X., Cai, T. Q., Cheng, K., Ippolito, M., Ren, N., Kaplan, R., Wu, K., Wu, T. J., Jin, L., Liaw, C., Chen, R., Richman, J., Connolly, D., Offermanns, S., Wright, S. D., & Waters, M. G. (2005). (D)-β-hydroxybutyrate inhibits adipocyte lipolysis via the nicotinic acid receptor PUMA-G. *Journal of Biological Chemistry*, *280*(29), 26649–26652. https://doi.org/10.1074/jbc.C500213200

Taing, K., Chen, L., & Weng, H. R. (2023). Emerging roles of GPR109A in regulation of neuroinflammation in neurological diseases and pain. *Neural Regeneration Research*, *18*(4), 763–768. https://doi.org/10.4103/1673-5374.354514

Tang, H., Lu, J. Y. L., Zheng, X., Yang, Y., & Reagan, J. D. (2008). The psoriasis drug monomethylfumarate is a potent nicotinic acid receptor agonist. *Biochemical and Biophysical Research Communications*, *375*(4), 562–565. https://doi.org/10.1016/j.bbrc.2008.08.041

Tang, Y., Zhou, L., Gunnet, J. W., Wines, P. G., Cryan, E. V., & Demarest, K. T. (2006). Enhancement of arachidonic acid signaling pathway by nicotinic acid receptor HM74A. *Biochemical and Biophysical Research Communications*, *345*(1), 29–37. https://doi.org/10.1016/j.bbrc.2006.04.051

Thangaraju, M., Cresci, G. A., Liu, K., Ananth, S., Gnanaprakasam, J. P., Browning, D. D., Mellinger, J. D., Smith, S. B., Digby, G. J., Lambert, N. A., Prasad, P. D., & Ganapathy, V. (2009). GPFM 09A is a G-protein-coupled receptor for the bacterial fermentation product butyrate and functions as a tumor suppressor in colon. *Cancer Research*, *69*(7), 2826–2832. https://doi.org/10.1158/0008-5472.CAN-08-4466

The IFNB Multiple Sclerosis Study Group. (1993). I expedited publication I Interferon beta-Ib is effective in relapsing-remitting multiple sclerosis . *Neurology*, *April*, 655–662.

Thompson, A. J., Banwell, B. L., Barkhof, F., Carroll, W. M., Coetzee, T., Comi, G., Correale, J., Fazekas, F., Filippi, M., Freedman, M. S., Fujihara, K., Galetta, S. L., Hartung, H. P., Kappos, L., Lublin, F. D., Marrie, R. A., Miller, A. E., Miller, D. H., Montalban, X., … Cohen, J. A. (2018). Diagnosis of multiple sclerosis: 2017 revisions of the McDonald criteria. *The Lancet Neurology*, *17*(2), 162–173. https://doi.org/10.1016/S1474-4422(17)30470-2

Tintore, M., Vidal-Jordana, A., & Sastre-Garriga, J. (2019). Treatment of multiple sclerosis — success from bench to bedside. *Nature Reviews Neurology*, *15*(1), 53–58. https://doi.org/10.1038/s41582-018-0082-z

Tunaru, S., Kero, J., Schaub, A., Wufka, C., Blaukat, A., Pfeffer, K., & Offermanns, S. (2003). PUMA-G and HM74 are receptors for nicotinic acid and mediate its anti-lipolytic effect. *Nature Medicine*, *9*(3), 352–355. https://doi.org/10.1038/nm824

Vinolo, M. A. R., Rodrigues, H. G., Hatanaka, E., Sato, F. T., Sampaio, S. C., & Curi, R. (2011). Suppressive effect of short-chain fatty acids on production of proinflammatory mediators by neutrophils. *Journal of Nutritional Biochemistry*, *22*(9), 849–855. https://doi.org/10.1016/j.jnutbio.2010.07.009

von Glehn, F., Dias-Carneiro, R. P. C., Moraes, A. S., Farias, A. S., Silva, V. A. P. G., Oliveira, F. T. M., Silva, C. E. B. G., de Carvalho, F., Rahal, E., Baecher-Allan, C., & Santos, L. M. B. (2018). Dimethyl fumarate downregulates the immune response through the HCA2/GPR109A pathway: Implications for the treatment of multiple sclerosis. *Multiple Sclerosis and Related Disorders*, *23*, 46–50. https://doi.org/10.1016/j.msard.2018.04.016

Voskuhl, R. R. (2020). The effect of sex on multiple sclerosis risk and disease progression. *Multiple Sclerosis Journal*, *26*(5), 554–560. https://doi.org/10.1177/1352458519892491

Wannick, M., Assmann, J. C., Vielhauer, J. F., Offermanns, S., Zillikens, D., Sadik, C. D., & Schwaninger, M. (2018). The immunometabolomic interface receptor hydroxycarboxylic acid receptor 2 mediates the therapeutic effects of dimethyl

fumarate in autoantibody-induced skin inflammation. *Frontiers in Immunology*, *9*(AUG), 1–10. https://doi.org/10.3389/fimmu.2018.01890

Waschbisch, A., Schröder, S., Schraudner, D., Sammet, L., Weksler, B., Melms, A., Pfeifenbring, S., Stadelmann, C., Schwab, S., & Linker, R. A. (2016). Pivotal Role for CD16+ Monocytes in Immune Surveillance of the Central Nervous System. *The Journal of Immunology*, *196*(4), 1558–1567. https://doi.org/10.4049/jimmunol.1501960

Wattjes, M. P., Rovira, À., Miller, D., Yousry, T. A., Sormani, M. P., De Stefano, N., Tintoré, M., Auger, C., Tur, C., Filippi, M., Rocca, M. A., Fazekas, F., Kappos, L., Polman, C., Barkhof, F., & Montalban, X. (2015). Evidence-based guidelines: MAGNIMS consensus guidelines on the use of MRI in multiple sclerosis - Establishing disease prognosis and monitoring patients. *Nature Reviews Neurology*, *11*(10), 597–606. https://doi.org/10.1038/nrneurol.2015.157

Werdenberg, D., Joshi, R., Wolffram, S., Merkle, H. P., & Langguth, P. (2003). Presystemic metabolism and intestinal absorption of antipsoriatic fumaric acid esters. *Biopharmaceutics and Drug Disposition*, *24*(6), 259–273. https://doi.org/10.1002/bdd.364

Wildner, P., Stasiołek, M., & Matysiak, M. (2020). Differential diagnosis of multiple sclerosis and other inflammatory CNS diseases. *Multiple Sclerosis and Related Disorders*, *37*. https://doi.org/10.1016/j.msard.2019.101452

Woodberry, T., Bouffler, S. E., Wilson, A. S., Buckland, R. L., & Brüstle, A. (2018). The emerging role of neutrophil granulocytes in multiple sclerosis. *Journal of Clinical Medicine*, *7*(12), 10–12. https://doi.org/10.3390/jcm7120511

Wu, F., Cao, W., Yang, Y., & Liu, A. (2010). Extensive infiltration of neutrophils in the acute phase of experimental autoimmune encephalomyelitis in C57BL/6 mice. *Histochemistry and Cell Biology*, *133*(3), 313–322. https://doi.org/10.1007/s00418-009-0673-2

Wu, Q., Wang, Q., Mao, G., Dowling, C. A., Lundy, S. K., & Mao-Draayer, Y. (2017). Dimethyl Fumarate Selectively Reduces Memory T Cells and Shifts the Balance between Th1/Th17 and Th2 in Multiple Sclerosis Patients. *The Journal of Immunology*, *198*(8), 3069–3080. https://doi.org/10.4049/jimmunol.1601532

Yadav, S. K., Soin, D., Ito, K., & Dhib-Jalbut, S. (2019). Insight into the mechanism of action of dimethyl fumarate in multiple sclerosis. *Journal of Molecular Medicine*, *97*(4), 463–472. https://doi.org/10.1007/s00109-019-01761-5

Yager, R. H. (1949). *E X P E R I M E N T A L DISSEMINATED ENCEPHALOMYELITIS IN*. *6*.

Zandi-Nejad, K., Takakura, A., Jurewicz, M., Chandraker, A. K., Offermanns, S., Mount, D., & Abdi, R. (2013). The role of HCA2 (GPR109A) in regulating macrophage function. *FASEB Journal*, *27*(11), 4366–4374. https://doi.org/10.1096/fj.12-223933

Zapolska-Downar, D., Siennicka, A., Kaczmarczyk, M., Kołodziej, B., & Naruszewicz, M. (2004). Butyrate inhibits cytokine-induced VCAM-1 and ICAM-1 expression in cultured endothelial cells: The role of NF-κB and PPARα. *Journal of Nutritional Biochemistry*, *15*(4), 220–228. https://doi.org/10.1016/j.jnutbio.2003.11.008

Zhou, X., Baumann, R., Gao, X., Mendoza, M., Singh, S., Katz Sand, I., Xia, Z., Cox, L. M., Chitnis, T., Yoon, H., Moles, L., Caillier, S. J., Santaniello, A., Ackermann, G., Harroud, A., Lincoln, R., Gomez, R., González Peña, A., Digga, E., … Baranzini, S. E. (2022). Gut microbiome of multiple sclerosis patients and paired household healthy controls reveal associations with disease risk and course. *Cell*, *185*(19), 3467-3486.e16. https://doi.org/10.1016/j.cell.2022.08.021

Zhu, H., Kwak, H.-J., Liu, P., Bajrami, B., Xu, Y., Park, S.-Y., Nombela-Arrieta, C., Mondal, S., Kambara, H., Yu, H., Chai, L., Silberstein, L. E., Cheng, T., & Luo, H. R. (2017). Reactive Oxygen Species–Producing Myeloid Cells Act as a Bone Marrow Niche for Sterile Inflammation–Induced Reactive Granulopoiesis. *The Journal of Immunology*, *198*(7), 2854–2864. https://doi.org/10.4049/jimmunol.1602006

Acknowledgments

The pursuit of a doctoral degree has been a significant part of my life, and the completion of my dissertation closed an important chapter. However, achieving this goal would not have been possible without the support of many people. I would like to express my gratitude to everyone who has been part of this journey, both professionally and personally.

First and foremost, I would like to thank my supervisor, Prof. Markus Schwaninger, for his valuable insights and guidance throughout my research, which were crucial. I appreciate the critical feedback that helped shape my thinking and challenged me to approach issues from different perspectives.

During my PhD, I had the opportunity to work with outstanding scientists. Special thanks to Prof. Markus Bleich, who provided incredible supervision during my stay in Kiel. I am also grateful to PD Dr. Misa Hirose for her fantastic assistance with my research on gut microbiota, and to Dr. Axel Künstler, whose gut analysis contributed to the data presented in this work. The collaboration with Dr. Sven Geisler on FACS measurement and analysis was invaluable, and I truly appreciate his help.

I would also like to thank all the doctoral students at our institute, with whom I had the pleasure of spending time, both during and outside of work. Activities like bowling, dinners, trips to the lakes, and playing board games made the more challenging moments enjoyable and bearable. These experiences allowed us to get to know each other better and create unforgettable memories. Special thanks to Dr. Marius Richter, who was a great help at the beginning of my PhD, and to my friends in the office: Doro, Dimi, and Franco, who always supported me during difficult times and with whom I shared both my achievements and setbacks.

I would like to extend my special thanks to our lab's technical assistants: Bea, Ines, Wiebke, Frauke, and Christine. I could always count on their expertise and advice, and your behind-the-scenes efforts are deeply appreciated. Additionally, I would like to thank Dr. Helge Müller-Fielitz, who was always willing to help, and Dr. Sonja Binder, whose incredible support during the analysis phase of my research was invaluable.

Finally, to my parents, Danuta and Janusz, who have always supported and encouraged me to pursue my passions and academic goals, thank you. To my siblings, Katarzyna and Sabina, your frequent visits provided me with much-needed distraction. And to my longtime friends, whose humor kept things in perspective, even when times were tough, thank you. You all reminded me that there is more to life than deadlines and drafts, and for that balance, I am incredibly grateful.